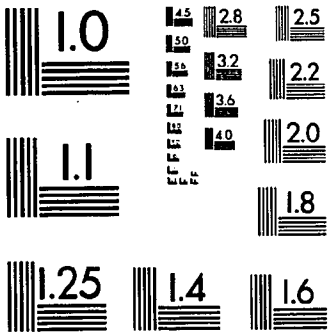

MICROCOPY RESOLUTION TEST CHART
NATIONAL BUREAU OF STANDARDS
STANDARD REFERENCE MATERIAL 1010a
(ANSI and ISO TEST CHART No. 2)

Dieter, Thomas

THE THERMAL AND PHOTOCHEMICAL BEHAVIOR OF RUTHENIUM DODECACARBONYL, (RU-3(CO)-12), SUPPORTED ON POROUS VYCOR GLASS

City University of New York PH.D. 1985

THE THERMAL AND PHOTOCHEMICAL BEHAVIOR OF RUTHENIUM DODECACARBONYL, $Ru_3(CO)_{12}$, SUPPORTED ON POROUS VYCOR GLASS.

by

THOMAS DIETER

A dissertation submitted to the Graduate Faculty in Chemistry in partial fulfillment of the requirements for the degree of Doctor of Philosophy, The City University of New York.

1985

This manuscript has been read and accepted for the Graduate Faculty in Chemistry in satisfaction of the dissertation requirement for the degree of Doctor of Philosophy.

Sept 9 1985
date

Harry D Gafney
Chairman of Examining Committee

19 Sept. 1985
date

David C. Lorke
Executive Officer

David C. Lorke

Arthur D Bakery

Harry D Gafney

Alfredo LaCava
Supervisory Committee

The City University of New York

ABSTRACT

THE THERMAL AND PHOTOCHEMICAL BEHAVIOUR OF
RUTHENIUM DODECACARBONYL, $Ru_3(CO)_{12}$,
SUPPORTED ON POROUS VYCOR GLASS.

by

Thomas Dieter

Adviser: Professor Harry D. Gafney

$Ru(CO)_5$ and $Ru_3(CO)_{12}$ adsorb onto Corning's code 7930 porous Vycor glass, PVG, without a change in their spectral properties, measured by optical transmission spectroscopy and diffuse reflectance FTIR spectroscopy (DRIFT). Adsorbed $Ru_3(CO)_{12}$ under CO is stable towards photoinitiated decomposition to $Ru(CO)_5$. Thermal or photochemical activation of the initially physisorbed cluster causes evolution of CO and leads to the chemisorbed species $HRu_3(CO)_{10}(OSi\equiv)$, identified by its optical and vibrational spectrum. The energy of activation for this process is 6.2 ± 0.3 kcal/mol. Under carbon monoxide the chemisorption is reversible, regenerating >90% of the physisorbed cluster. The energy of activation for the backreaction is 5.1 ± 0.2 kcal/mol.

From solution the sterically demanding substituted trimer $Ru_3(CO)_9(PPh_3)_3$ does not adsorb onto PVG. Although

the supported species can be obtained by co-sublimation of PPh_3 and $Ru_3(CO)_{12}$ it decomposes under vacuum at room temperature.

PVG supported $Ru_3(CO)_{12}$ thermally decarbonylates in vacuum to yield CO-covered ruthenium crystallites. After thermal decomposition in the presence of oxygen CO-covered, partially oxidized ruthenium species are observed on the surface. Reduction of the oxidized metal under flowing H_2 at 200°C and subsequent recarbonylation with CO yields a new IR band at 2031 cm^{-1}, assigned to agglomerated ruthenium metal.

The chemisorbed cluster $HRu_3(CO)_{10}(OSi\equiv)$ is a thermally and photochemically active catalyst for the isomerization of 1-pentene to cis- and trans-2-pentene with turnover numbers in excess of 400. Thermal catalysis initially yields cis- and trans-isomers in a ratio of ca. 1:1.2 before reaching the thermodyamic ratio of 1:3.2. The ratio of 2-pentene isomers produced by photoinitiated catalysis is in the order of 1:5 and constant over several cycles.

In fluid solution $Ru_3(CO)_{12}$ photochemically reacts with L = 1-pentene, PPh_3, and $P(t\text{-}Bu)_3$ to form the substituted monomer $Ru(CO)_4L$ with limiting quantum yields of decomposition of $8.0\pm0.7\times10^{-2}$, $5.7\pm0.4\times10^{-2}$, and $8.4\pm0.5\times10^{-2}$ respectively. The monosubstituted $Ru(CO)_4PPh_3$ reacts with PPh_3 to form $Ru(CO)_3(PPh_3)_2$ under photochemical conditions and with CO to regenerate ruthenium dodeca-

carbonyl in a thermal backreaction at room temperature. At temperatures above 30°C a thermal substitution of $Ru_3(CO)_{12}$ with PPh_3 leads to the substituted trimer $Ru_3(CO)_9(PPh_3)_3$. The activation energy of this reaction has been calculated to 24.2±1.2 kcal/mol.

ACKNOWLEDGEMENTS

I would like to thank the members of the thesis committee, especially my adviser Professor Harry D. Gafney, for their time and their expertise which they frequently and freely provided. Dr. Gafney, you taught me how to focus on the important when my vision was clouded by details. I am very grateful to Professor David Baker, Professor Thomas Strekas, and Professor George Axelrad for their kind assistance, to Professor David C. Locke who, as Executive Officer of the Graduate Program, solved administrative problems faster than anyone I know, and the staff of the Chemistry Department for their relentless support. No acknowledement would be complete without mentioning those members of the staff who make experimental science possible; Bob Wurman who promptly repaired my broken instruments, Randy Smith who surprised me many times with his exceptionally well organized stock room, Paul Schaedler who built my high pressure optical cell, and Ottmar Safferling who always offered me a cup of coffee and who crafted excellent glassware from sketchy designs. Last but not least many thanks to my parents who sacrificed much to get me started and to my best friend Marilyn who kept me going.

TABLE OF CONTENTS

LIST OF FIGURES

LIST OF TABLES

1. INTRODUCTION

1.1. GENERAL INTRODUCTION

In recent years the chemical industry in America and Western Europe has experienced a dramatic increase in expenditure for human resources, raw materials, energy, and general operating cost. Although a worldwide recession in combination with conservation efforts resulted in an oversupply of oil and several other basic raw materials, this positive development can only be viewed as temporary. It is therefore our obligation to use this hiatus for researching long-term strategies, dealing with an effective use of our scarce and exhaustable resources.

In addition to securing a supply of raw materials, the removal of undesired reaction by-products has received much attention in recent years. The once common practice to 'bury and forget' toxic wastes for the sake of short-term profitability fully justifies this attention. In most cases, the uncontrolled dumping of toxic waste has come back to haunt us and has, especially in Europe, severely tainted the reputation of the entire chemical industry. Unfortunately, as every experimental chemist will attest, chemical reactions rarely proceed to completion, often converting only a fraction of the starting material to the desired product. Although generally optimized, production

scale reactions generate significant amounts of waste, some of which is highly toxic and persistent. Advances in chemical engineering have provided us with tools to contain such pollutants and convert them into non-hazardous materials. However, many of these waste management technologies are expensive and burdened with a disposal problem of their own. From an economic point of view it is therefore advantageous to develop chemical processes that are not only fast and energy efficient but also highly selective, generating little or no unwanted products.

Catalysis is a viable method of controlling rate and direction of a chemical process and has captured the imagination of chemists and engineers for many years. The function of a catalyst is to accelerate the rate at which equilibrium is attained, i.e. to lower the activation energy for the conversion of reactants to reaction products. The principle actions of a catalyst have been summarized by Schrauzer (1):

1. Catalysts increase reaction rates by their ability to relax restrictions imposed by quantum mechanical selection rules of spin and angular momentum.

2. Catalysts bring reaction participants together in energetically and sterically favorable fashion (proximity effect).

3. Catalysts introduce efficient alternative reaction pathways by virtue of specific interactions with the substrate(s).

From its origin in the last century, industrial catalysis has remained primarily a technology which draws on many fields such as organic chemistry, surface chemistry, chemical kinetics, thermodynamics, solid-state physics, ceramic, and physical metallurgy. No unified theory of catalysis exists, and there are frequently several alternative, and not necessarily mutually exclusive, theoretical 'explanations' for any given set of facts (2). As usual, in our quest for viable catalytic systems, we attempt to learn from Nature; enzymatic processes are fast, occur at low temperature, and are highly selective. Man has yet to design a catalyst that rivals enzymatic and photosynthetic efficiency.

1.2. HETEROGENEOUS CATALYSIS

Heterogeneous catalysis still accounts for the great majority of commercially-used catalytic processes, primarily in the petroleum refining industry. The term describes the enhancement in the rate of a chemical reaction brought about by the presence of an interface between two phases (3). Catalysts are manufactured by depositing a coating of precious metals or metal oxides on an inorganic substrate

in order to both increase the effective surface area of the metal and to dilute the catalyst for better temperature control. How the coating is applied, as well as the physical properties of the substrate (i.e. the presence of acid and base functionalities on the surface which may also act as catalysts), markedly affect the activity, the specificity, the lifetime, and the poison-tolerance of the catalyst (4). Dependence on these variables complicates the manufacturing of heterogeneous catalysts with reproducible and constant activities and selectivities. Further problems associated with heterogeneous catalysis are limitations in surface area per gram of catalyst, due to the formation of rather large metal crystallites, > 35 Å, and the temperature requirements of the reaction, typically 250 - 550°C. The number of alternative reactions that can occur and their ability to successfully compete with the desired process increases rapidly with temperature, leading to a low selectivity. Heterogeneity and high temperature also complicate the characterization of the reactant-catalyst-support system and hinder systematic research on the improvement of activity and selectivity. These disadvantages are balanced, however, by a superior stability of the heterogeneous system and a facile separation of catalyst and reactants.

1.2.1. RUTHENIUM IN HETEROGENEOUS CATALYSIS

Many heterogeneous catalytic systems are based on group VIII transition metals and ruthenium catalysts can be found in a wide range of applications. Therefore even the attempt to categorize the use of ruthenium metal and ruthenium oxides would go far beyond the scope of this introduction. An excellent review, recently published by Rard (5), discusses the chemistry and thermodynamics of ruthenium and some of its inorganic compounds and aqueous species. Rard pointed out that Ru, similar to many second row transition metals, has a very complicated chemistry and that much of the thermodynamics associated with ruthenium compounds are still poorly understood.

A recent review of the Fischer-Tropsch Synthesis by M. E. Dry (6) lists ruthenium as a very active catalyst for the hydrogenation of carbon monoxide. It is most active in the pure metal form, i.e. supports and/or promoters appear to have no beneficial effect other than increasing the surface area of the catalyst. The activities of many research workers in the field of heterogeneous, ruthenium-based catalysis (7,8,9,10) may serve as evidence for ruthenium's high potential as a catalyst for converting synthesis gas to a variety of high molecular weight hydrocarbons. However, in spite of the great number of catalytic systems that have been reported in the literature, a comprehensive theory, linking the effects of temperature, catalyst

dispersion, and chemical and geometric properties of the support material to the observed product mixture remains in its infancy.

1.3. HOMOGENEOUS CATALYSIS

A catalytic reaction is termed homogeneous if the reactants and the catalyst are in the same phase. The earliest observed cases of catalysis in solution are the frequently encountered acid- or base-catalyzed reactions. More recently the term homogeneous catalysis has been specifically applied to a solution of organometallic compounds in which a central metal atom is surrounded by coordinating ligands. Depending on the nature of these ligands the metal may be in a low positive, zero, or negative oxidation state and several structures may coexist in solution (2). The prominent feature of most organometallic catalysts is the presence of vacant coordination sites at which facile substrate adsorption and/or coordination occurs (11,12,13,14,15). Compared to mononuclear complexes the use of transition metal clusters, complexes with at least one metal-metal bond, has a potential for chemoselective and stereoselective reactions (16,17). Active sites in a metal complex are commonly generated by ligand dissociation and, as such, the active species is often a transient intermediate in the reaction sequence and difficult to identify. In spite of these difficulties, many

solution reactions have been followed by kinetic and spectroscopic analysis, and stoichiometric and catalytic processes have been well-characterized. It is expected that a knowledge of the steric and electronic effects, that a given set of ligands exerts on the central metal, will enable us to custom design catalysts for specific reactions. However, several critical disadvantages remain associated with homogeneous transition metal catalyzed reactions; side-reactions, such as oxidations, are likely to reduce the solution-concentration of the active species and the separation of the reactants from the catalyst typically requires a distillation. Also, energetically more demanding transformations, such as the activation of carbon-carbon and carbon-hydrogen bonds in saturated hydrocarbons as well as the hydrogenation of the carbon-oxygen triple bond in CO remain relatively unkown in homogeneous catalysis.

As mentioned earlier, the lack of information regarding catalysts and catalyst-reactant systems and the inability to control reactions at the molecular level have severely restricted the understanding of heterogeneous catalysis by metal surfaces. Since this information can be acquired if the metal is dissolved in fluid solution, a strong interest in transition metal complexes and clusters has developed. Transition metal clusters are on the borderline between the molecular state and the metallic state. Although their solubility in hydrocarbon solvents is generally low, intensely colored solutions, 10^{-3} to

10^{-4} Molar in cluster, can be prepared. Beginning in 1975 with Muetterties (18), Ugo (19), and Lewis and Johnson (20), numerous papers and reviews have put forward the idea that homogeneous reactions, catalyzed by transition metal clusters, may be used to model heterogeneously catalyzed reactions (21,22). We can summarize the reasons for the great interest in homogeneous catalysis by organometallics:

1. Development of new organo-transition metal complexes capable of catalyzing reactions with high activity and selectivity under mild conditions.

2. Development of asymmetric catalysts (23).

3. Research on catalysts that are capable of activating stable bonds such as the bond in molecular nitrogen and C-H and C-C bonds in alkanes.

4. Modeling of heterogeneous catalysts using transition metal clusters in order to gain insights in the processes occurring on gas-metal interfaces.

The role of transition metals in homogeneous catalysis has been discussed in several books (1,14,24) and review articles (4,25). Figure 1 summarizes several important processes that employ a variety of transition metal salts, compounds and complexes.

CATALYSIS USING Ru-COMPOUNDS:

Homologation:

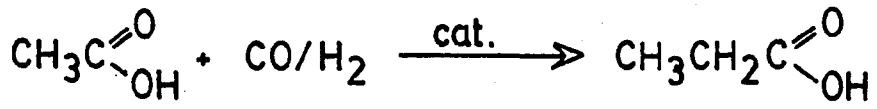

Carbonylation:

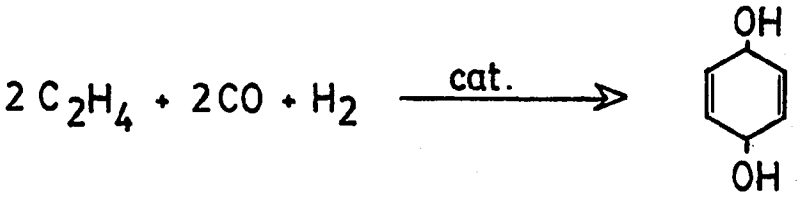

Isomerization:

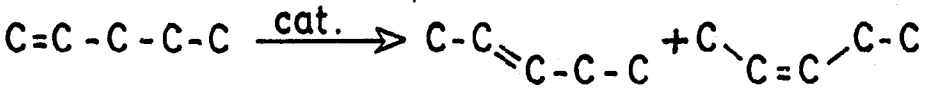

Hydrosilylation:

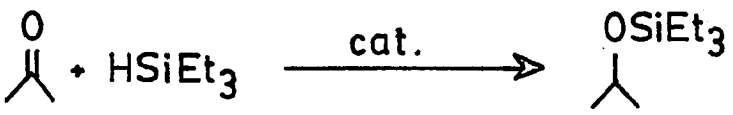

Fig. 1. Examples for transition metal catalyzed reactions

1.3.1. RUTHENIUM DODECACARBONYL, $Ru_3(CO)_{12}$

The air-stable, gold-orange colored ruthenium trinuclear compound was discovered as early as 1910 but was not characterized as such (26,27). Using X-ray diffraction techniques the similarity of its structure to that of $Os_3(CO)_{12}$ was determined less than twenty five years ago (28,29,30) and and exact geometric data were not available until 1977 (31). $Ru_3(CO)_{12}$ is a coordinatively saturated, diamagnetic transition metal cluster with three metal to metal bonds, six equatorial, and six axial carbonyl groups (Figure 2). Churchill and coworkers determined the average axial Ru-CO bondlength to 1.942Å and the average equatorial bondlength to 1.921Å. The axial Ru...O vectors, average 3.071Å, are also longer than the equatorial Ru...O vectors with an average of 3.048Å. The distortion of the axial Ru-C-O moieties by about 7° was explained as the result of van der Waals distortion caused by interaction of the closely packed carbonyl groups. Ru-Ru bonds within the cluster triangle were found to be not strictly equivalent showing an average of 2.8515Å with a difference of 0.0080±0.0006Å. $Ru_3(CO)_{12}$ belongs to the symmetry point group D_{3h} and group theory predicts four IR-active fundamentals (3 E' and 1 A_2''), two axial and two radial (Figure 3). Although for $Ru_3(CO)_{12}$ the fourth band is only poorly resolved (32), absorptions in the carbonyl region at

$Ru_3(CO)_{12}$

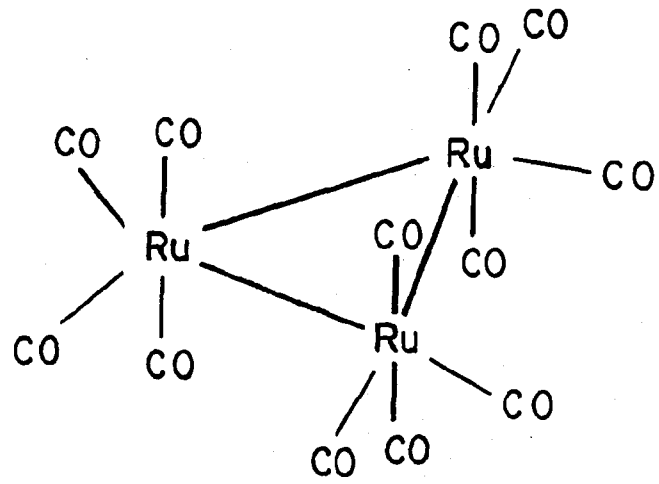

$Ru\text{-}CO_{ax}$ = 1.942 Å

$Ru\text{-}CO_{eq}$ = 1.921 Å

$Ru\ldots O_{ax}$ = 3.071 Å

$Ru\ldots O_{eq}$ = 3.048 Å

Ru - Ru = 2.8515 Å

Fig. 2. The $Ru_3(CO)_{12}$ cluster and its bondlengths

IR-active vibrations of $Ru_3(CO)_{12}$

point group D_{3h}

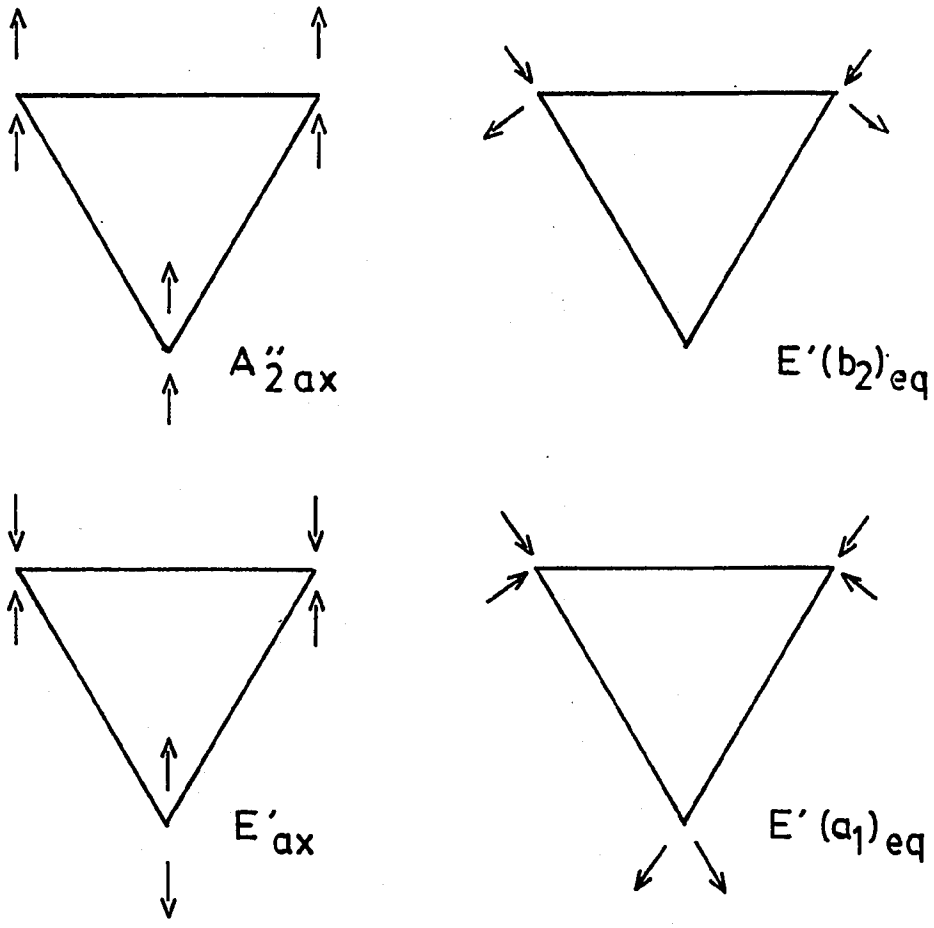

Fig. 3. Vibrations of the D_{3h} ruthenium cluster

2060-2062 (vs), 2030-2033 (s), 2018 (sh,w) and 2010-2012 cm^{-1} (m) have been reported. Quicksall and Spiro (33) assigned the high frequency vibration to a purely axial A_2'', the intense vibration in the 2033 cm^{-1} region to an axial E" or E', and the band in the 2010 cm^{-1} region to a radial E'. This assignment is in conflict with interpretations put forward by Kaesz and coworkers and other groups (34,35,36), proposing an assignment of axial E' and A_2'' for the high frequency bands and radial E' for the vibrations at 2018 and 2012 cm^{-1}. The nature of the metal-metal bond in $Ru_3(CO)_{12}$ was studied by UV photoelectron spectroscopy and Granozzi and coworkers (37) suggested a d^8 electron configuration in a pseudo octahedral environment for each Ru atom and an antibonding character with respect to the Ru-Ru ring for the lowest unoccupied molecular orbital (LUMO). Gray and coworkers (38) supported this analysis and assigned the lowest energy band in the electronic spectrum at 390 nm to a σ to σ^* transition (Figure 4).

1.3.2. RUTHENIUM IN HOMOGENEOUS CATALYSIS

Ruthenium, either in a higher oxidation state or zero valent as in many carbonyl complexes, has a record of catalytic activity in homogeneous solution.

Strohmeier and Weigelt (39) reported the use of $RuCl_2(CO)_2(PPh_3)_2$ for the homogeneous hydrogenation of

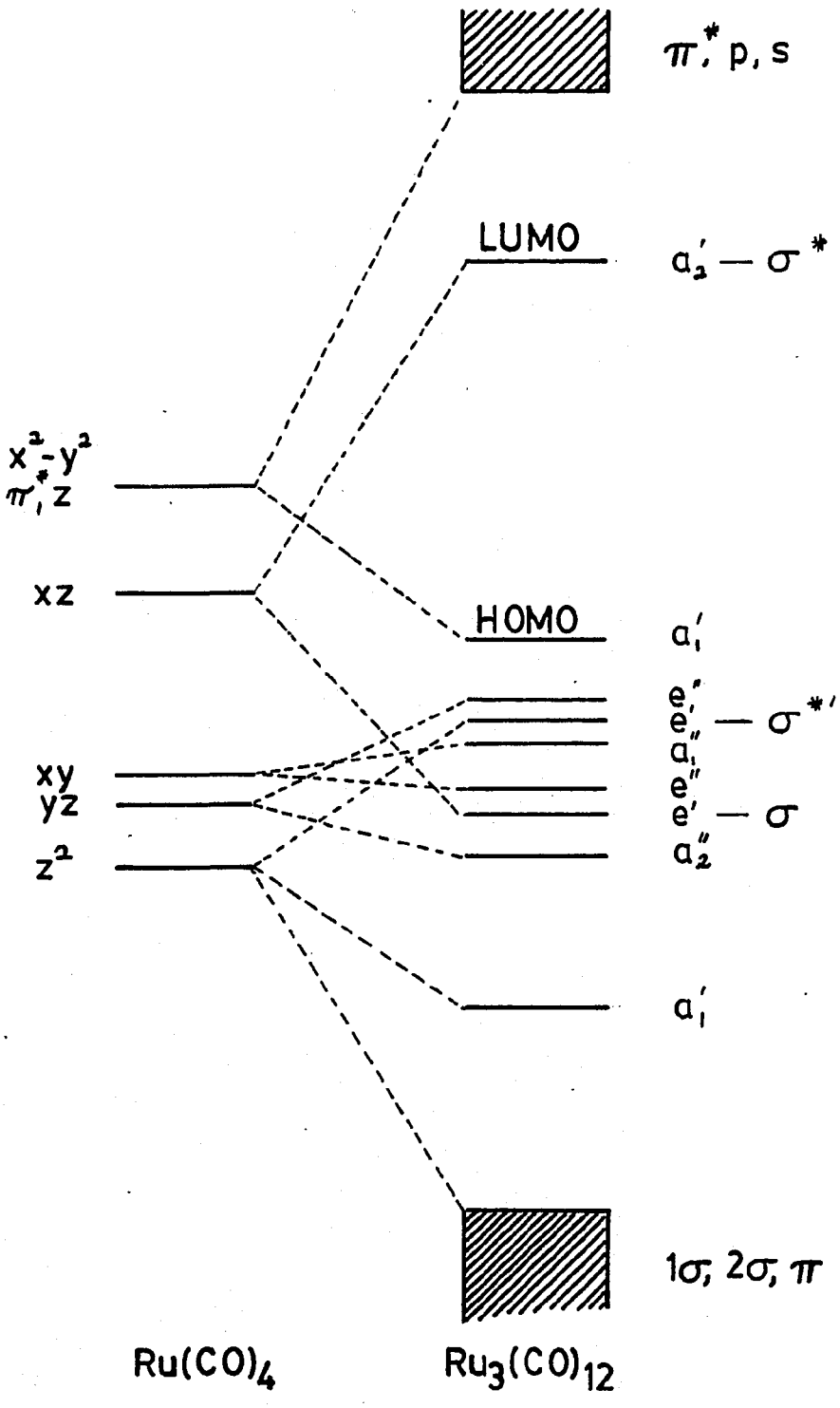

Fig. 4. Energy diagram for the ruthenium cluster (175)

aldehydes. The same reaction was performed by Sanchez-Delgado and de Ochoa (40) using the precursors $RuHCl(CO)(PPh_3)_3$, $RuHCl(PPh_3)_3$, $RuCl_2(PPh_3)_3$, and $Ru(CO)_3(PPh_3)_2$. Although no hydrogenation occurred at 25°C and 1 atm of H_2, aromatic aldehydes were rapidly reduced at 100°C and 1000 psi H_2. It is noteworthy that in the reduction of propionaldehyde to 1-propanol with $RuHCl(CO)(PPh_3)_3$, using a substrate to catalyst ratio of 100,000, turnover numbers of up to 20,000 after 3 days have been achieved. The catalyst could be re-used without any appreciable loss in its activity.

Although ruthenium carbonyls do not possess the same level of activity as the ruthenium species mentioned above, many publications report their use as catalyst precursors. The effectiveness of $Ru_3(CO)_{12}$ as a catalyst for the carbonylation of acetylene has been described (41) as early as 1968. The hydrocarbonylation was performed under anhydrous conditions in THF or dioxane at 150 - 250°C.

Valle and coworkers (42) refluxed 1-pentene with $Ru_3(CO)_{12}$ in n-hexane. GC analysis showed that the olefin was isomerized and that the equilibrium composition of 3% 1-pentene, 23% cis-2-pentene, and 74% trans-2-pentene was reached within a few hours. Knifton (43) studied the homologation of aliphatic carboxylic acids catalyzed by RuO_2, $Ru_3(CO)_{12}$, and $H_4Ru_4(CO)_{12}$, coupled with alkyl or hydrogen iodide promoters in acetic acid solution. He noted a strong dependence of yield and selectivity on syngas

composition and operating pressure which was typically between 50 and 500 atm. No homologation was observed in the absence of the halogen promoter. A hydrogenation of carbon monoxide to alcohols, catalyzed by cobalt and ruthenium carbonyls at 180 - 200°C and 200 atm, was observed by King and coworkers (44). Their catalytic system was prepared from $Ru_3(CO)_{12}$ and was spectroscopically shown to contain $Ru(CO)_5$ as its principal component. The wide range of applications that ruthenium dodecacarbonyl has found in homogeneous catalysis is further exemplified by a study of asymmetric hydrogenation of ã,ß-unsaturated carboxylic acids, conducted by Johnson and coworkers (45). Johnson's group reduced the carboxylic acids with hydrogen in the presence of $Ru_3(CO)_{12}$ and three different chiral phosphinites. Best results were obtained in THF at 125°C with 40 atm of H_2 pressure.

The above examples show that ruthenium-catalyzed homogeneous reactions, with few exceptions, require rather high temperatures and operating pressures. These requirements are not surprising if one considers that $Ru_3(CO)_{12}$, like many other transition metal carbonyls, is coordinatively saturated and thermodynamically stable. Before catalysis can occur a vacant coordination site must be created in the complex by thermal dissociation of a labile ligand such as CO. The reactants must then penetrate the stabilizing solvent shell, bind to the active site, dissociate after the reaction, and leave the solvent shell. The activity of a

particular catalyst depends on the number of moles of reactant that complete this process per mole of catalyst per unit time and is conveniently expressed in the turnover number. Compared to thermal activation, which raises the energy content of the entire complex until one or more of its bonds rupture, the use of light may offer a method to selectively remove a ligand without affecting the other bonds in the system. Thus at ambient or low temperature photochemistry may offer a route to the generation of a metal complex which contains a vacant coordination site and which is catalytically active.

1.3.3. PHOTOCHEMICAL STUDIES IN SOLUTION

Many recent investigations of the photochemistry of transition metal complexes in ambient temperature homogeneous solution indicate that activation, *i.e.* ligand dissociation can be initiated by absorption of visible or ultraviolet light by the catalyst precursor (46,47,48,49). Porter (50) pointed out that inorganic complexes in excited states undergo a number of different chemical reactions. These are sometimes the counterpart of thermal reactions, but in many cases the photochemical pathway is distinctly different from that of the thermal reaction. Selective irradiation of optical absorption bands of transition metal compounds may lead to population of electronic excited states that are strongly anti-bonding with respect to

specific metal-ligand interactions (51,52). Population of the lowest excited state of transition metal clusters is known to have a destabilizing effect with respect to the metal-metal σ bond and may result in cluster fragmentation (53). Therefore photochemistry can not only provide a route to the preparation of active catalysts at low temperature, but may in fact generate genuinely new catalysts with properties unavailable through thermal activation. However, it is necessary to differentiate between photoactivation and photosensitized catalysis (54). While the latter requires continued photolysis, photoactivation necessitates only photogeneration of the active species; the actual catalytic cycle occurs as a dark reaction. Recent publications report several reactions, catalyzed by photoactivated and/or photosensitized transition metal carbonyls. Examples are polymerizations (55), olefin isomerizations (53,56,57,58), metatheses (59), and olefin dimerizations or oligomerizations (60).

Investigations of the photochemistry of ruthenium species have mostly involved $Ru_3(CO)_{12}$ or phosphine substituted trimers and monomers and catalysis studies have concentrated on isomerization reactions (53,57,61). As early as 1974 Johnson, Lewis, and Twigg (62,63) pointed to differences between the thermo- and photochemical behavior of the ruthenium cluster; 390 nm photolysis of $Ru_3(CO)_{12}$ in the presence of carbon monoxide or phosphine ligands leads to quantitative yields of mono- and di-substituted monomers

(Figure 5). During thermal reactions with the same donor ligands, however, the metal-metal triangle remains intact (64). Wrighton and coworkers (53) elaborate on the photocatalytic activity of Fe, Ru, and Os trimers for alkene isomerization and for the reaction of alkenes with silanes at room temperature. Photogeneration of mononuclear catalysts for M = Fe or Ru and cluster catalysis for M = Os is postulated. A comparison of the catalytic activities of $Ru(CO)_4PPh_3$ and $Ru_3(CO)_9(PPh_3)_3$ is of special interest since clusters generally have low energy optical absorptions, allowing for initiation of photochemical reactions by visible light. For both complexes the photogeneration of a thermally active catalyst has been shown. However, differences in the inital ratio of trans- to cis-pentene were observed which indicate a sensitivity of the reaction to the catalyst precursor (61,65). Cleavage of a Ru-Ru bond and formation of a di-radical was assumed to be the primary chemical result upon light absorption (66). Poe and coworkers (67) studied the photofragmentation of $Ru_3(CO)_{12}$ to $Ru(CO)_5$ in several organic solvents under CO. They report limiting quantum yields between $5.1\pm0.8 \times 10^{-2}$ to $10.5\pm2.2 \times 10^{-2}$, the values being essentially independent of the irradiation wavelength. The presence of a reactive intermediate that can either revert to $Ru_3(CO)_{12}$ or react further with CO to yield $Ru(CO)_5$ as a stable product is proposed in favour of the diradical intermediate. Flash

Reactions of $Ru_3(CO)_{12}$ with PPh_3

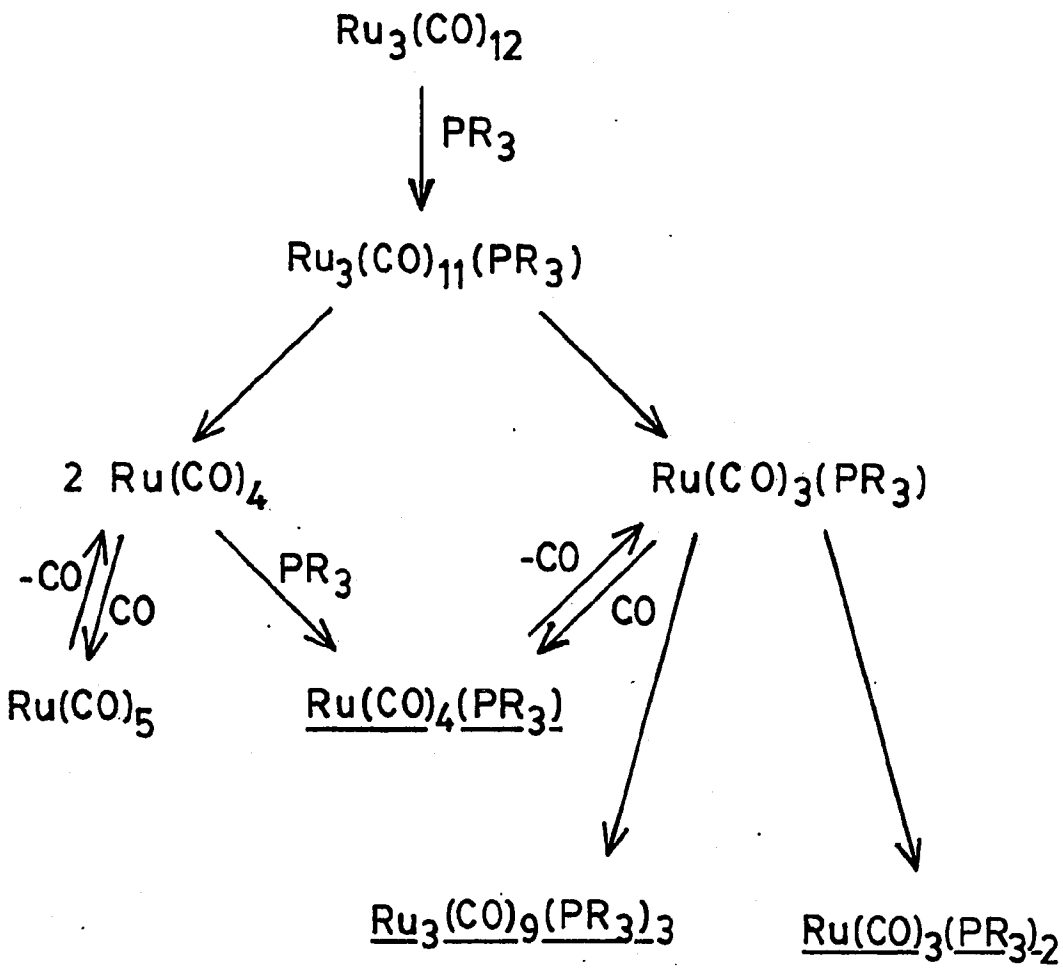

(stable products are underlined)

Fig. 5. Reactions of $Ru_3(CO)_{12}$ with PPh_3

photolytic studies performed by Ford and coworkers (68) indicate the presence of two reactive intermediates, each key to independent pathways, leading respectively to photofragmentation (wavelength > 390 nm) or to ligand photosubstitution (wavelength < 315 nm) of $Ru_3(CO)_{12}$ (Figure 6).

1.4. HYBRID CATALYSIS

In the preceding sections we have elaborated on several of the disadvantages associated with heterogeneous and homogeneous catalysis. Attempts to unify the two concepts and to combine their respective advantages have been in progress for several years as evidenced by the work of Strohmeier and coworkers who compared homogeneous Ir-, Rh-, and Pt-based catalysts with their heterogenized counterparts (69). Heterogenized homogeneous catalysts, also termed hybrid catalysts, can be prepared by supporting transition metal carbonyls on materials such as polymers or inorganic oxides (4). A hybrid catalyst retains many of the properties of a homogeneous species, such as control of the catalyst on a molecular level in conjunction with high activity, while enjoying the additional benefit of easy catalyst-reactant separation and catalyst stability, commonly associated with heterogeneous systems. Several reports have already appeared linking high catalytic

Flash Photolysis Studies of $Ru_3(CO)_{12}$

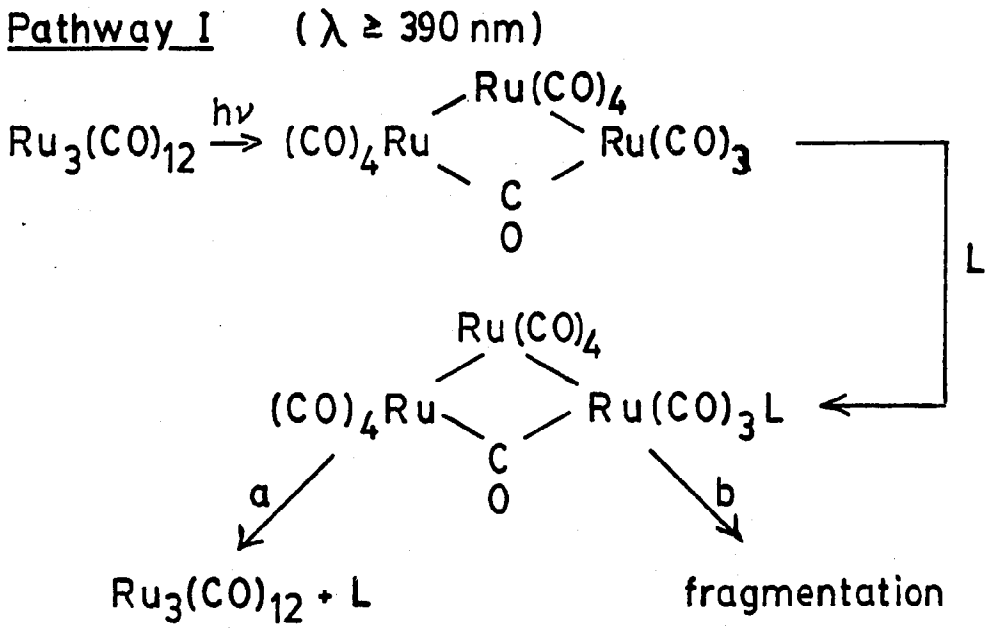

Pathway II ($\lambda \leq 400$ nm)

$$Ru_3(CO)_{12} \xrightarrow[S]{h\nu} Ru_3(CO)_{11}S + CO$$

$$Ru_3(CO)_{11}S \underset{k_b}{\overset{k_a}{\rightleftharpoons}} Ru_3(CO)_{11} + S$$

$$Ru_3(CO)_{11} + CO \xrightarrow{k_c} Ru_3(CO)_{12}$$

Fig. 6. Flash photolysis results (68)

activities and selectivities to catalysts derived from oxide supported metal carbonyls. The active species in homogeneous catalysis are coordinatively unsaturated and Smith and Basset (70) pointed out that immobilization of such species on an insoluble support can prevent intermolecular reactions leading to aggregation into inactive compounds, and thus stabilize unsaturation. However, the material used to hybridize an organometallic species does not necessarily behave as an "inert support". Rather, it may possess surface functionalities capable of catalyzing reactions on their own. Polymeric support materials and phosphines-bridges, which may be used to attach transition metal complexes to inorganic oxides, are sensitive to temperature, solvents, and ultraviolet light. Consequently, in addition to being capable of withstanding the reaction conditions and possessing a large surface area, the effect of the support material on the reactions of the immobilized metal complex must be known. Yermakov (71) recently reviewed the field of oxide-anchored transition metal complexes and distinguished between the following support materials:

1. Organic polymers
   (see review by Ciardelli et al. (72))
2. Graphite
   (see lecture by Vol'pin (73))

3. Inorganic Oxides

   A. Complexes anchored to functionalized oxides

   B. Complexes anchored on nonfunctionalized surfaces

In spite of the concentrated efforts of many research groups throughout the world, however, the field of hybrid catalysis is progressing slowly. Basset and Choplin conclude (74) that the strategy for developing hybrid systems is much closer to that followed in homogeneous catalysis than that followed in heterogeneous catalysis: the characterization of a supported complex must be as complete as possible before starting the study of a catalytic reaction (the lack of observation of such a procedure could lead to similar problems in characterizing catalytically active species as encountered in heterogeneous catalysis). Unfortunately many of the tools available for monitoring fast reactions in homogeneous solution and identifying active species are not available to the surface scientist. Although significant advances have occurred in the development of analytical instrumentation to probe surfaces and adsorbed species, only a few, if any, of these techniques have a time resolution sufficient to detail the extremely fast catalytic reactions and to identify the activated complexes. Additional difficulties arise from the inhomogeneity of the support and changes that it undergoes in the

course of a catalysis reaction, e.g. the swelling of polymers due to incorporation of solvents. In our attempt to characterize the reactions of immobilized ruthenium complexes we decided to exclude as many variables from our reaction system as possible. Our discussion of hybridized complexes will therefore be limited to transition metal compounds that are directly adsorbed onto inorganic oxides.

1.4.1. IMMOBILIZED RUTHENUM COMPLEXES

In this section we will discuss the thermal chemistry of ruthenium carbonyls stabilized on inorganic oxides. A wide selection of substrates, including SiO_2, Al_2O_3, MgO, and zeolites, have been used to primarily support the trimer $Ru_3(CO)_{12}$ (75,76,77). Sanchez-Delgado and coworkers (78) adsorbed the trimer onto silica and studied the catalysis of a hydrogenation and isomerization of 1-hexene by the cluster and its fragmentation products (Figure 7). A catalytic activity was only observed for the pink form (B) and the grey form (D). Although initial observations were rather confusing and sometimes contradictory, some important parameters became quickly apparent; the presence of basic and/or acidic surface functionalities has implications for the stability of the adsorbed metal carbonyl and the amount of surface water that is available to the catalyst may effect the product distribution. Differences in the thermal

$Ru_3(CO)_{12}$ on Silica

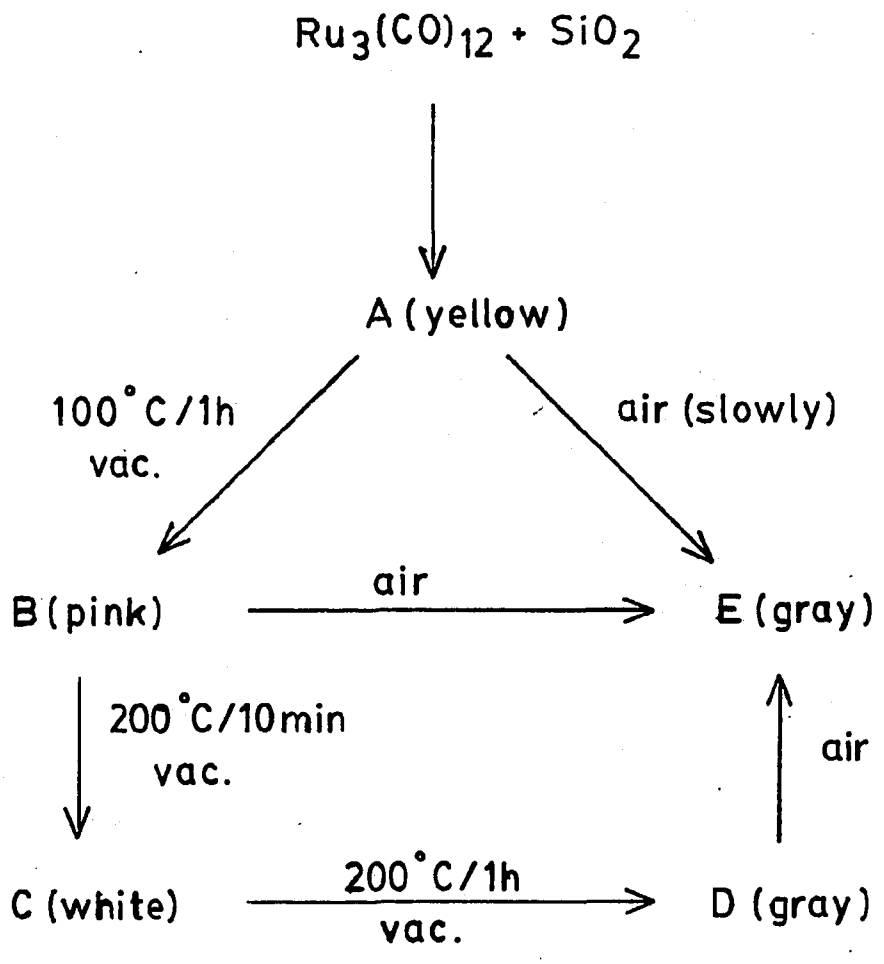

Fig. 7. Reactions of $Ru_3(CO)_{12}$ according to Sanchez - Delgardo (78)

pretreatment of the support material and failure to effectively exclude air and moisture from the reaction system explained many of the conflicting results. Kuznetsov and coworkers (79) reported that $Ru_3(CO)_{12}$ adsorbs onto alumina and silica with its metal framework intact. The similarity of the infrared absorption for $Ru_3(CO)_{12}/Al_2O_3$ and $Ru_3(CO)_{12}/SiO_2$ to those of the cluster in solution is striking and has been interpreted as an initial physisorption of the ruthenium trimer onto the support. The complex can be decomposed on the support by reaction with CO, O_2, H_2, or surface hydroxyls yielding mononuclear ruthenium species. Thermal decomposition in vacuum produces Ru crystallites on the surface of the support (79,80,81,82, 83). The oxidation of $Ru_3(CO)_{12}$ on alumina under O_2 produces IR bands at 2132 (w), 2050 (br), and 1993 cm^{-1} (br). Thermal degradation of the trimer on silica has been found to produce weak bands at 2130, 2110, and 2079 cm^{-1} in addition to those observed for the initial trimer (84). Doi and Yano (85) studied the photochemistry of $Ru_3(CO)_{12}$ supported on silica and reported an UV-visible maximum at 330 nm and IR bands at 2075 (sh), 2063 (s), 2031 (s), and 2000 cm^{-1} (sh) upon adsorption of the ruthenium trimer onto nonporous Carbosil. After photolysis with 310 nm light they observed a disappearance of the UV-visible absorption concurrent with an appearance of IR bands at 2060 (s), 1990 (m), and 1945 cm^{-1} (m) and conclude that a $Ru(CO)_4/SiO_2$ species is photochemically produced on the silica surface

(Figure 8). Basset and coworkers (86) reported initial IR absorptions of 2063 (s), 2032 (m), and 2018 cm^{-1} (m,sh) on silica which change to absorptions at 2111 (w), 2077 (m), 2066 (m), 2033 (s,br), and 1995 cm^{-1} (sh) upon treatment under vacuum at 80°C. They assigned this new set of bands to the formation of a grafted molecular cluster $HRu_3(CO)_{10}(OSi\equiv)$, resulting from the oxidative additon of a surface silanol group into the metal-metal bond of the original physisorbed trimer (Figure 9). Basset postulates that such grafted clusters decompose only above 100°C to produce, upon aggregation, ruthenium metal particles covered with CO and some oxidized Ru(II) carbonyl surface species. Electron microscopy studies by Simpson and Whyman (87) show that thermal decomposition of $Ru_3(CO)_{12}$ under H_2 at 350 - 400°C results in the formation of very small metal particles with a crystallite size between 15 and 20Å. A greatly enhanced activity and selectivity for complete hydrogenolysis of straight chain aliphatic hydrocarbons to methane was claimed to occur under conditions directly comparable to conventional ruthenium-based catalysis. Since the metal crystallites are dispersed on a high surface area support, an observed catalytic activity for synthesis gas reactions is not surprising. Infrared analysis of the reaction system shows a strong band at 2030 cm^{-1}, characteristic of CO linearly adsorbed on fully reduced silica-supported ruthenium metal (88).

Reactions of $Ru_3(CO)_{12}$ on Silica

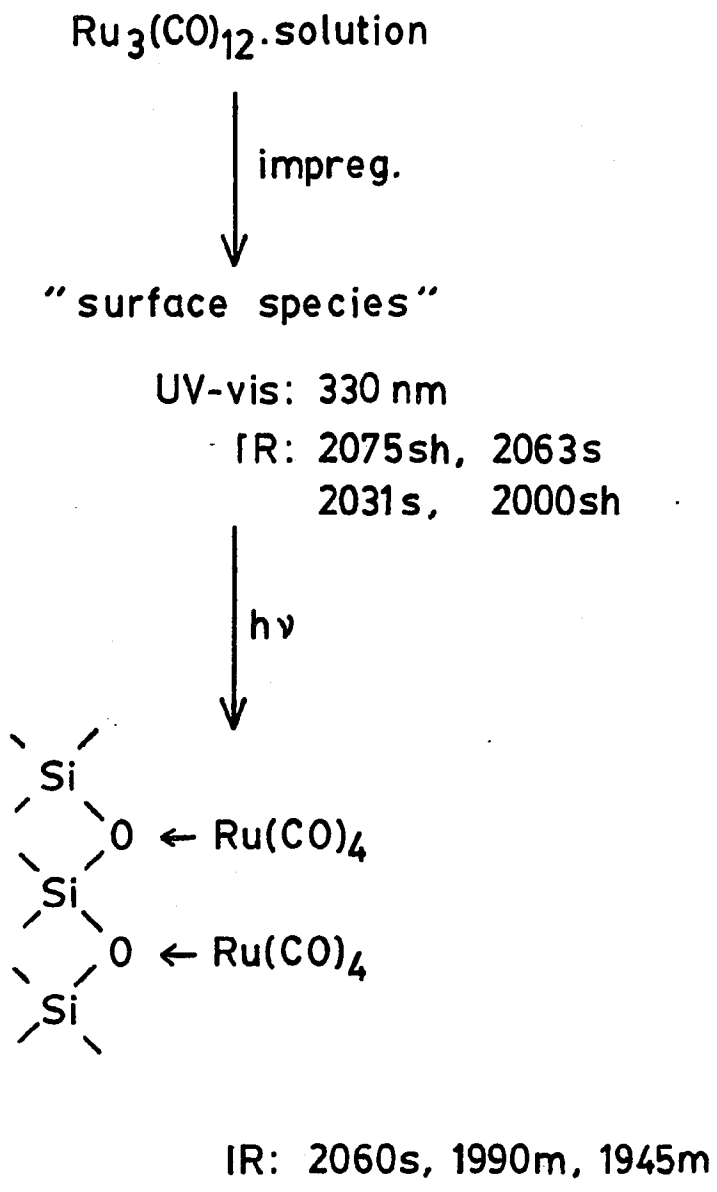

Fig. 8. Interaction of the ruthenium trimer with silica, proposed by Doi and Yano (85)

REACTIONS OF $Ru_3(CO)_{12}$ WITH SiO_2

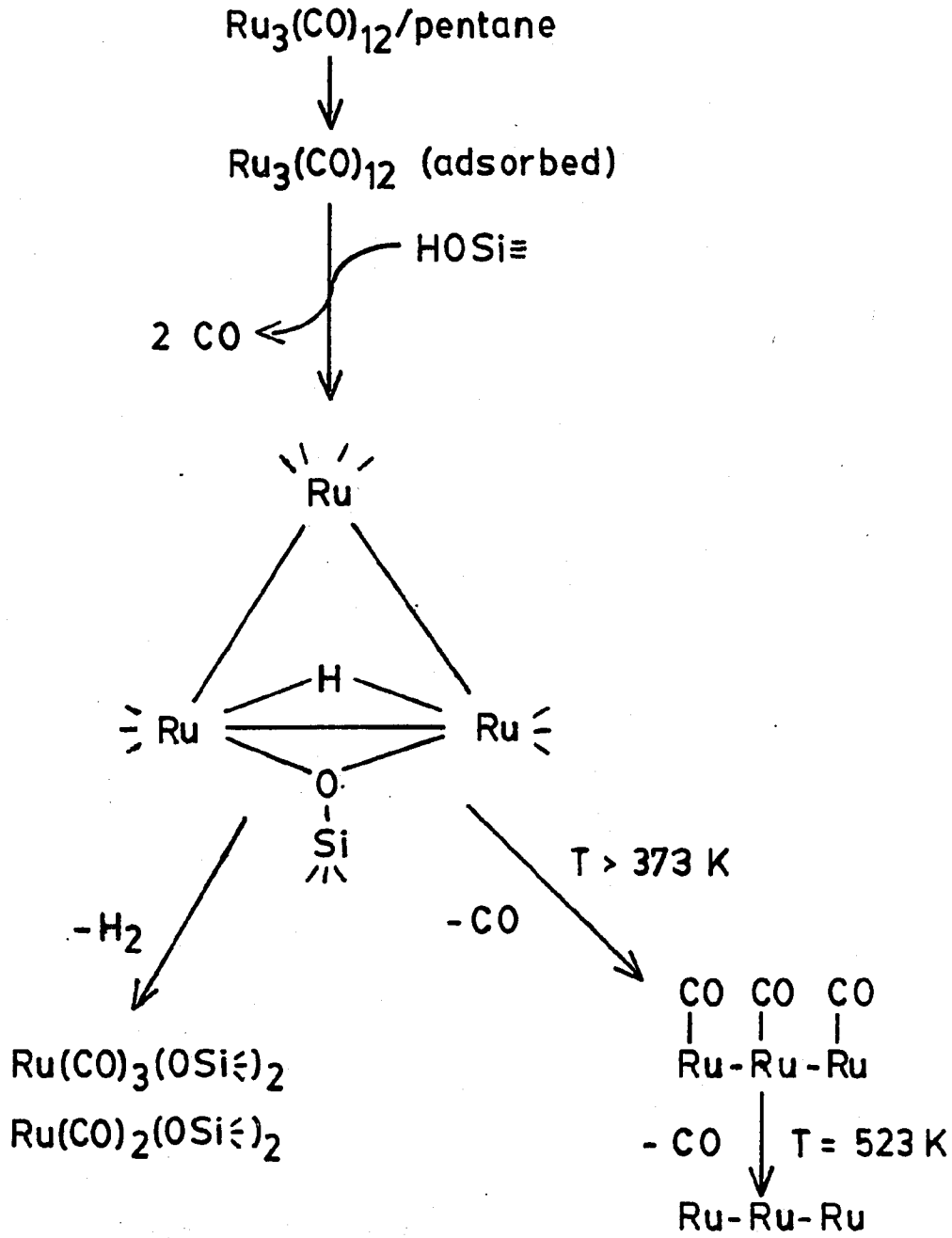

Fig. 9. Interaction of the ruthenium trimer with silica, proposed by Basset and coworkers (86)

Catalytic activations of carbon monoxide on metal surfaces and metal cystallites have been reviewed by Vannice (89). He notes significant differences between the IR spectra of CO adsorbed on reduced and oxidized Ru cystallites. Brown and Gonzalez (90) found that the major CO band on a reduced 6% Ru/SiO_2 catalyst was at 2030 cm^{-1} whereas a strong 2080 cm^{-1} band and two medium intensity bands at 2135 and 2030 cm^{-1} were observed on the oxidized sample. The 2080 cm^{-1} band was assigned to linearly adsorbed CO on Ru, and the last two bands were assigned to CO adsorbed on a surface oxide and on Ru atoms perturbed by neighboring oxygen atoms, respectively. Bradshaw (91) noted that the collective carbon monoxide stretching mode in the CO/Ru(001) system varied between 1981 and 2061 cm^{-1} as a function of the CO coverage and postulates the equivalency of this mode to the A_2'' vibration of the ruthenium cluster (Table I).

1.5. PHOTOCHEMICAL STUDIES OF HYBRID CATALYSTS

In the preceding discussion it was pointed out that hybrid catalysis may offer the advantage of controlling the supported catalyst on a molecular level. However, part of this advantage is lost in the process of thermally activating the transition metal complex; since many of its bond energies are of comparable magnitude, raising the vibrational energy content of the entire complex may lead to a

Compound	cm^{-1}	ref.
$Ru_3(CO)_{12}$[a]	2061 vs, 2031 s, 2012 m	t.w.
$Ru_3(CO)_{12}$[b]	2060 vs, 2030 s, 2010 m	(85)
$Ru(CO)_5$[a]	2035 s, 2000 vs	t.w.
$Ru(CO)_5$[b]	2035 s, 1999 vs	(53)
$Os_3(CO)_{12}$[a]	2070 vs, 2037 vs, 2017 m	(53)
$Os(CO)_5$[b]	2034 s. 1991 vs	(53)
$Ru_3(CO)_{12}/SiO_2$	2075 sh, 2063 s, 2031 s, 2000 sh	(85)
$Ru_3(CO)_{12}/SiO_2$	2063 s, 2032 s, 2018 sh	(86)
$Ru(CO)_4/SiO_2$	2060 s, 1990 m, 1945 m	(85)
$Ru_3(CO)_{12}$/PVG	2064 s, 2035 m, 2018 sh	t.w.
$HRu_3(CO)_{10}(OSi\equiv)$	2109 w, 2078 s, 1069 s, 2034 m,br 2017 sh, 1999 sh,	t.w.

a = isooctane, b = heptane

Table I. IR bands of ruthenium and osmium complexes

multitude of possible reactions. On the other hand, photoactivation and/or photosensitized catalysis of hybrid systems offers potentially higher selectivity, yet it has received limited attention even though the primary photochemical events of a complex interacting with a support material may differ from those observed in fluid solution. Some studies have appeared suggesting that photolysis is not only a means to realizing the advantages of hybrid systems, but also an opportunity to initiate reactions not found in homogeneous solution (59,92,93,94).

In solution, $Cr(CO)_6$ does not catalyze 1,3-hydrogen shifts or cis-trans isomerization of 1,3-dienes (95). However, photolysis of chromium carbonyl supported on porous Vycor glass (PVG) leads to an adsorbed species which catalyzes the isomerization of 1,3-dienes with an activity comparable to that found for tungsten carbonyl (96). Jackson and Trusheim (97) investigated the photochemistry of silica gel-supported $Fe(CO)_5$. Their results indicate a formation of $Fe_3(CO)_{12}$ rather than $Fe_2(CO)_9$, which is observed upon photolysis of $Fe(CO)_5$ in non-coordinating solvents (46,97). Wrighton and coworkers (93) detailed the photochemical behavior of $Ru(CO)_4L$ and $Ru_3(CO)_9L_3$ confined to the surface of silica gel. The results illustrate the low surface mobility of the transition metal monomers of cluster fragments since photodeclusterification of the immobilized substituted trimer was reversible. The steric effects of a series of phosphorus ligands in

$M_3(CO)_9(PR_3)_3$ clusters, where PR_3 represents a phosphorous donor ligand and M represents Fe or Ru, on the photocatalyzed isomerization of 1-pentene have been examined by Wrighton's group (66). It was noted that alkene complexes of Ru are much more labile than the corresponding complexes with Fe which themselves are labile at 25°C. It was also found that the nature of the phosphor donor can significantly alter the chemistry of the photochemical system. Bulky ligands favoured the formation of cis-2-pentene over trans-2-pentene.

Most of the reports discussed above describe the photochemistry of hybrid systems in qualitative terms. In part this is due to the difficulties encountered in applying fast reaction techniques to probe photogenerated intermediates adsorbed onto opaque supports (98,99,100). Unfortunately the opacity of materials such as silica gel (amorphous silica) or alumina (Al_2O_3), both available and used in form of high surface area powders, complicates the application of absorption spectroscopy and flash photolysis since these techniques are based on the transmission of light. Quantification of thermal and photochemical reactions are further hindered by the high degree to which photolyzing and analyzing light beams are scattered by a powdered support. It appears that transparency to light is a helpful property for studying model systems in hybrid catalysis. A support material that satisfies this criterion is Corning's code 7930 porous Vycor glass.

1.6. POROUS VYCOR GLASS

Porous Vycor glass (PVG) is a surface-hydroxylated, transparent (wavelength > 230 nm) glass which has a myriad of precisely controlled pores or cavities interconnected throughout the glass in a random three-dimensional array. PVG is available in the form of plates of various thicknesses, rods, spheres, and powders. It is composed of 96% SiO_2, 3% B_2O_3, and 1% NaO_2 and Al_2O_3 and can be prepared with pore sizes comparable to those of commercially available silica gels (101,102,103). Silica gels are porous materials, formed by gelling a silica sol (102). However, the size and number of these pores determine the opacity of a material and pore dimensions in excess of 100 Å seriously impede the use of UV-visible spectroscopy as an analytical tool. Silica gel and PVG possess many similarities (101,102,103) such as the presence of surface hydroxyls (Si-OH), referred to as silanol groups. These silanol groups are slightly acidic (104) and undergo cation-exchange with ions in fluid solution (105,106) is observed; e.g.:

$$\text{Si-OH} + \text{Na}^+ \longrightarrow \text{Si-O}^-\text{Na}^+ + \text{H}^+ \qquad (1)$$

The number of hydroxyl groups per unit area, termed the silanol number, depends on the extent of hydration and previous thermal treatment (107). In spite of obvious similarities between PVG and silica gel there is evidence

that different types of hydroxyls are present in both materials (108,109).

In addition to chemical factors, there is a growing realization that the reactivity of an adsorbate is influenced by the dimensionality of the support. A transition metal compound dissolved in fluid solution is freely accessable from all directions. However, hybridizing the complex on a rigid support such as silica gel, alumina, or magnesium oxide limits its geometric accessibility. The imposed restrictions are a function of the particular support material and vary in wide boundaries. Many supports, particularly amorphous materials such as PVG and silica gel, lack the geometric regularity that produces an equivalence of surface sites. These irregular materials are fractals and are characterized by the fractal or Hausdorff dimension which, if smaller than the Euclidian dimensions, can impose constraints that yield reaction pathways not found in fluid solution (110,111). The dimensionalities of PVG and silica gel are quite different; the fractal dimension of silica gel (112) is 2.94±0.02 whereas recent measurements by Jortner and coworkers yield a fractal dimension of 1.72±0.12 for PVG (113). Although latter value may not be of absolute physical significance it suggests that PVG is a highly restrictive environment. As noted by Pfeifer and Avnir (110,111), chemical factors may become secondary to geometric factors in governing a surface-confined molecule's kinematics and modes of interaction. A

distinction between chemical and geometric factors and how these factors are manifested in changes in reactivity patterns, however, awaits further data on the reactivity of molecules confined to surfaces of different dimensionalities.

1.7. POROUS VYCOR GLASS AS A CATALYST SUPPORT

Although the use of silica gel has been far more extensive (114), the advantages of variable cavity structure, mechanical strength, acid resistance, thermal stability, and stability towards regenerative procedures have led to the use of PVG as a catalyst support (115,116). Elemental metals or metal oxides supported on PVG are known to catalyze metathesis, isomerization, polymerization, and hydrogenation reactions (117,118,119,120,121,122,123,124, 125). Transition metals on porous Vycor glass catalyze the cracking, dehydrocyclization, dehydroisomerization, and dealkylation of hydrocarbons and the dehydration of alcohols (123,126,127,128,129,130). PVG impregnated with Pt catalyzes the oxidation of SO_2 and the conversion of auto exhaust (131,132). Although these examples illustrate the viability of using PVG as a catalyst support, surprisingly little information is available on its use with transition metal carbonyls in hybrid catalysis.

Adams, Gardner, and Parkyns utilized PVG as a support for a Raman study of thermally-activated, adsorbed $Mo(CO)_6$

(133). In two patents, Vanderspurt reported that thermally-activated $Re_2(CO)_{10}$ adsorbed onto PVG catalyzed selective hydrogenations. In addition, thermal activation between 323 and 523° K generated a hybrid catalyst which was more active in the conversion of unsaturated aldehydes to unsaturated alcohols than the conventional Re_2O_7 supported on glass (134). A patent issued in Germany indicates that $Fe(CO)_5$, adsorbed onto porous Vycor beads, is thermally decomposed to elemental iron and iron oxide (135).

This thesis work is intended to expand our knowledge of PVG-supported metal complexes into the realm of PVG-supported transition metal clusters. Attention will be focused on the thermo- and photochemistry of $Ru_3(CO)_{12}$ dissolved in fluid solution and hybridized on the Vycor glass. Differences in the observed reactivity of the cluster will be explained and compared to the reported chemistry of $Ru_3(CO)_{12}$ supported on silica gel and alumina.

2. EXPERIMENTAL SECTION

2.1. MATERIALS

$Ru_3(CO)_{12}$ was obtained from Pressure Chemical Company and used without further purification since its UV-visible and IR spectra in hexane solution were identical to published spectra. Furthermore, purification by sublimation at 60°C and 10^{-4} torr yielded no change in the spectral properties of the ruthenium cluster. $Ru(CO)_5$ (62), $RuHCl(CO)(PPh_3)_3$ (136), and $Ru_3(CO)_9(PPh_3)_3$ (137,138) were prepared according to literature procedures, and their electronic and infrared spectra agreed with published spectra. Triphenylphosphine, PPh_3, (Pfaltz & Bauer) was purified by recystallization from ethanol. 1-pentene (J. T. Baker) was passed through chromatographic grade alumina (J. T. Baker, lot number 33154) and freshly distilled. Triphenylsilanol, $HOSiPh_3$, (Pfaltz & Bauer, lot number T30905) was recrystallized from benzene. Tris(t-butyl)phosphine, $P(t\text{-}Bu)_3$, (Alpha Ventron Co.) and carbon monoxide, CO, (Linde) were used as received since their reported purity was >99%. IR grade KBr, dried at 120°C for several days, was used for preparing samples for infrared analysis. Spectral grade solvents were used as received. Reagent grade solvents were dried over CaH_2 and distilled immediately prior to use. A special solvent recovery and purification

still was developed to provide dry solvents, distilled and transferred under nitrogen (Figure 10).

Code 7940 porous Vycor glass (PVG) was obtained from the Corning Glass Works and used as either a fine powder (>620 mesh), a coarse powder (420 - 520 mesh), or as transparent plates. Plate PVG was available in form of 25 x 18 x 4 mm samples with rippled surface (chill marks) or as flat, highly transparent plates of dimension 25 x 8 x 1 mm. To insure reproducibility, the glass samples were extracted with water in a 250 ml Soxhlet extractor for 24 hours in order to remove inorganic ions and water soluble cutting oil, introduced during sample preparation from larger plates. PVG was then dried under reduced pressure ($p < 20$ torr) at 60°C and calcined in air at 500°C for >24 hours. Prior to calcination thick PVG pieces had to be thoroughly dehydrated in a vacuum oven since mechanical stress, caused by rapid evaporation of water at 500°C, would otherwise crack most samples. As expected, this problem was not encountered with 1 mm thick glass plates. Calcined PVG samples were stored at 500°C until immediately prior to impregnation with the metal complex. Pieces of 4 mm thickness were equilibrated to room temperature in a desiccator over $CaCl_2$.

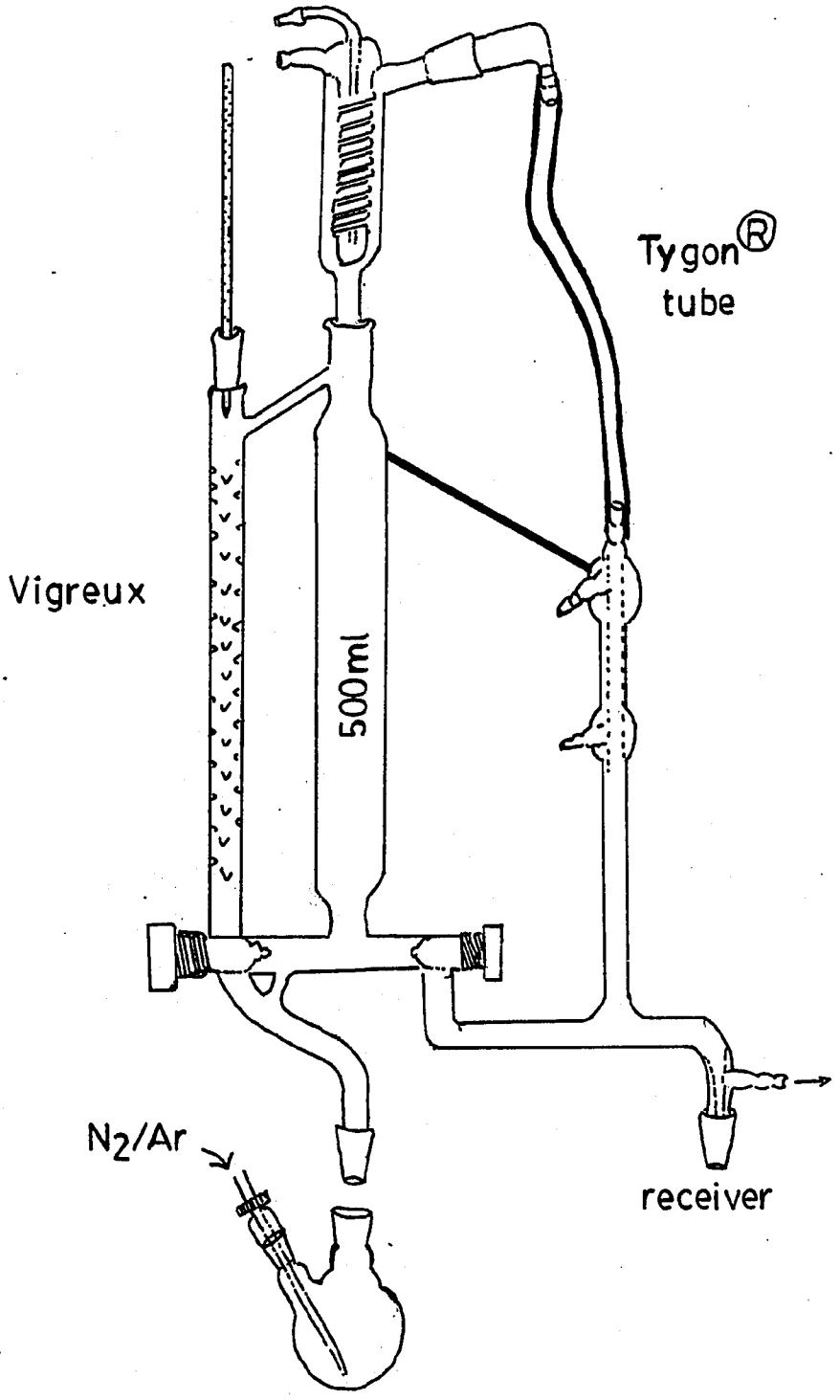

Fig. 10. Solvent purification/recovery still

2.2. IMPREGNATION PROCEDURE

Impregnation was by conventional procedures (139,140,141). Calcined samples, either in powdered or plate form, were placed in 5-40 ml of a 10^{-3} - 10^{-4} M solution of the metal complex in 2,2,4-trimethylpentane or n-pentane for > 12 hours (Figure 11). The number of moles adsorbed was calculated from the change in optical density of the impregnating solution after appropriate corrections for the amount of solvent retained in the pores of the support material (typically 5%) had been made. To minimize the error due to evaporation of solvent, impregnation was performed at low temperature (typically -18°C - 0°C). The solvent incorporated during impregnation was removed at room temperature under flowing N_2 (PVG powder only) or under high vacuum (powder and plate PVG) to better than 99.9% (142). Drying times depended on the boiling point of the particular solvent and were generally minimized to prevent undesirable reactions and standardized for every series of experiments. Reactions of supported metal carbonyls were quantified by measuring the UV-visible spectrum of the surface species. To obtain reproducible readings, the impregnated PVG samples of 4 mm thickness were rigidly mounted with a Teflon holder in a previously described (143) quartz or Pyrex cell. The cell assembly could be connected to a vacuum line and evacuated to < 10^{-3} torr through a ℔ 10/30 joint with a high

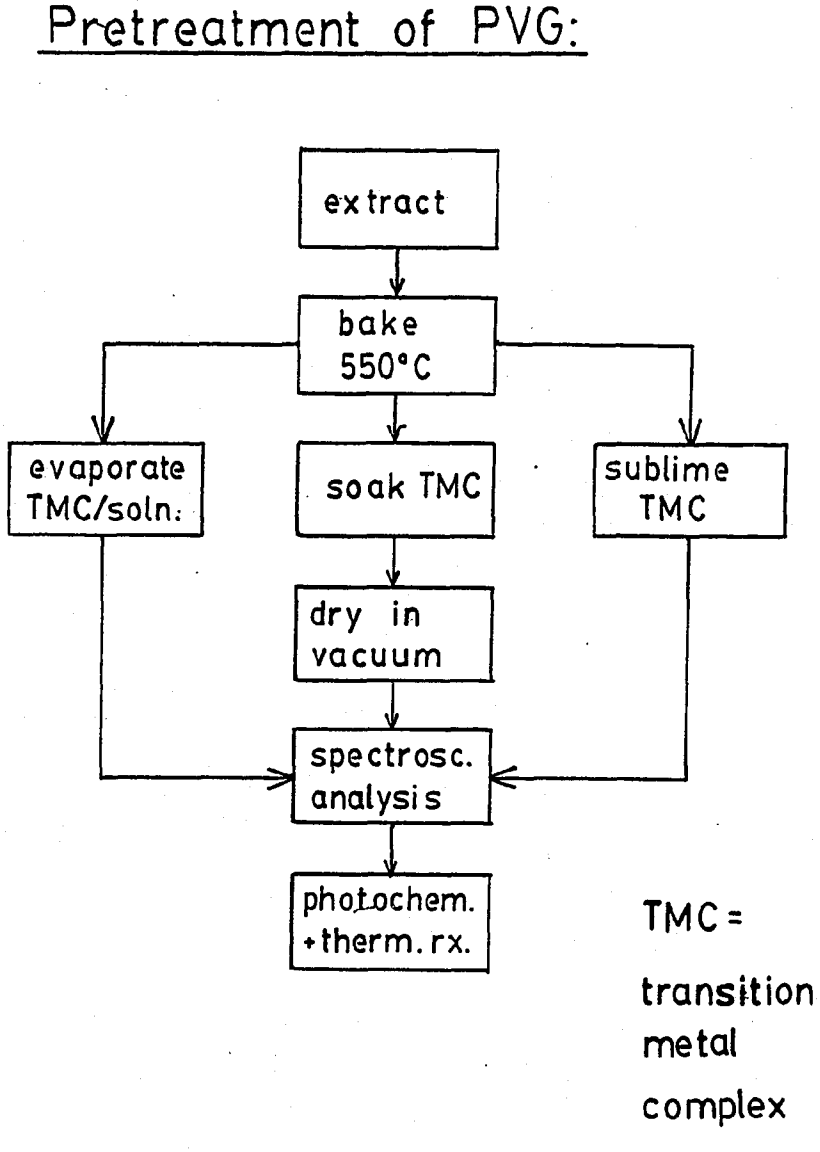

Fig. 11. Impregnation procedure

vacuum valve. In order to avoid contamination, a single vacuum line was dedicated to solvent removal. Final evacuation before photolysis and addition of gases to the sample were performed on a line, mounted of a mobile steel cart. The line consisted of a Welch rotary oil pump, liquid nitrogen trap, a 250 ml gas reservoir, and four greaseless high vacuum valves (Ace Glass) with ℔ 10/30 joints (Figure 12). A pressure of 10^{-4} torr could be reached and was measured with a Leybold-Heraeus Combitron 330 with one Pirani and one Penning gauge (range: 760 to 10^{-6} torr). Gas pressures between 100 and 760 torr were determined with a volume-compensated mercury manometer. To compensate for the optical absorbance of the PVG, a reference piece was mounted in a comparable cell and placed in the reference beam of the spectrometer. Plates of 1 mm thickness were mounted in a modified 1 cm x 1 cm quartz cell. A 14/28 quartz joint was sealed to a standard fluorimetry cell and, as shown in Figure 13, was attached to an upper section with a high vacuum valve and a ℔ 10/30 joint. The latter was then attached to the vacuum line and evacuated ($p \leq 10^{-4}$ torr). A second type of cell top (Figure 14) enabled the introduction of freeze-pump-thaw-degassed liquids into the cell under vacuum. Again a plate of similar thickness was mounted in a 1-cm x 1-cm quartz cell, sealed under nitrogen and placed in the reference beam of the spectrometer. With high surface loadings (i.e. 10^{-6} - 10^{-7} moles of $Ru_3(CO)_{12}$

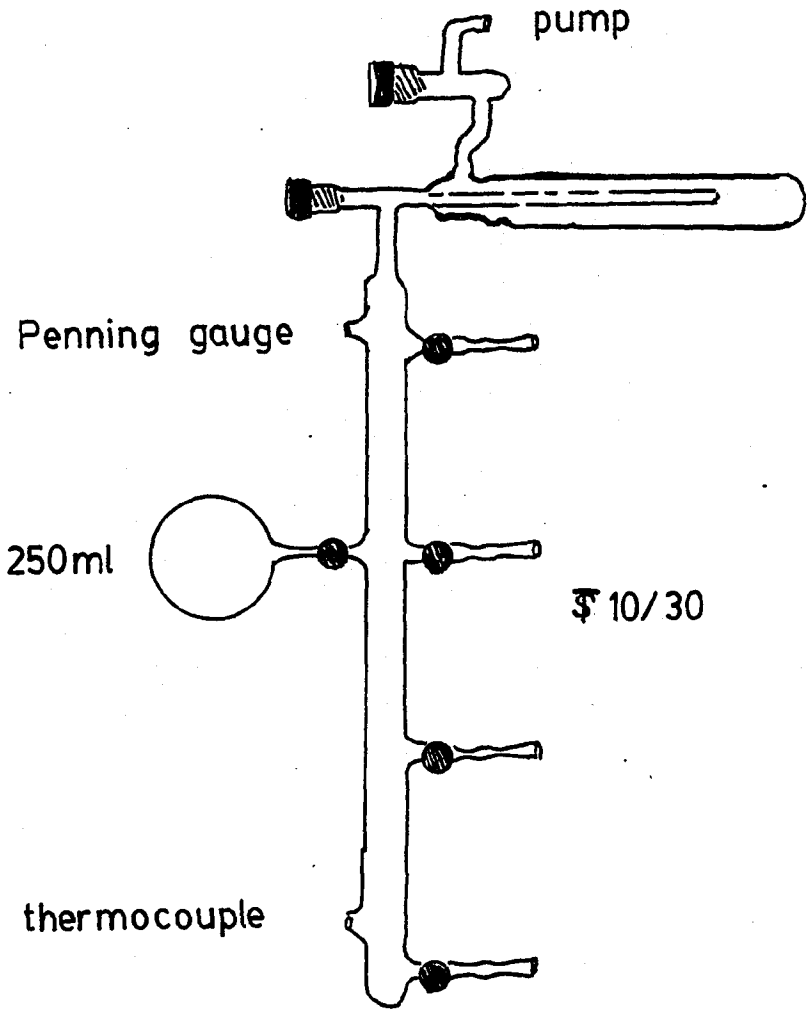

Fig. 12. Vacuum line mounted on a steel cart

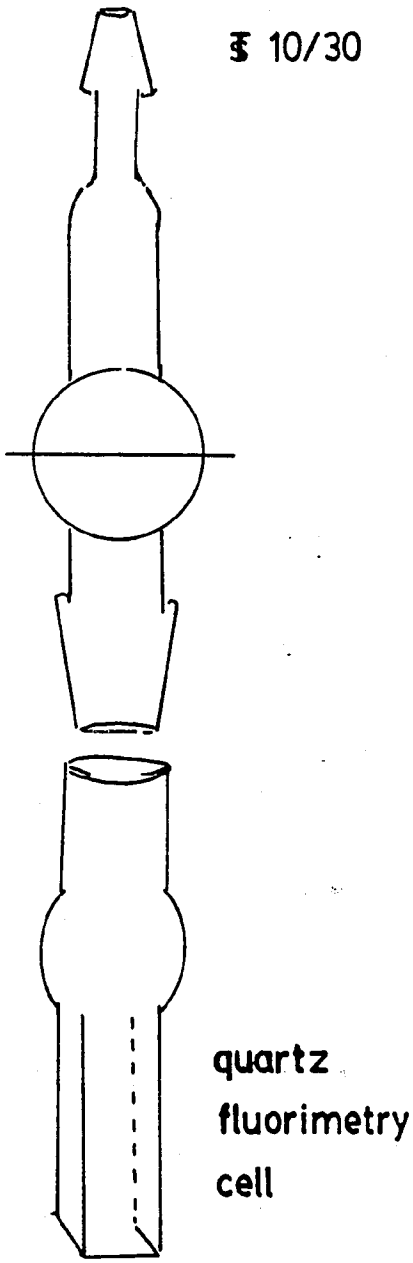

Fig. 13. Quartz cell with regular top

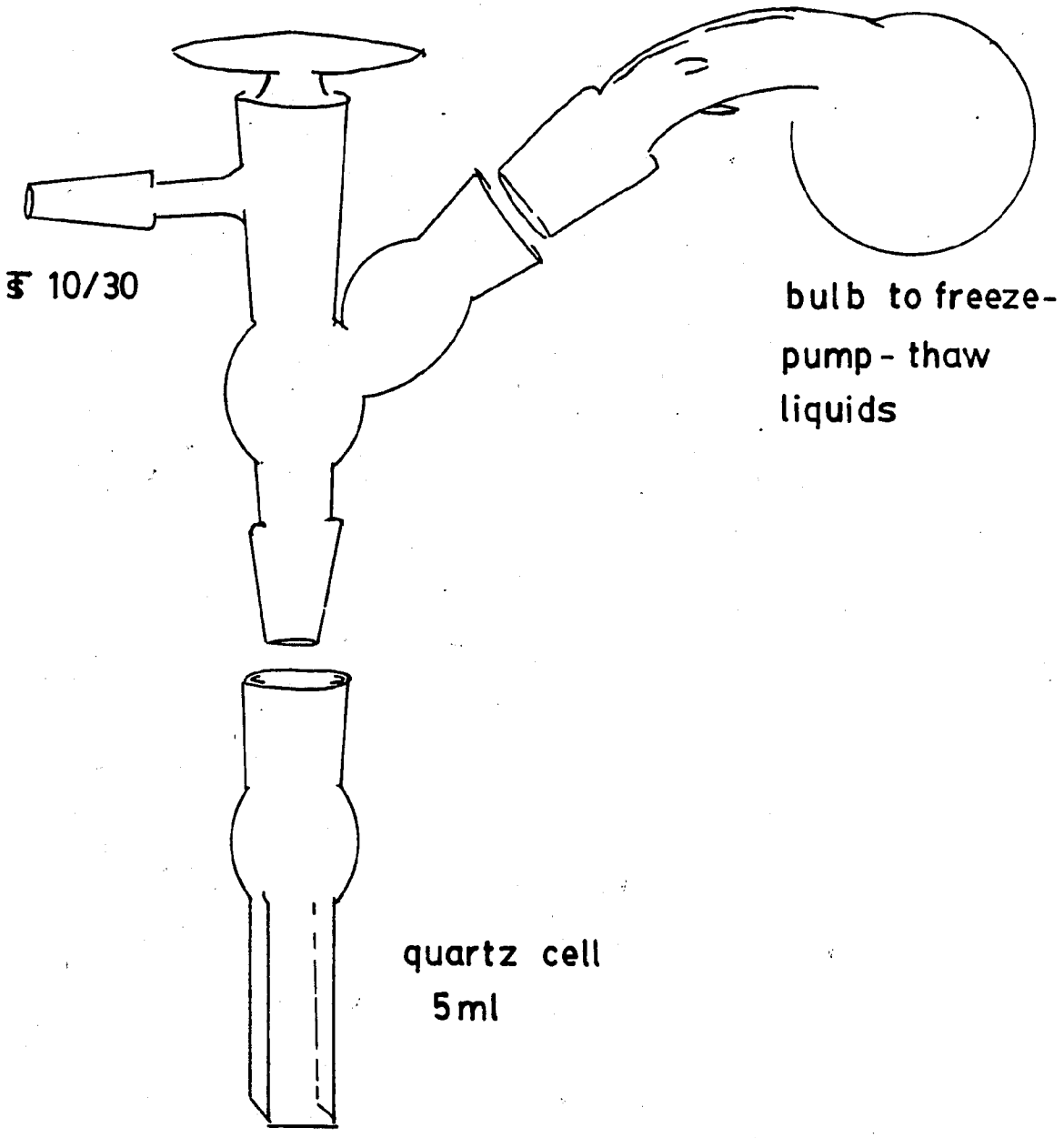

Fig. 14. Quartz cell with special top to freeze-pump-thaw liquids prior to admission

per gram of PVG), the absorbance change was determined by monitoring the ligand field band at 390-nm (molar absorptivity = 7000 $M^{-1}cm^{-1}$), whereas with lower loadings, the change was determined at the intense 238-nm MLCT band (molar absorptivity = 35,000 $M^{-1}cm^{-1}$) (Figures 15 and 16). Dehydrated porous Vycor glass has a large surface area and readily adsorbs moisture from the environment. Under experimental conditions it is therefore difficult to maintain PVG in a dehyrated state. However, since minute differences in water content between sample and reference plate significantly affect the UV spectrum at wavelengths < 250 nm, a special procedure was required to quantify reactions at low surface loadings. For dilute samples, i.e. < 10^{-8} moles/gram, the electronic spectrum was measured on 1 mm plates against a reference blank which had just been treated with pure solvent and dried for time periods identical to those of the actual sample. The uncertainty in the transmittance spectrum of the supported complex, primarily caused by reflection of the analyzing beam, could thus be limited to 20%, introducing a corresponding error into the calculation of moles adsorbed.

In the absence of solvent, impregnation was by sublimation. The calcined PVG sample, either crushed or in plate form, was suspended above the solid complex in an evacuated round bottomed flask (Figure 17). The flask was maintained at 50°C for times between 30 min and 2 hours and

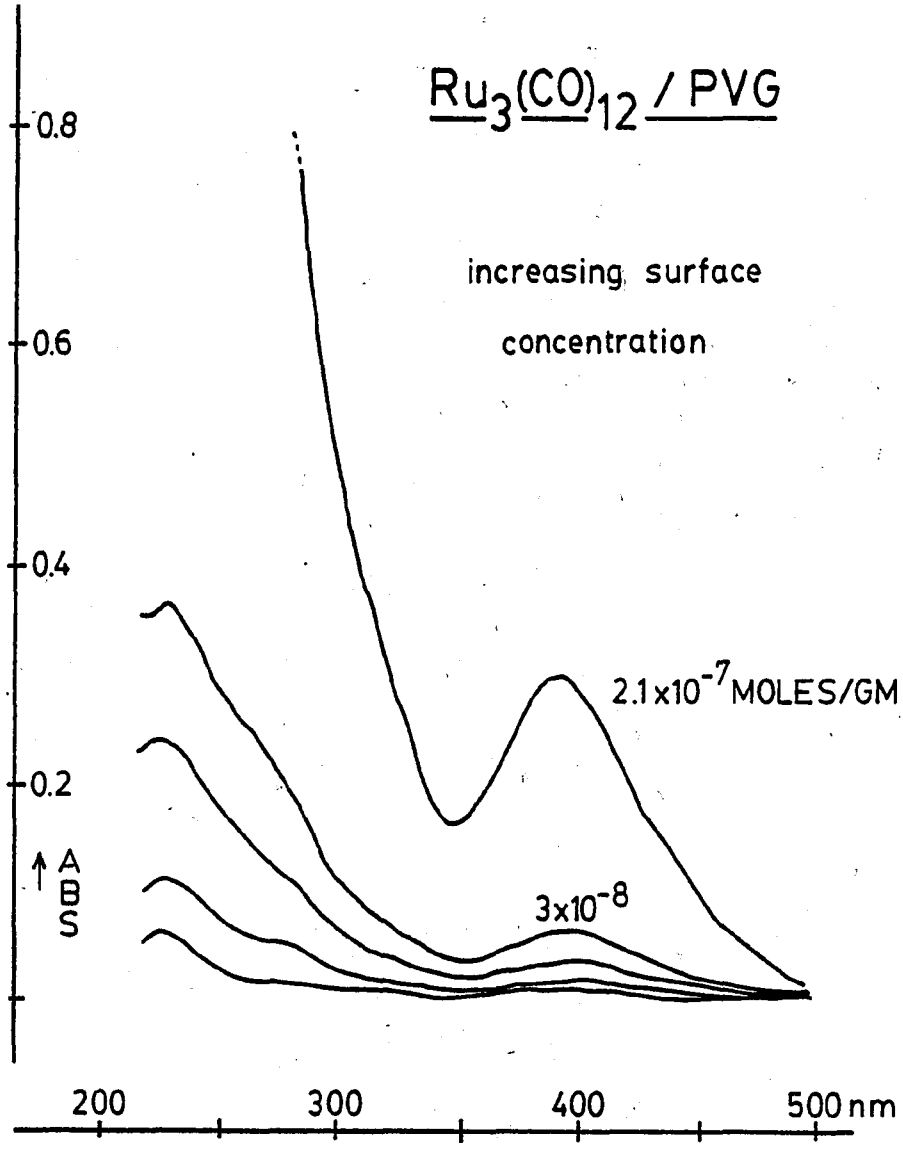

Fig. 15. $Ru_3(CO)_{12}$ supported on PVG at various surface concentrations

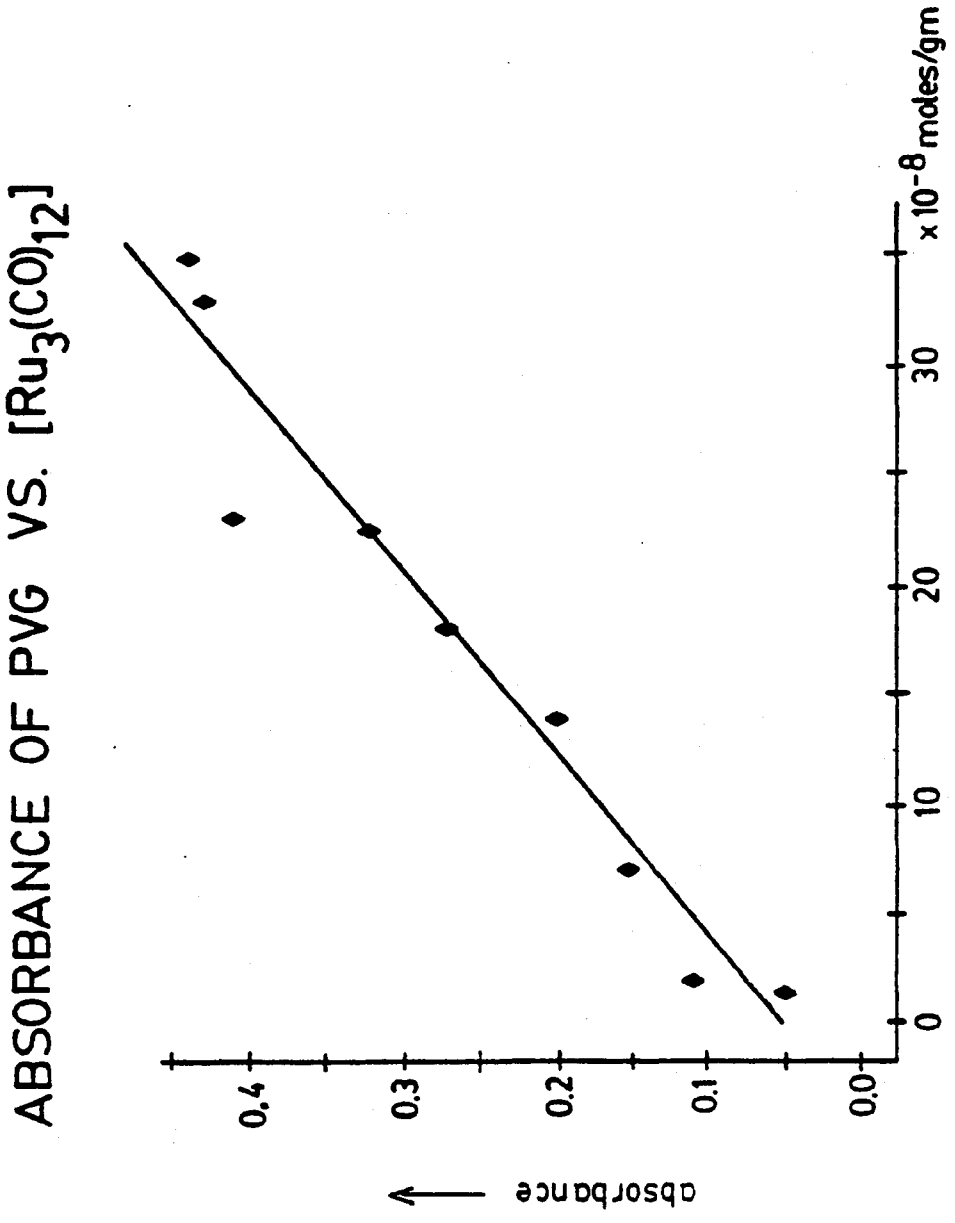

Fig. 16. Plot of the absorbance of impregnated plate PVG vs. the $Ru_3(CO)_{12}$ surface concentration

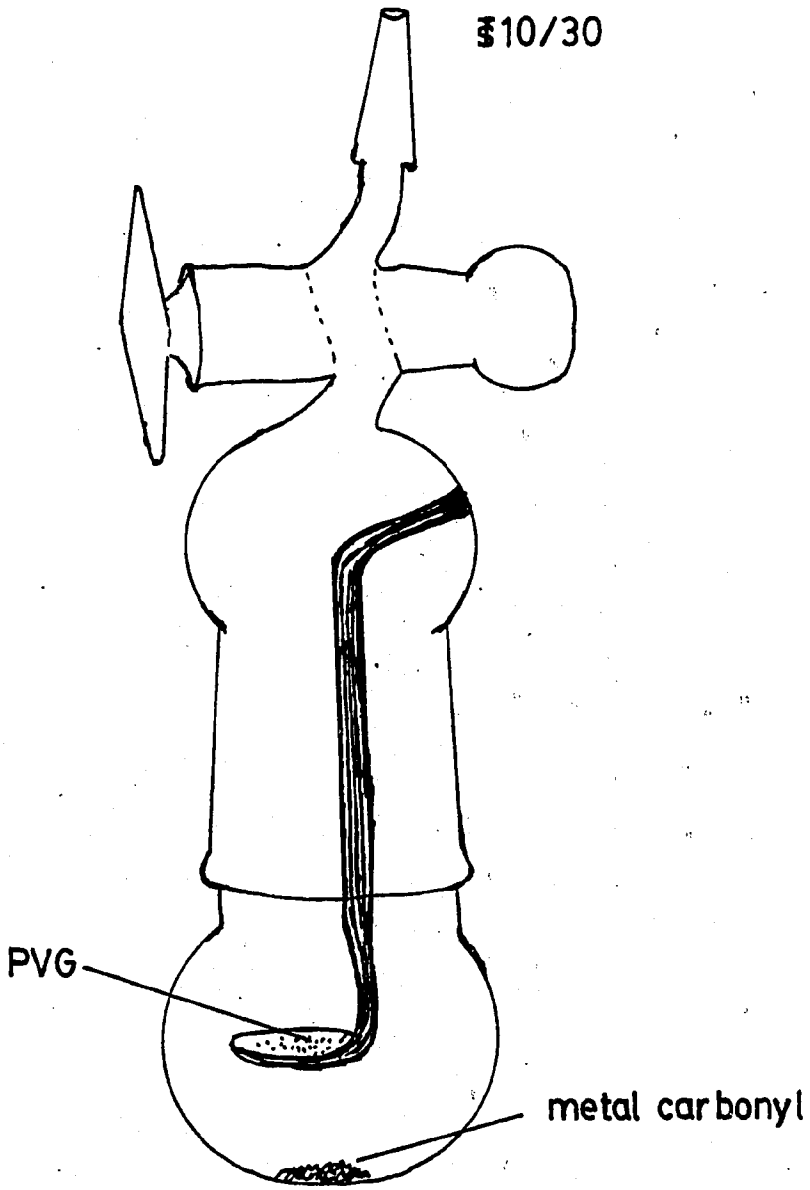

Fig. 17. Sublimation apparatus

the moles adsorbed was determined by spectral comparison with samples impregnated by solution procedures. Spectra recorded at different locations on the same sample plate were all within experimental error. All manipulations of the impregnated samples were under a protective atmosphere of N_2.

2.3. DEUTERATION OF POROUS VYCOR GLASS

The isotopic exchange of surface hydroxyl groups, -OH, of the PVG against deutroxyl groups, -OD, was performed in a stainless steel high pressure reactor (2 liter volume, Parr Instruments). The reactor was charged with 1 gram of powdered PVG, <630 mesh, and 5 ml of D_2O under 100 torr of N_2 and heated to 150°C for 24 hours. The -OH/-OD exchange was only partial and could be quantified by FTIR techniques. In order to achieve complete exchange, the procedure was repeated three times and all transfers were performed under a protective atmosphere of dry N_2. To simplify the -OH/-OD exchange and to be able to perform support impregnation from solution or gas phase under total exclusion air or nitrogen, a special impregnation apparatus was designed. As shown in Figure 18 the apparatus consists of a quartz tube that can be charged with plate or powdered support material and heated under vacuum to > 550°C. A demountable pyrex bulb contains the liquid, degassed by

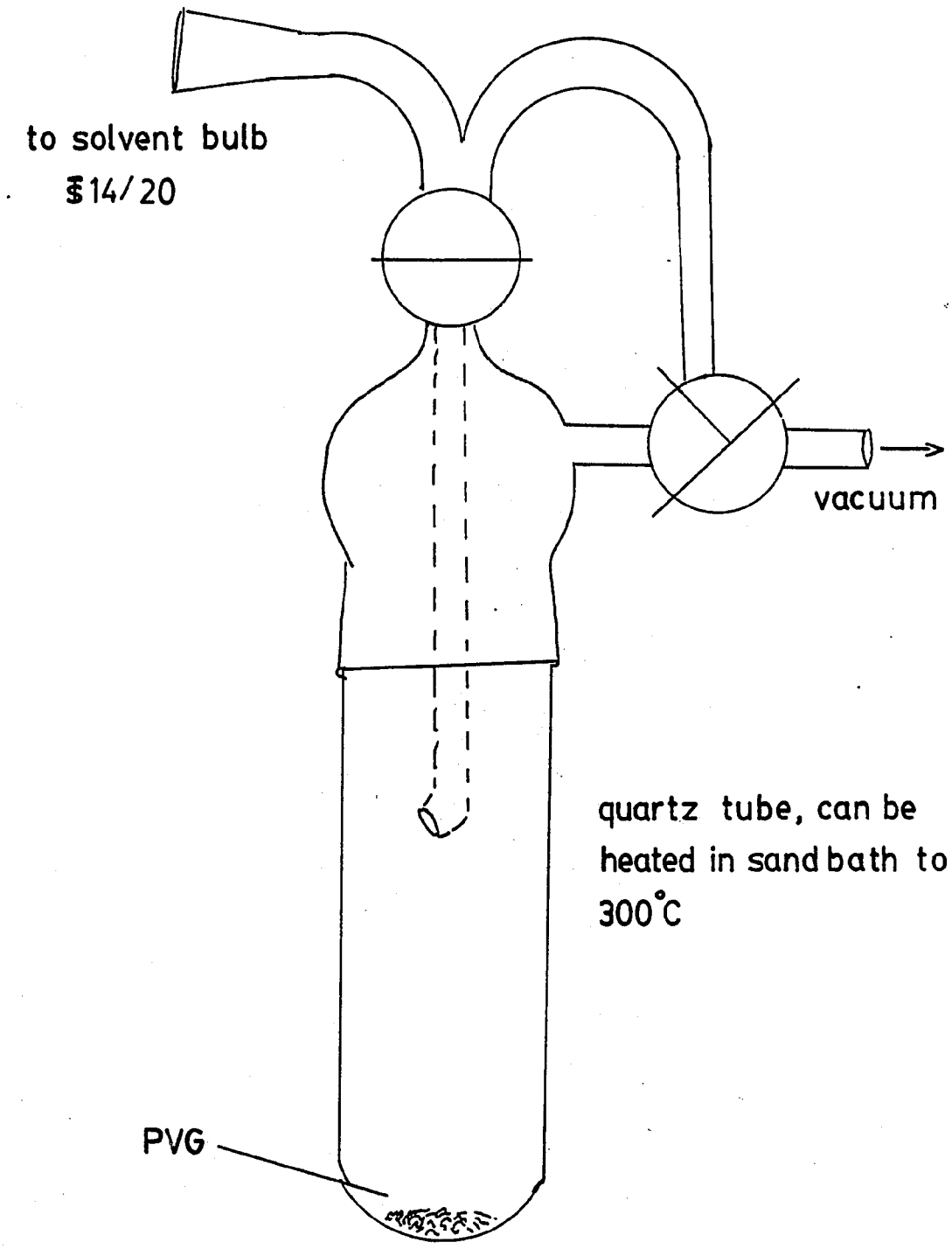

Fig. 18. Vacuum impregnation apparatus

repeated freeze-pump-thaw cycles, before it is transferred into the main chamber under vacuum.

2.4. PHOTOCHEMICAL PROCEDURES

Solutions of transition metal carbonyls were degassed by three freeze-pump-thaw cycles. For experiments where the removal of a gaseous reaction product was required, a stream of Ar or N_2, saturated with the particular solvent, was passed through the solution. Impregnated plates of PVG were rigidly mounted with a Teflon holder in the rectangular quartz or pyrex cells described earlier and evacuated prior to any experiment. Unless otherwise specified, all samples were irradiated in vacuo ($p \leq 10^{-2}$ torr). The plate samples and samples in fluid solution were irradiated in a Rayonet reactor (The Southern New England Ultraviolet Corporation), equipped with 254, 300, or 250 nm bulbs or by using a 350 Watt high pressure mercury arc lamp (Illumination Industries) (Figure 19). Impregnated powdered samples in the vacuum chamber of a Harrick Scientific FTIR diffuse reflectance accessory (DRIFT) were irradiated with a 254 nm penlamp (Analamp, Model 90-0001-01) or a filtered (wavelength $\geq$ 350 nm) high pressure mercury arc lamp (SA Instruments). In each experimental arrangement the excitation intensity was determined by ferrioxalate actinometry (144,145) and ranged from 10^{-6} to 10^{-9} Einstein/sec-cm^2.

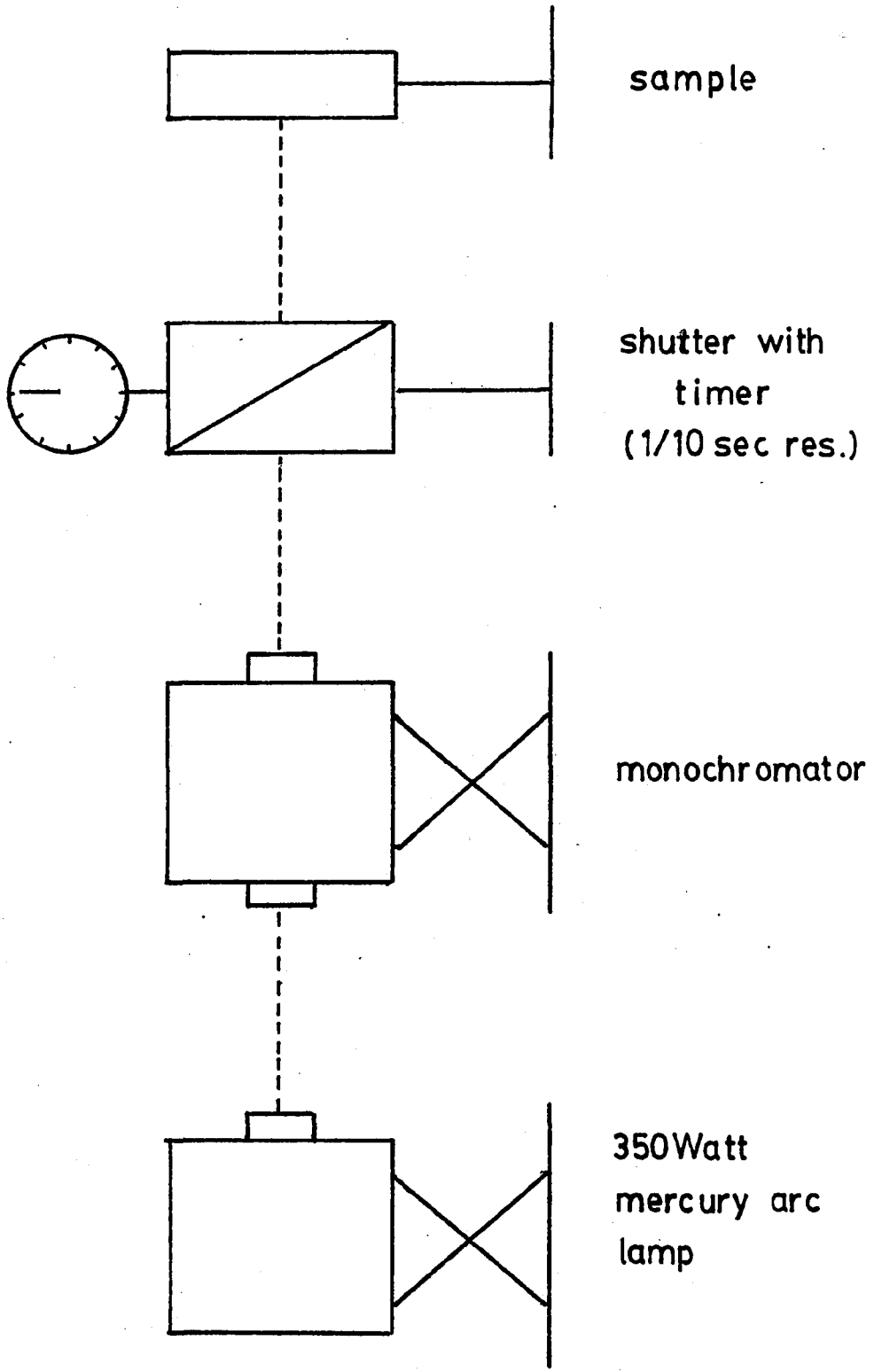

Fig. 19. Photolysis set-up for 350W mercury arc lamp

UV-visible spectra were recorded during photolysis, and gaseous photoproducts were collected with a Toepler pump and quantitatively transferred to a Gow-Mac Model 69-100 gas chromatograph using a sample loop with a volume of 4.7 ml. The GC was equipped with a rhenium-tungsten thermal conductivity detector, a 6' x 1/4" OD stainless steel column, packed with 80/100 mesh 5Å molecular sieve (Supelco). Ar (CP grade, Matheson) or N_2 carrier gas was used. The detector response, calibrated with known pressures of CO, H_2, and CH_4 in the photolysis cell, was linear in the number of moles of gas. In all measurements, except where indicated, the gas chromatographic conditions were an oven temperature of 100°C, a flow rate of 40 ml/min, and a detector current of 150 mA. The detector response was displayed on a Shimadzu R-111 recorder.

Gaseous products of olefin isomerization reactions were collected in a gas tight syringe (Hamilton Company) or directly transferred via a 6-port valve (Supelco, loop size 1 or 5 ml) and analyzed on a Varian Aerograph series 1520 gas chromatograph, equipped with FID detector. A 20' x 1/8" OD stainless steel column containing tricresyl phosphate deposited on 100/120 mesh Chromosorb PAW (Supelco) or a 2m x 1/8" OD stainless steel column with GP 80/100 Carbopack C/0.19% picric acid (Supelco) was used to separate the various olefins. Peaks in the chromatogram were identified by injection of standard samples. Conditions used throughout were a N_2 flow rate of 20 ml/min, an oven

temperature of 100°C (50°C for the Carbopack column), and a detector temperature of 130°C.

2.5. PHYSICAL MEASUREMENTS

UV-visible spectra were recorded on a Cary 14, adapted to accomodate the larger rectangular cells, or a Perkin-Elmer 320 photometer, equipped with a thermostated cell holder for 1 cm^2 cells. The temperature, controlled by a Haake FK 2 temperature bath, was variable from 5 to 90±1°C. UV spectra were recorded relative to blank PVG which had been treated in a manner similar to that of the impregnated sample.

Infrared spectra of solutions or KBr discs were recorded on a polystyrene film calibrated Perkin-Elmer Model 1330 spectrometer with Model 1600 data station or on a Nicolet 5DX FTIR. Diffuse reflectance FTIR spectra of complexes adsorbed onto powdered PVG or silica gel, diluted with KBr (1:30), were recorded on a Nicolet 5DX FTIR equipped with an intensified IR source, an MCT type B detector maintained at 77 K, and a Harrick Scientific diffuse reflectance accessory. Unless otherwise noted the instrument gain was set to the limiting value of 8 and a total of 10 interferograms were averaged for each spectrum. The interferograms were terminated under Happ-Ganzel apodization and converted to Kubelka Munk units for quantitative comparison. All spectra were ratioed against a

background spectrum of blank, calcined PVG, diluted with KBr (1:30). Solution spectra were recorded by using a demountable liquid cell with KBr or CaF_2 windows and a 0.5 mm Teflon spacer.

For nuclear magnetic resonance experiments, a 200 MHz IBM/Bruker Model WP200SY multinuclear FT-NMR spectrometer with liquid helium-cooled magnet was employed. The spectrometer was equipped with a hydrogen-selective 200 MHz probe head and two broad band probes, covering the frequency regions from 8 - 29 and 23 - 84 MHz.

2.6. APPARATUS FOR CATALYSIS EXPERIMENTS

The catalytic reactor system was of modular design and could be modified in accordance with the experimental requirements. The reactor support system was used for continuous flow, pulse, or batch studies under pressures ranging from vacuum to 3500 psi and could be connected to either one of two reactor cells (Figures 20-22).

Cell A:

This cell was constructed for photochemical studies on impregnated plate PVG under high pressure conditions. After evaluation of several published designs for high pressure optical cells (146,147,148,149,150,151) our cell was built from a 2" ID stainless steel 4-way pipe fitting, rated to withstand 14,000 psi. One arm of the fitting had an

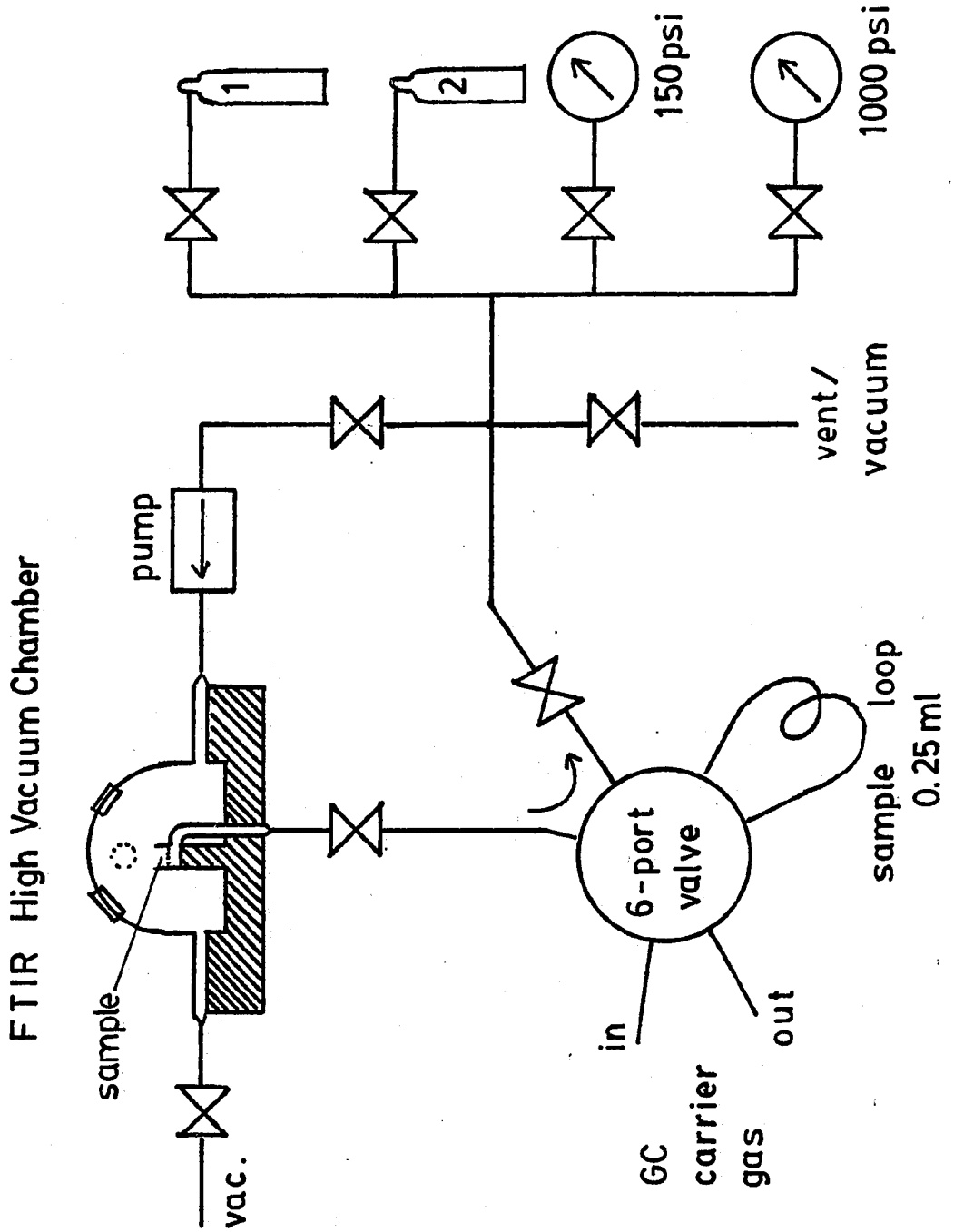

Fig. 20. Catalysis reactor system for circulating gases

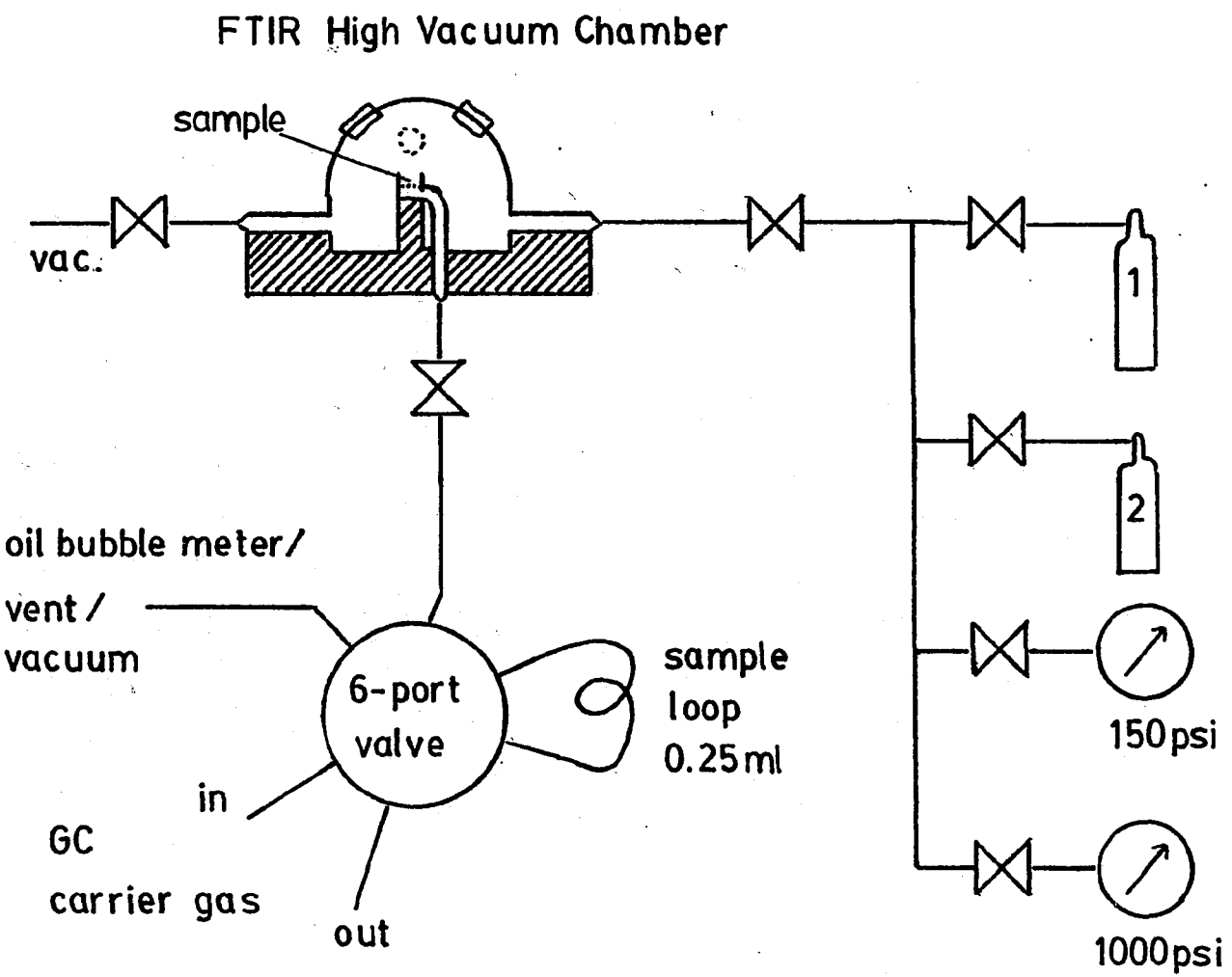

Fig. 21. Catalysis reactor system for batch mode

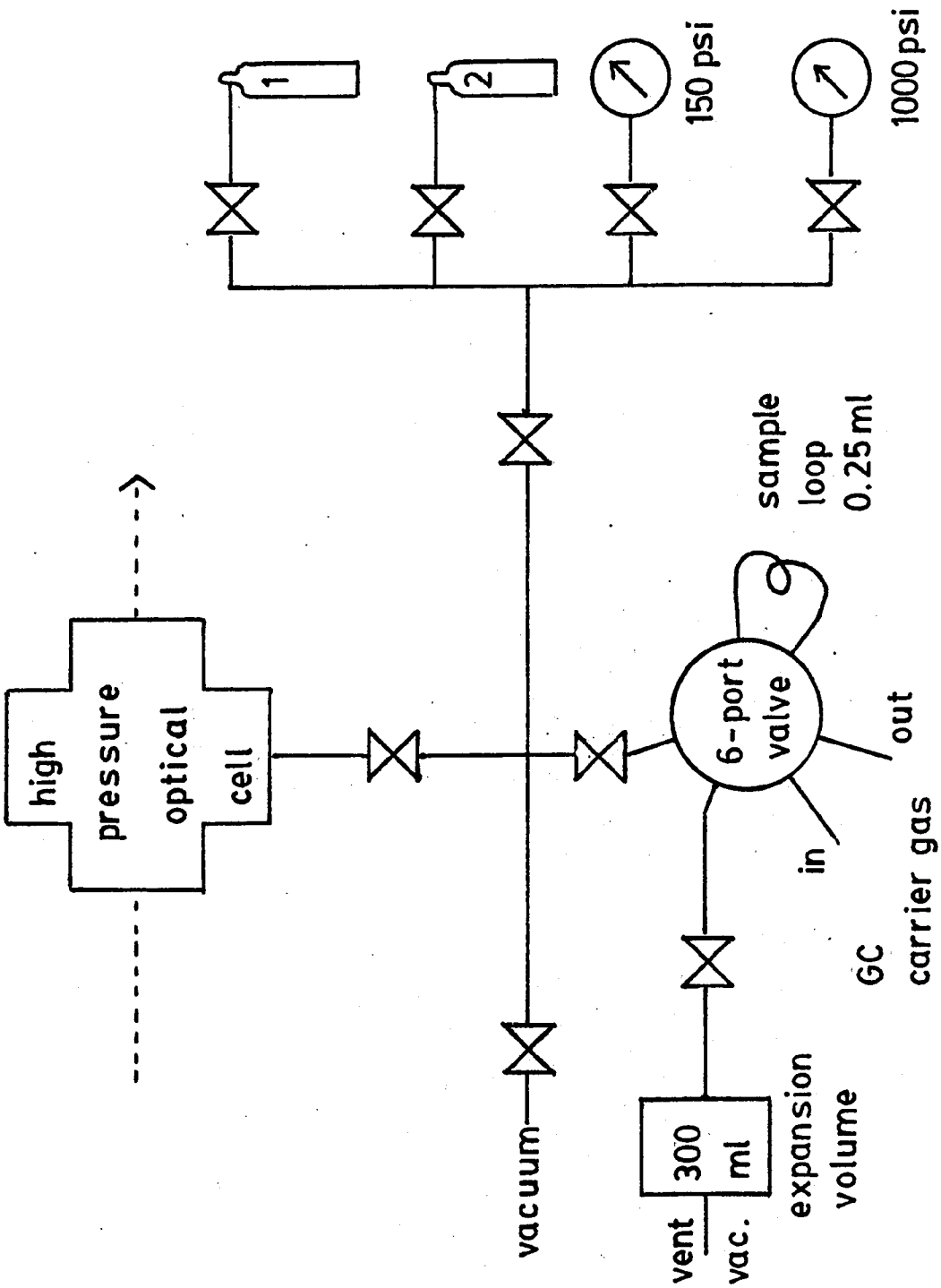

Fig. 22. Catalysis reactor system supporting high-pressure optical cell

adjustable Teflon sample holder for mounting impregnated PVG plates, while the other three arms had removable window plugs containing 0.75" diameter x 0.5" thick quartz windows (Figures 23-25). The window arrangement allowed the impregnated PVG plate to be photolyzed and the reaction progress to be monitored by absorption and emission spectroscopy. The cell body was designed to withstand a pressure of 10^4 psi and was operated under a maximum pressure of 3×10^3 psi. In addition to optical monitoring, the high pressure cell could be attached to the reactor support system, shown in Figure 23, allowing for a periodic sampling of the gas phase and gas chromatographic analysis. For operating pressures $\leq$1.2 atm one of the cell windows could be replaced by a GC septum allowing sampling of the gas phase in the cell by syringe.

CELL B:

This reactor cell was used to monitor changes in the IR spectrum of the supported transition metal complex during a catalytic reaction. The cell consisted of a commercial high vacuum chamber (HVC) supplied by Harrick Scientific that was mounted in the diffuse reflectance attachment of the Nicolet FTIR. The chamber was fitted with one 10x2 mm quartz observation/photolysis window and with two 19x2 mm IR-transparent windows made of KBr or CaF_2. Two connections allowed for addition and removal of gases. A third connection, terminating underneath the sample cup, enabled

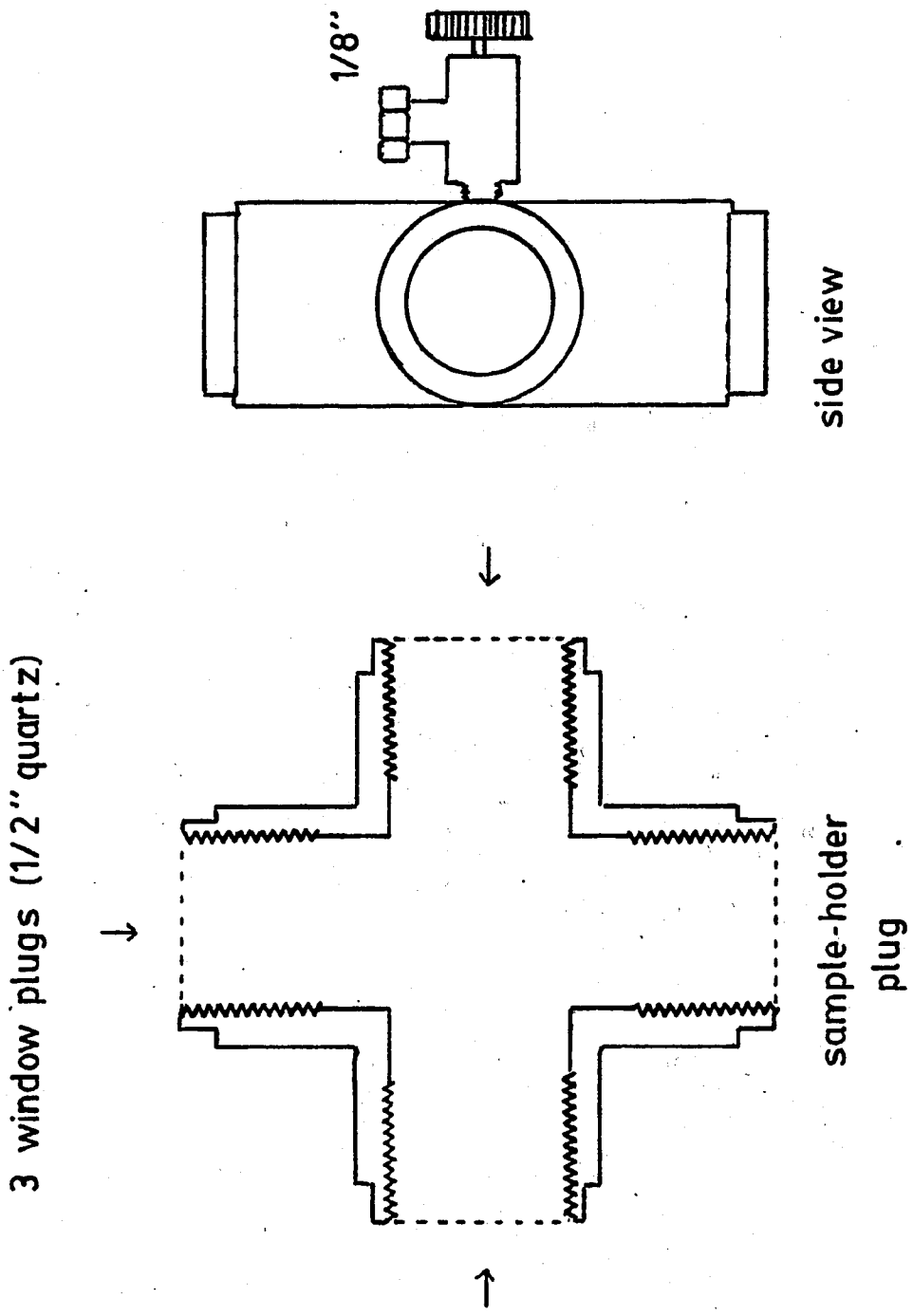

Fig. 23. High-pressure optical cell, front and side view

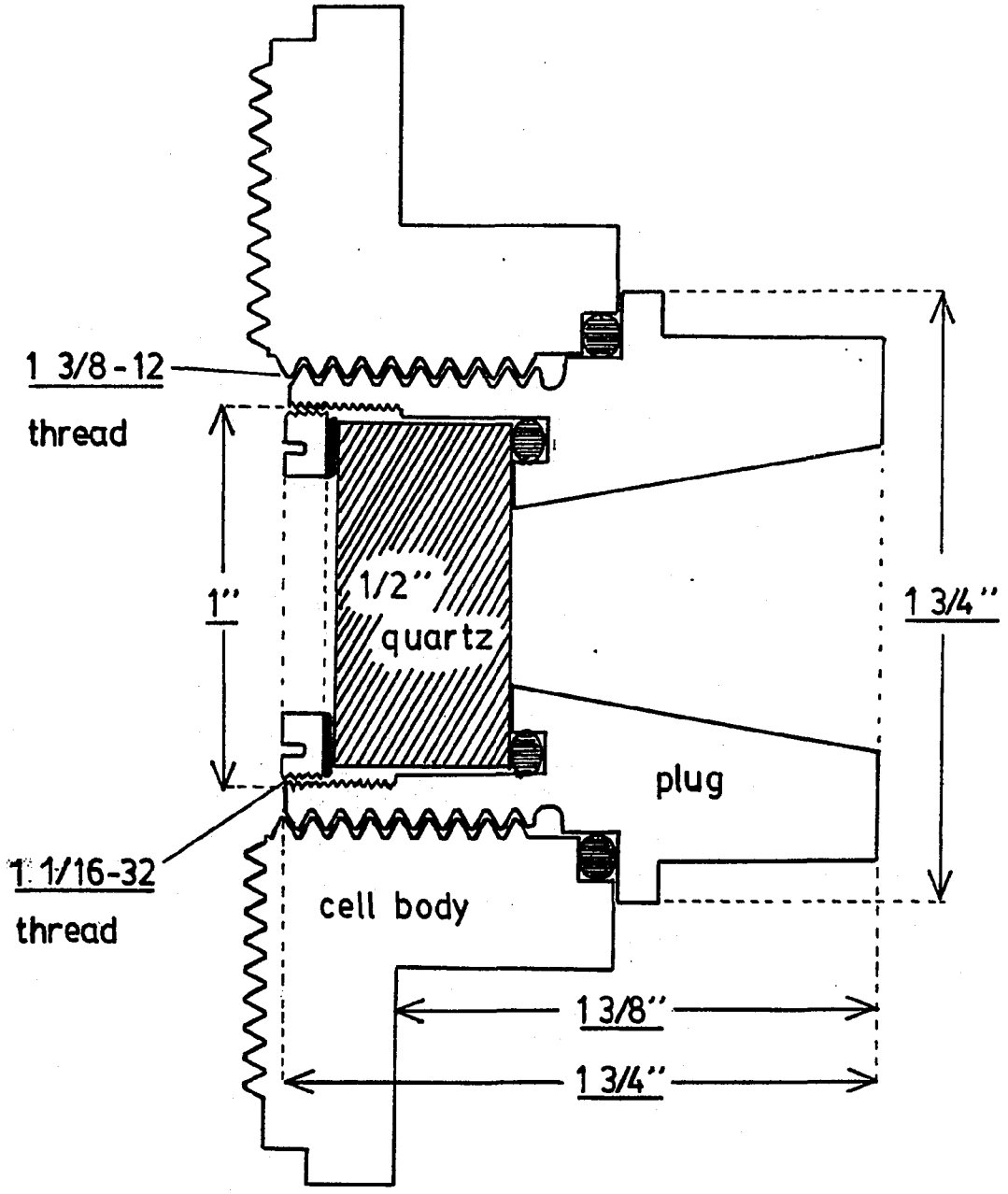

Fig. 24. High-pressure optical cell, window plugs

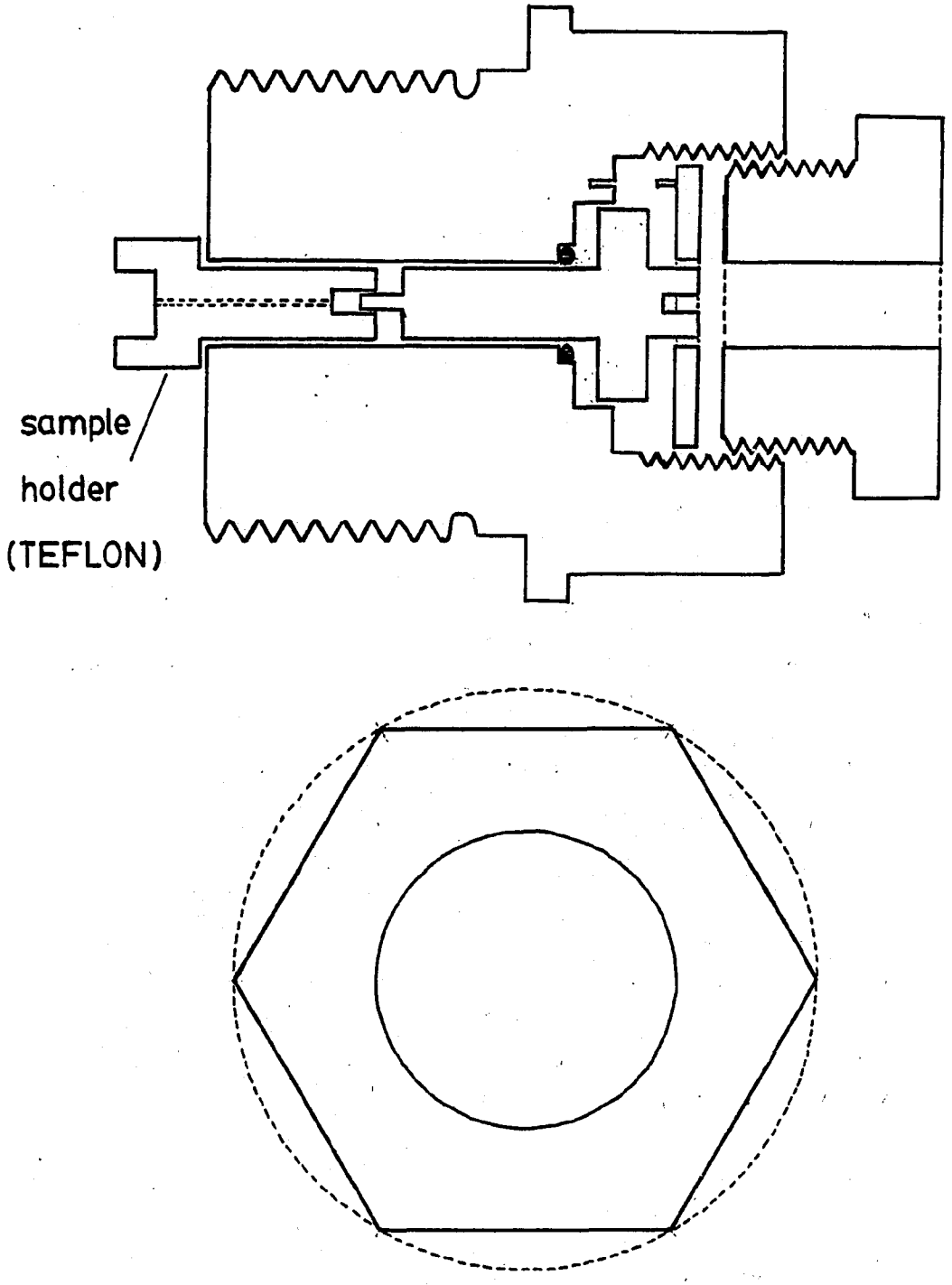

Fig. 25. High-pressure optical cell, sample holder plug

the circulation of gases through the PVG/KBr sample. The cell could therefore be operated in a batch, pulse, or flow mode. The sample cup in the center of the cell accepted up to 300 mg of a PVG/KBr mixture and could be heated to 650°C using a 7 W heater and an Omega Engineering Mode 49 proportional temperature controller. To induce a reaction the sample could also be photolyzed, using one of the light sources described earlier.

3. RESULTS

3.1. CHARACTERIZATION OF PVG

Although the properties of porous Vycor glass have been extensively studied, its application as a support material for transition metal carbonyls is relatively new. Since we intended to use vibrational and optical spectroscopy qualitatively and quantitatively to characterize surface reactions we had to improve our understanding of the chemical and spectral properties of PVG.

UV-visible spectroscopy: Plate PVG is transparent to visible and near UV light; measured against air at 250 nm a 1 mm thick plate shows an absorbance of 0.6 units. Above 350 nm physical sample handling introduces an error of $< \pm 0.003$ absorbance units, measured by repeated removal and reinsertion of the sample into the spectrometer and probably caused by minute changes of the angle between the PVG surface and the direction of the analyzing light beam. This error increases to ± 0.01 in the UV, requiring a careful handling of the sample during quantitative studies and low surface loadings. Below ca. 300 nm the molecular water content of the Vycor glass has a significant impact on the optical spectrum, probably by causing changes in the refractive index. Adsorption of water onto the support results in a decrease of absorbance at 255 nm and a pronounced increase at 220 nm (Figure 26). As a consequence,

differences in absorbance as large as 0.2 units between 220 and 300 nm are observed on comparing two blank pieces of PVG. However, rigorous standardization of the sample and reference pretreatment was found to limit the error to 0.015 absorbance units. No evidence of a permanent change of the UV-visible spectrum due to incorporation of hydrocarbon solvents was found. Drying of plate-PVG containing pentane at room temperature and under reduced pressure for 15 min yields a spectrum identical to the original with an error margin solely due physical handling. However, it is important to use rigorously anhydrous solvents since moisture adsorbed onto the support during impregnation, will desorb at a much lower rate than the hydrocarbon solvent and introduce an experimental error into subsequent measurements. The reverse effect is noticed when PVG with a significant content of bulk water is impregnated in dry pentane. Water is extracted into the solvent and causes a slight increase in the ultra violet absorbance of the pentane or pentane/$Ru_3(CO)_{12}$ solution. FTIR spectra of the support after impregnation show a substantially decreased water band at 3450 cm^{-1} (Figure 27).

IR spectroscopy: Several unsuccessful attempts were undertaken to characterize PVG and adsorbed species by transmission IR. Plate PVG with a thickness > 0.1 mm is opaque to infrared radiation with the exception of windows between 3100 and 2100 cm^{-1} and above 3800 cm^{-1}

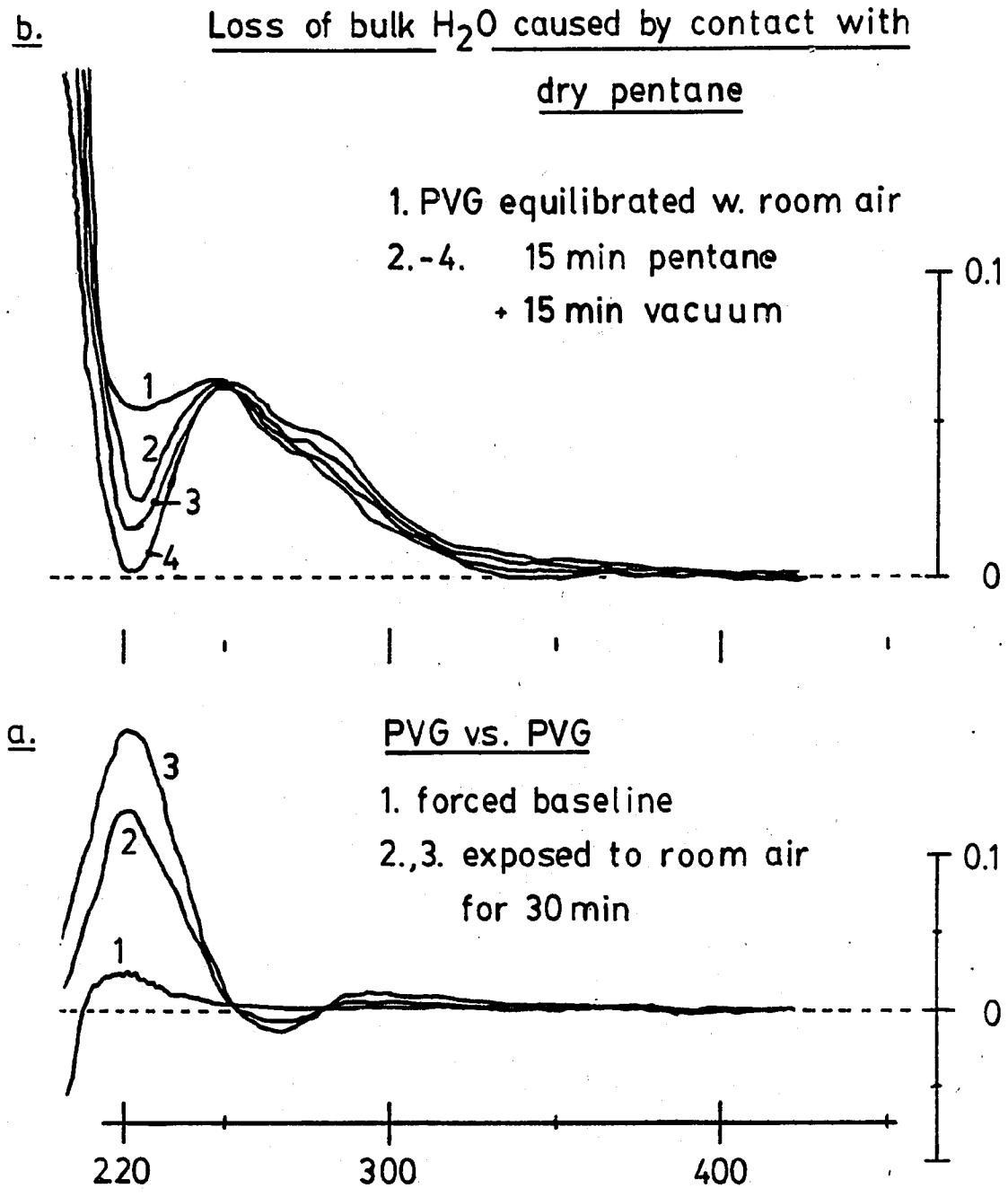

Fig. 26a. UV-vis of PVG upon adsorption of moisture

Fig. 26b. Loss of molecular (bulk) water from PVG through contact with dry n-pentane

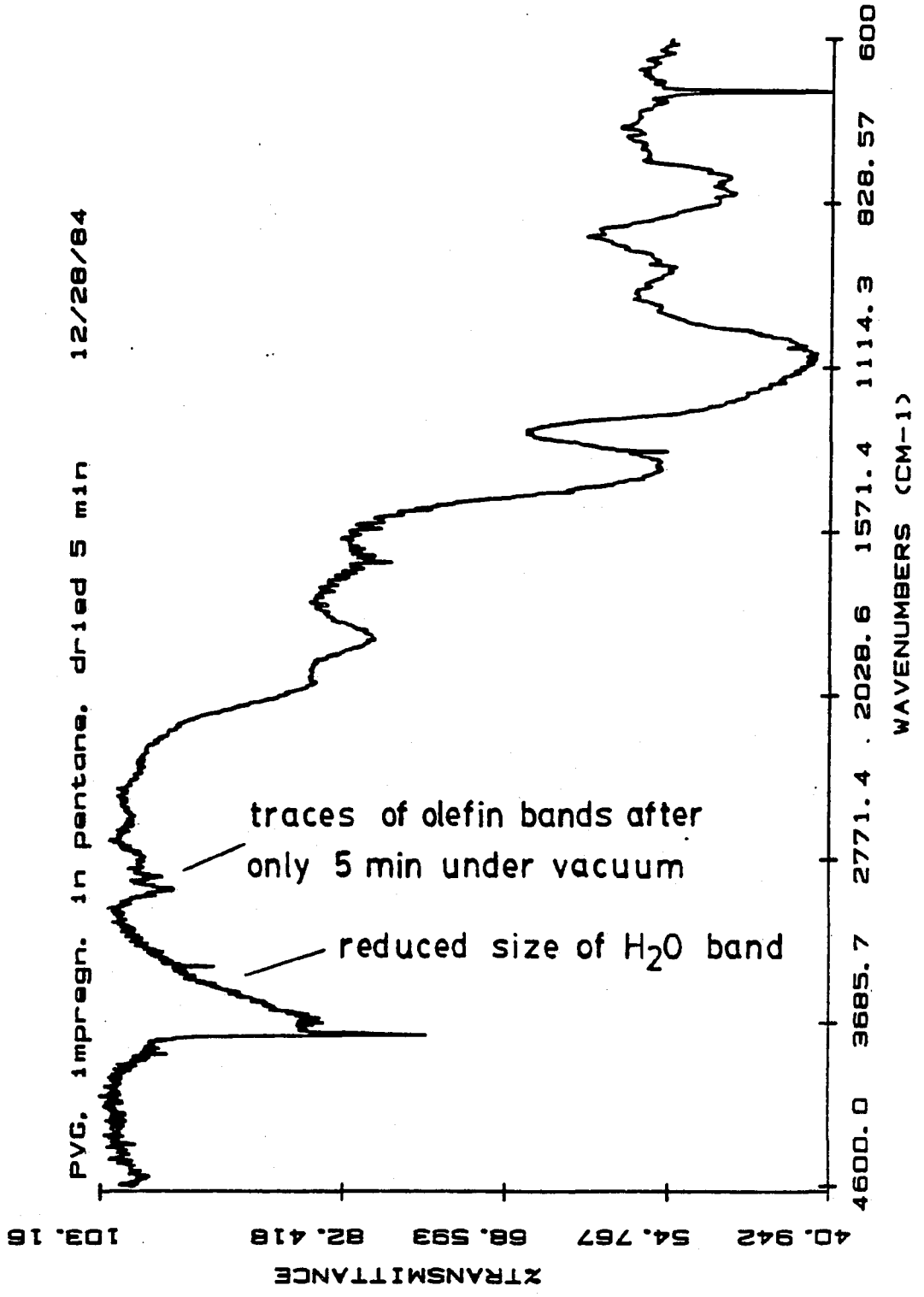

Fig. 27. PVG after impregnation with pentane (IR)

(Figure 28). A mull of powdered PVG in Fluorolube yields a spectrum for wavenumbers > 1400 cm^{-1} but obtained spectra are difficult to reproduce in a quantitive manner. Also, an extraction of the adsorbed metal cluster into the Fluorolube appears possible and a marked decrease in intensity of the sharp band at 3745 cm^{-1} points to an interaction of Fluorolube with surface silanol groups (Figure 29). Since physisorbed metal complexes also interact with these surface functionalities the integrity of the metal complex/PVG adduct may be compromised. The use of Fourier transform diffuse reflectance IR (DRIFT) yields reproducible spectra under pressures of various gases and at temperatures between 25 and 650°C. The spectra show a sharp band at 3745 cm^{-1}, commonly associated with free Si-OH (152,153), a very weak shoulder at 3702 cm^{-1}, associated with hydroxyl groups attached to boron (154), a shoulder at 3650 cm^{-1}, due to associated surface hydroxyls, and a broad band centered at 3450 cm^{-1} associated with bulk water present on the surface of PVG (Figure 30). Upon deuteration, the intensity of the bands between 3650 and 3745 cm^{-1} decreases and a new band at 2760 cm^{-1} with a shoulder at 2740 cm^{-1} appears in the spectrum (Figure 31).

Dehydration of PVG: The loss of water from the surface of PVG was monitored by thermogravimetry between 30 and 800°C and by diffuse reflectance FTIR between 25 and 600°C. Thermogravimetric analysis shows that heating thin

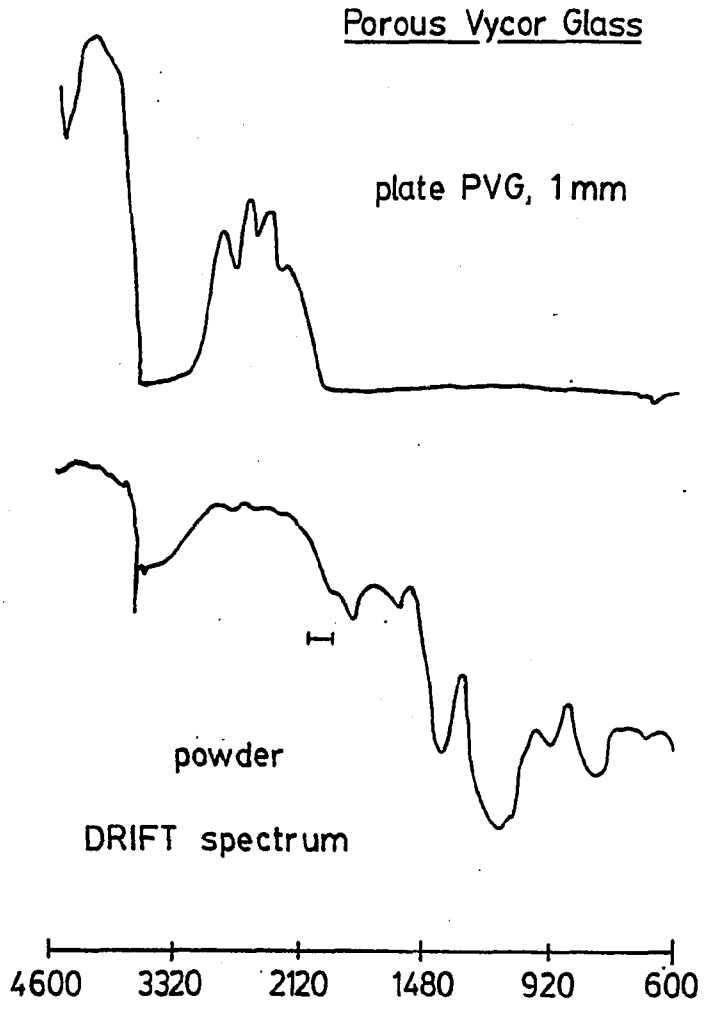

Fig. 28. IR of plate PVG vs. DRIFT of powdered PVG

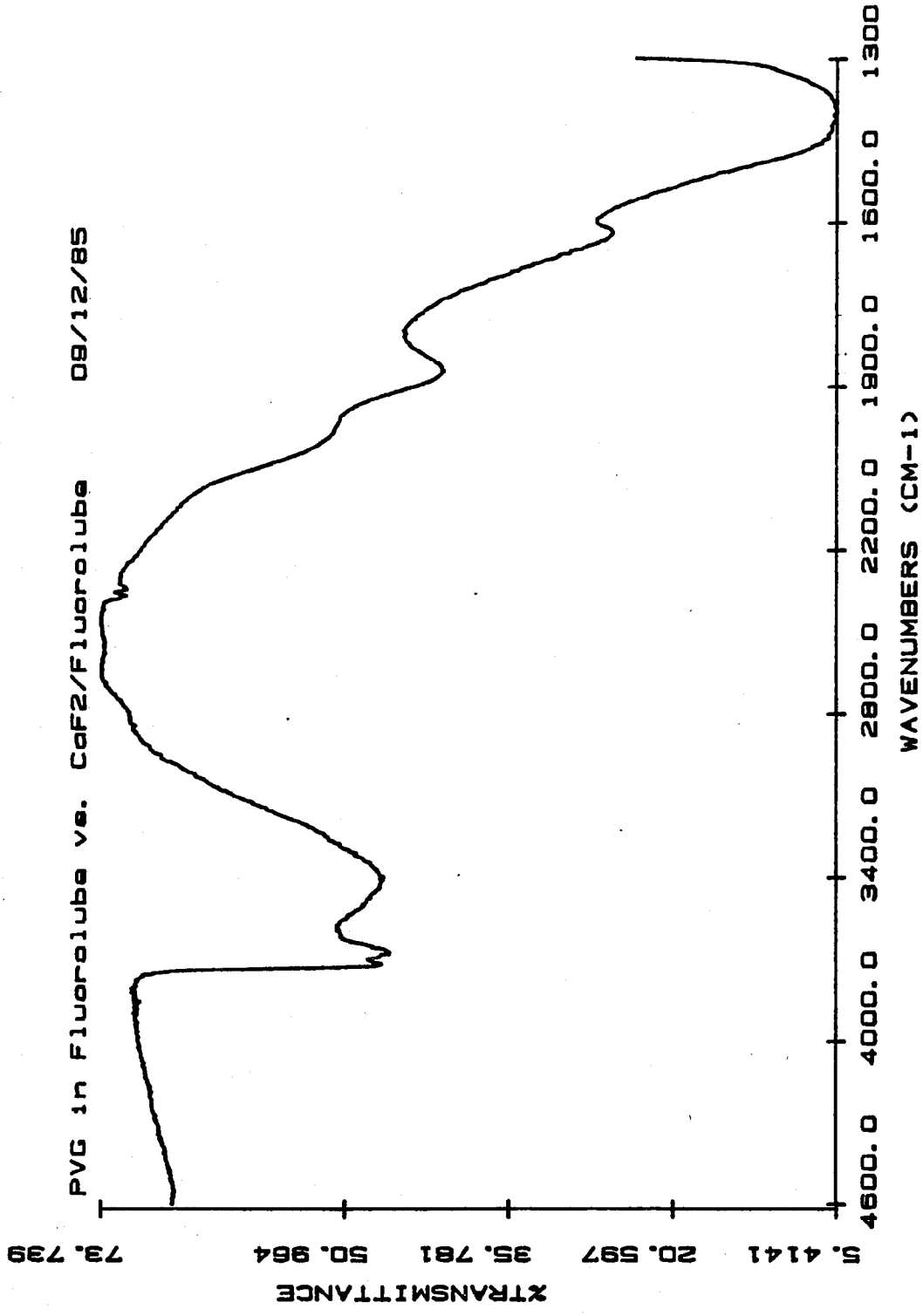

Fig. 29. IR of powdered PVG in Fluorolube

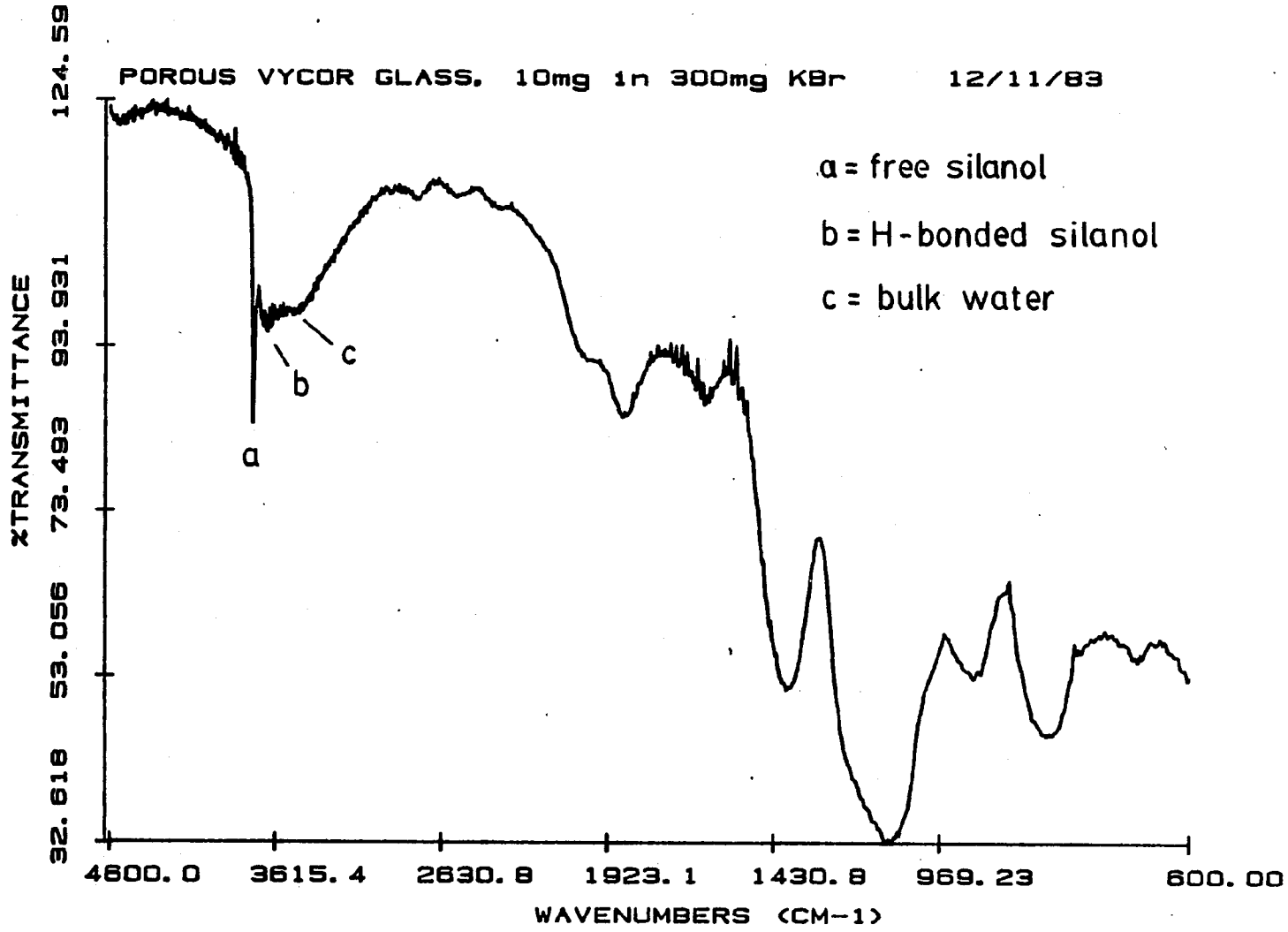

Fig. 30. DRIFT spectrum of powdered PVG

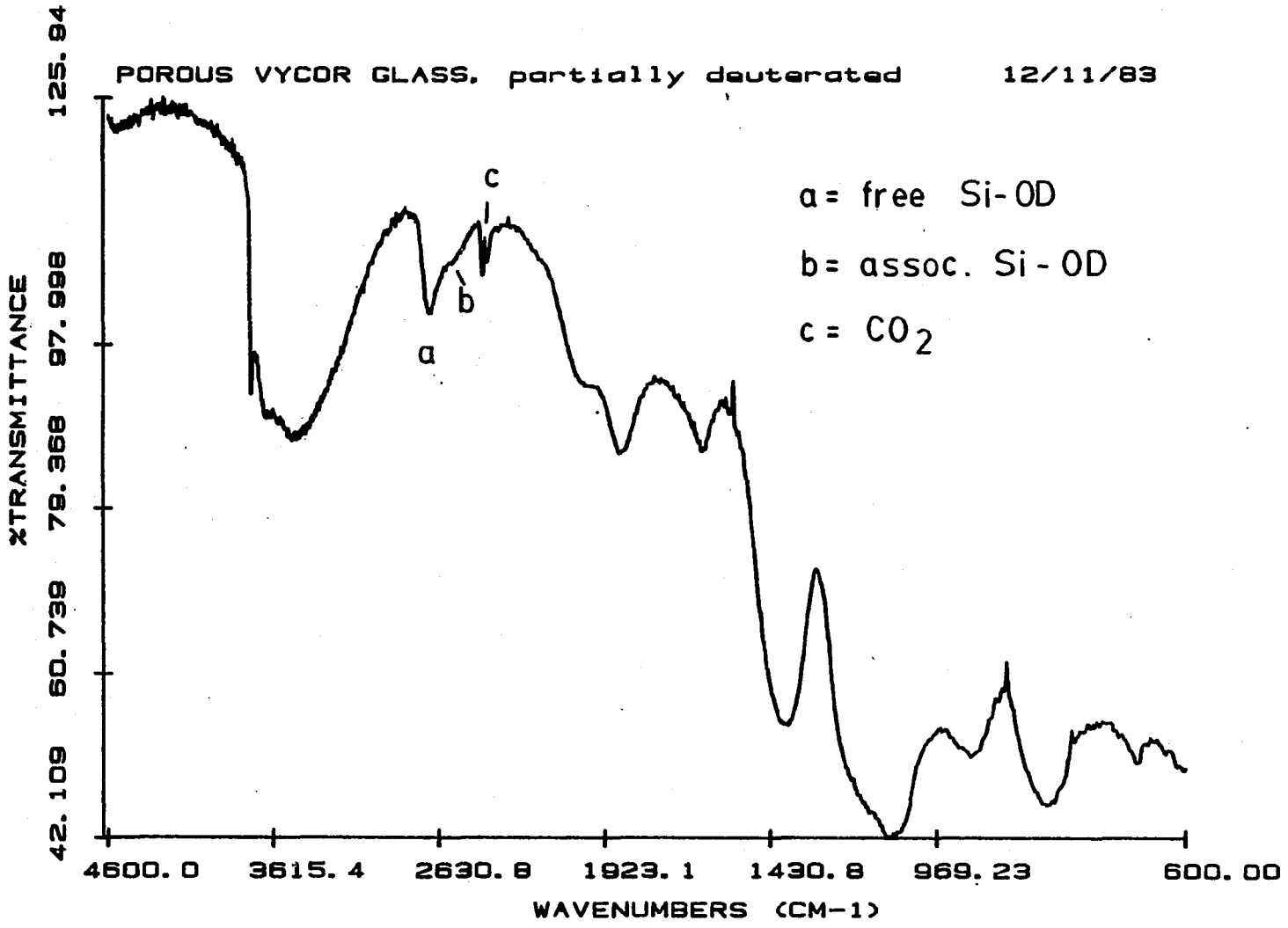

Fig. 31. DRIFT of partially deuterated PVG

PVG plates, equilibrated with room air, to 130°C causes a rapid loss of approximately 2.5% of the initial weight (Figure 32). This corresponds to a loss of physisorbed or bulk water from the surface. Raising the temperature to 400°C eliminated another 0.25% water but at a much slower rate. Condensation of surface silanol groups according to the equation

$$2\ \text{Si-OH} \rightleftharpoons \text{Si-O-Si} + H_2O \qquad (2)$$

becomes a significant reaction above ca. 550°C, indicated by a sharp increase of the water loss rate to 0.85% per hour. Total water loss over a period of 18 hours at 550°C, however, is limited to ca. 5% and samples can be rehydrated to 100% of the original weight. At temperatures above 650°C the rate of dehydration is further accelerated to 2.4% per hour but decreases to <.1% per hour after the total loss has reached 5%. PVG samples which have been subjected to temperature of 1200°C and above solidify to a non-porous glass which can not be rehydrated or impregnated with metal carbonyl. These results are consistent with a reported reduction in surface area above 800 to 900°C due to irreversible condensation of silanol groups in the pores of PVG.

The thermogravimetric results were consistent with diffuse reflectance FTIR spectra recorded as a function of temperature. Temperatures up to 200°C reduce the intensity

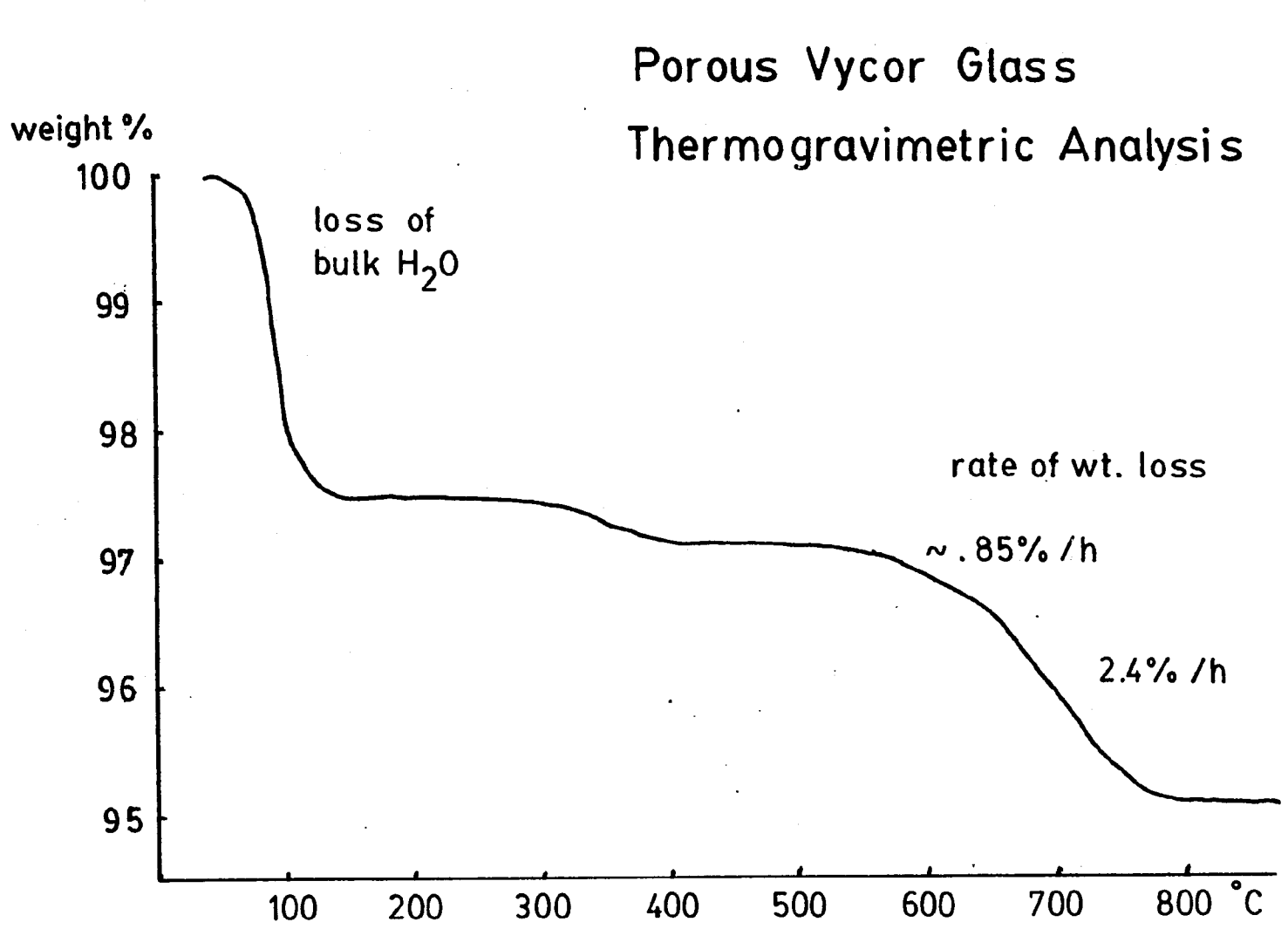

Fig. 32. Thermogravimetric analysis of PVG

of the 3450 cm^{-1} band, characteristic of physisorbed water, without significantly affecting the vibrational characteristics of free and associated silanol groups. At 300 to 400°C the number of associated Si-OH groups diminishes and at a temperature of 500°C only free silanol functionalities remain on the surface (Figure 33). During the thermal treatment the strong vibrations due to freely vibrating SiO-H shifts from 3745 cm^{-1} at 25°C, to 3739 cm^{-1} at 200°C, and finally to 3737 cm^{-1} at 600°C.

3.2. SOLUTION REACTIONS

The solubility of transition metal clusters in hydrocarbon solvents is generally low. $Ru_3(CO)_{12}$ dissolves in non-coordinating solvents such as 2,2,2-trimethylpentane (isooctane) or n-pentane to yield a maximum solution concentration of 5×10^{-4} moles/liter. In the absence of oxygen and water, hydrocarbon solutions of $Ru_3(CO)_{12}$ are thermally stable and show little evidence for photochemical reactivity. In the presence of O_2, however, a slow oxidation leads to the precipitation of black RuO_2; the formation of $[HRu_3(CO)_{11}]^-$ has been reported if water is present in the solvent (155,156,157). The solubility of the ruthenium trimer in chlorinated solvents such as $CHCl_3$ and CCl_4 was found to be greater but is at the expense of thermal and photochemical stability. The observed UV-visible spectra of

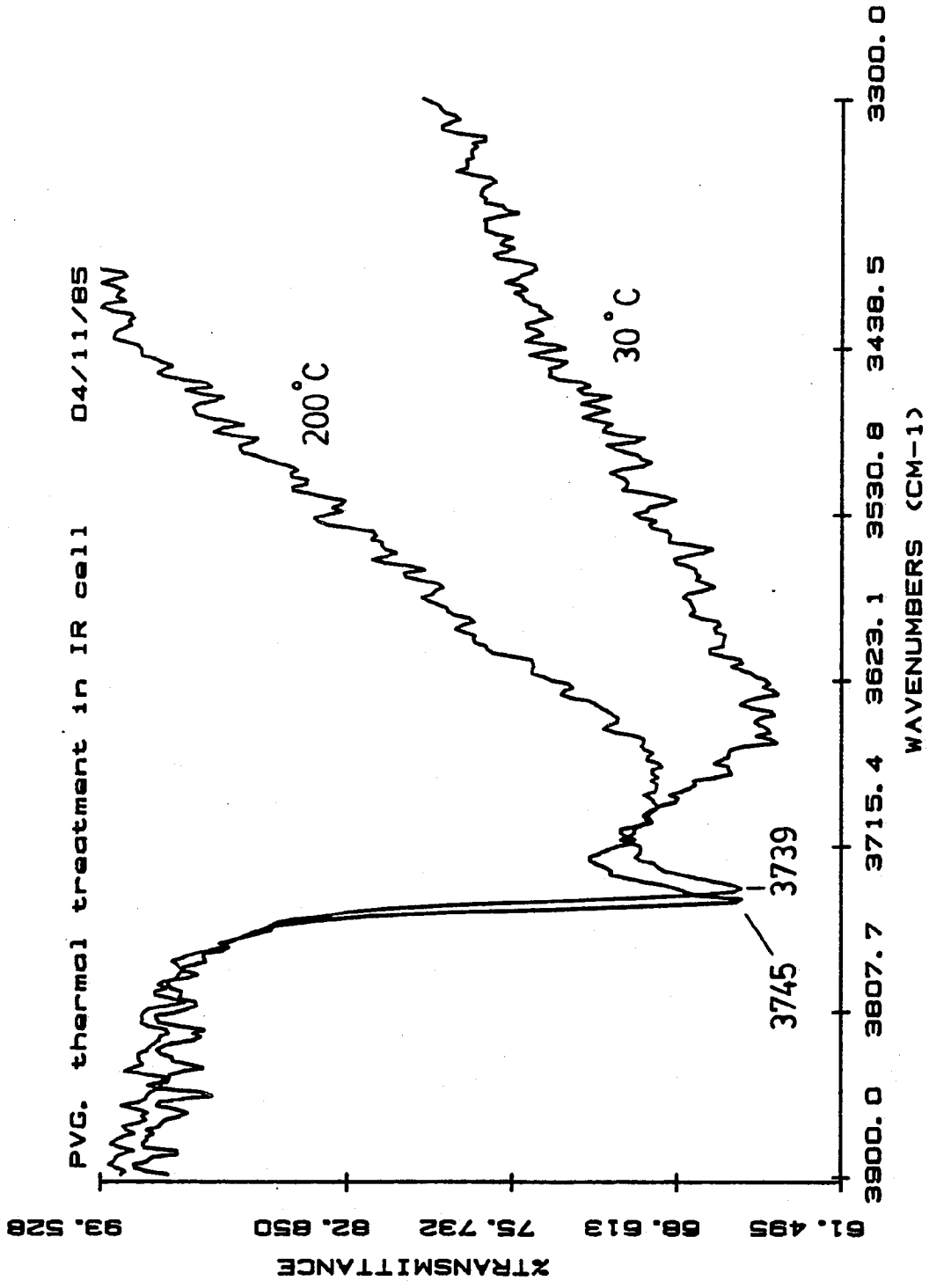

Fig. 33. IR spectrum of silanol/water bands during thermal dehydration of PVG

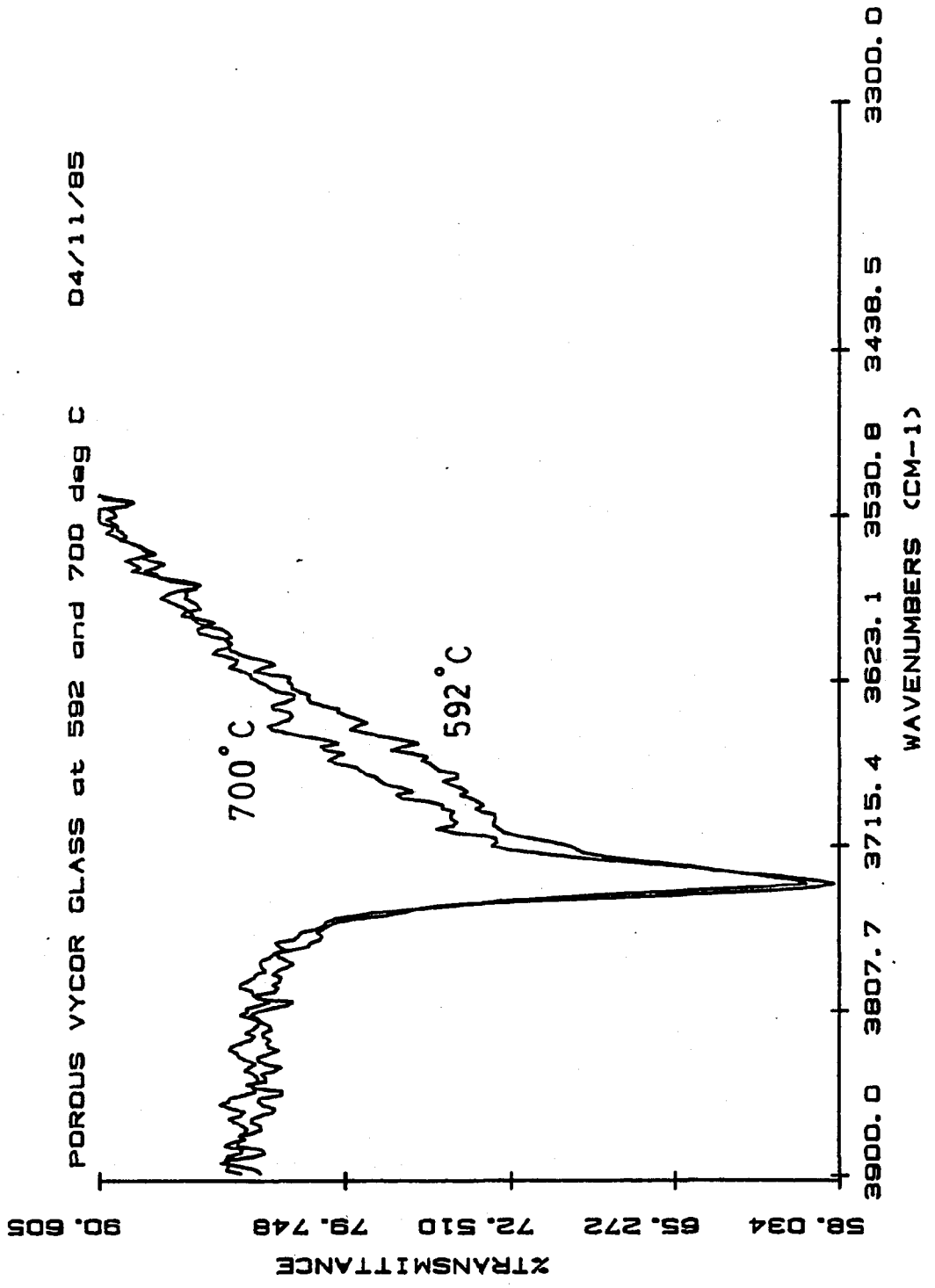

Fig. 34. IR spectrum of dehydrated PVG

solutions containing $Ru_3(CO)_{12}$ exhibit an intense band at 238 nm (molar absorptivity = 35,000 $M^{-1}cm^{-1}$), a weak shoulder at 270 nm, and a band at 395 nm (molar absorptivity = 7,000 $M^{-1}cm^{-1}$) (Table II). The latter band is temperature-dependent and shifts to 400 nm upon heating to 60°C or to a higher frequency upon cooling. IR spectra show three clearly resolved bands at 2061 (vs), 2031 (s), and 2012 cm^{-1} (m). The reported low-intensity band at 2018 cm^{-1} can only be seen as a weak shoulder in very concentrated solutions.

3.2.1. THERMAL REACTIONS IN SOLUTION

As expected from published data, which report that high temperatures and pressures of CO are required to decompose the trimer to $Ru(CO)_5$, no reaction is observed at ambient temperature between $Ru_3(CO)_{12}$ in homogeneous solution and dissolved carbon monoxide. This stability of the ruthenium cluster towards the weak sigma-donor carbon monoxide is contrasted by its reactivity towards stronger sigma-donors such as phosphines; thermal reaction at temperatures above 25-30°C with L = PPh_3 is first order in $Ru_3(CO)_{12}$ and yields the equatorially substituted cluster $Ru_3(CO)_9(PPh_3)_3$ which can be detected by its strong UV-visible absorptions at 385 nm and 505 nm (Figure 35). The IR absorptions have a very low intensity and can not be

Complex	abs. max. [nm]	absorptivity x 10^{-3}	ref.
$Ru_3(CO)_{12}$	395	7	(175)
	270 sh	-	
	238 (MLCT)	35.5	
$Ru_3(CO)_{12}$[a]	395	7	t.w.
	270 sh	-	
	238	35	
$Ru(CO)_5$	260 sh	5.7	(175)
	236 (MLCT)	8.4	
$Ru(CO)_5$[a]	260 sh, 236	-	t.w.
$Ru_3(CO)_9(PPh_3)_3$	387	12.8	(175)
	508	12.3	
$Ru_3(CO)_9(PPh_3)_3$[b]	385, 505	-	t.w.
$Ru_3(CO)_9(PBu_3)_3$[b]	485	-	t.w.
$Ru_3(CO)_{12}$/EtOH[c]	330	-	t.w.
$RuHCl(PPh_3)_3$[d]	470, 520	-	t.w.
$Ru_3(CO)_{12}$/PVG	238, 395	ratio 1:5	t.w.
$Ru(CO)_5$/PVG	260	-	t.w.
$HRu_3(CO)_{10}(OSi\leq)$	330	-	t.w.
$Ru_3(CO)_9(PPh_3)_3$/PVG	385, 505	ratio 1:1	t.w.

a = isooctane, b = Ch_2Cl_2, c = pentane, d = benzene

Table II. UV-visible bands of ruthenium complexes

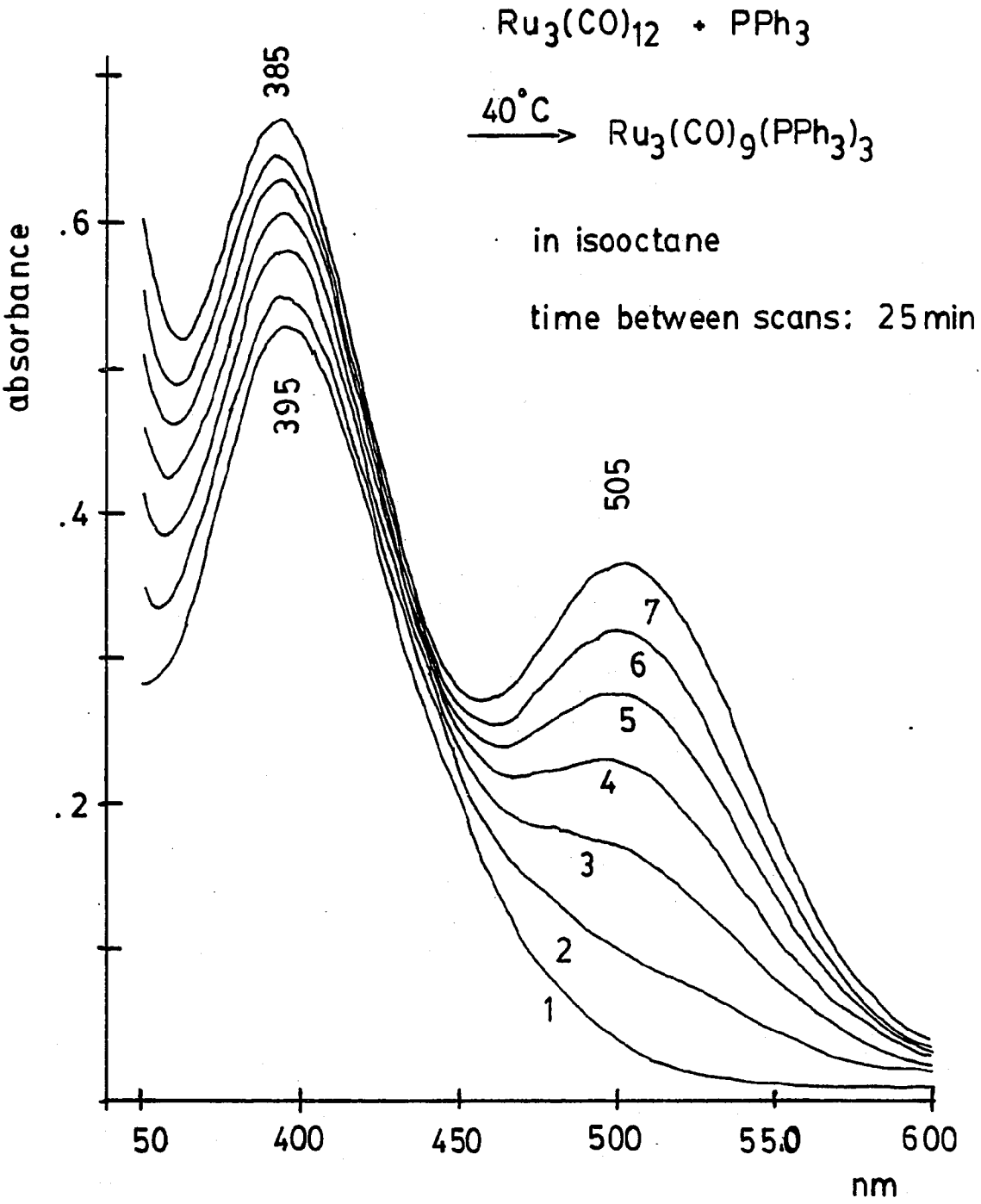

Fig. 35. Formation of $Ru_3(CO)_9(PPh_3)_3$ from reaction of $Ru_3(CO)_{12}$ with PPh_3

detected in hydrocarbon solvents, indicating a significant decrease in symmetry for this species. The solubility of the substituted trimer in benzene or CCl_4 is appreciably higher and the spectrum in these solvents is characterized by three very weak bands at 2075, 2048 and 2022 cm^{-1}, two medium bands at 1984 and 1974 cm^{-1}, and a shoulder at 1953 cm^{-1}. Due to the problems discussed above, published band frequencies for $Ru_3(CO)_9(PPh_3)_3$ differ significantly (Table III). However, our results are identical for both solvents and agree well with the spectrum published by Poe and Twigg (158). The rate constant for reaction 3, determined at temperatures between 40 and 60°C, are summarized in Table IV.

$$Ru_3(CO)_{12} + 3PPh_3 \xrightarrow{\Delta} Ru_3(CO)_9(PPh_3)_3 + 3CO \quad (3)$$

Arrhenius plots of 1/k vs. 1/T yield an activation energy of 24.2±1.2 kcal/mol for this reaction (Figure 36).

Under our experimental conditions and in carbon monoxide-saturated chlorocarbon or benzene solutions $Ru_3(CO)_9(PPh_3)_3$ proved to be stable towards substitution or cluster fragmentation. However, a slow thermal decomposition of the substituted trimer in chlorinated solvents was observed yielding IR bands at 2135 (m), 2073 (ms), 2033 (ms), and 2018 cm^{-1} (m).

Thermal reaction of $Ru_3(CO)_{12}$ with $P(t\text{-}Bu)_3$ also

Compound	cm^{-1}	ref.
$Ru_3(CO)_9(PPh_3)_3$[a]	2075 vw, 2048 vw, 2022 vw, 1984 m, 1974 m, 1953 sh	t.w.
$Ru_3(CO)_9(PPh_3)_3$[b]	1985 s, 1975 s, 1958 m	(158)
$Ru_3(CO)_9(PPh_3)_3$[a]	2046 vw, 1978 sh, 1970 s, 1933 s, 1929 s, 1920 sh	(176)
$Ru_3(CO)_{11}PPh_3$	2097 m, 2046 s, 2030 sh, 2023 sh, 2014 s, 1996 sh, 1986 m, 1972 sh, 1960 sh	(177)
$Ru_3(CO)_{11}PPh_3$[a]	2098 m, 2047 w, 2014 sh, 1986 vw, 1974 sh	t.w.
$Ru(CO)_4PPh_3$[c]	2061 s, 1987 m, 1955 vs	(178)
$Ru(CO)_4PPh_3$[d]	2061 m, 1988 w, 1955 s	t.w.
$Ru(CO)_3(PPh_3)_2$[e]	1900 s	(53)
$Ru(CO)_3(PPh_3)_2$[d]	1909 s	t.w.
$Ru(CO)_4P(t\text{-}Bu)_3$[d]	2059 m, 1983 w, 1945 s	t.w.

a = CCl_4, b = decaline, c = heptane, d = CH_2Cl_2, e = methylcyclohexane

Table III. IR bands of phosphine substituted ruthenium carbonyls

A] rx.: $Ru_3(CO)_{12}.ads \xrightarrow{\Delta} HRu_3(CO)_{10}(OSi\equiv)$

temp. (Celsius)	rate constant
30.0	2.32×10^{-4}
33.0	3.21×10^{-4}
38.0	3.23×10^{-4}
41.5	3.27×10^{-4}
47.5	4.63×10^{-4}

B] rx.: $HRu_3(CO)_{10}(OSi\equiv) + 2CO \xrightarrow{\Delta} Ru_3(CO)_{12}.ads$

temp. (Celsius)	rate constant	p_{CO} (torr)
42.0	2.43×10^{-5}	160
44.0	2.51×10^{-5}	160
51.0	2.96×10^{-5}	160
64.5	3.39×10^{-5}	160
64.5	8.03×10^{-5}	760
69.0	5.28×10^{-5}	160

C] rx.: $Ru_3(CO)_{12} + 3PPh_3 \xrightarrow{\Delta} Ru_3(CO)_9(PPh_3)_3 + 3CO$

$[Ru_3(CO)_{12}] = 1.2 \times 10^{-4}$ M

$[PPh_3] = 1.0 \times 10^{-3}$ M

solvent: isooctane

temp. (Celsius)	rate constant
40.0	2.78×10^{-5}
45.0	4.37×10^{-5}
51.0	5.73×10^{-5}
55.0	1.40×10^{-4}
60.5	3.20×10^{-4}

Table IV. Rate constants for the activation of $Ru_3(CO)_{12}$

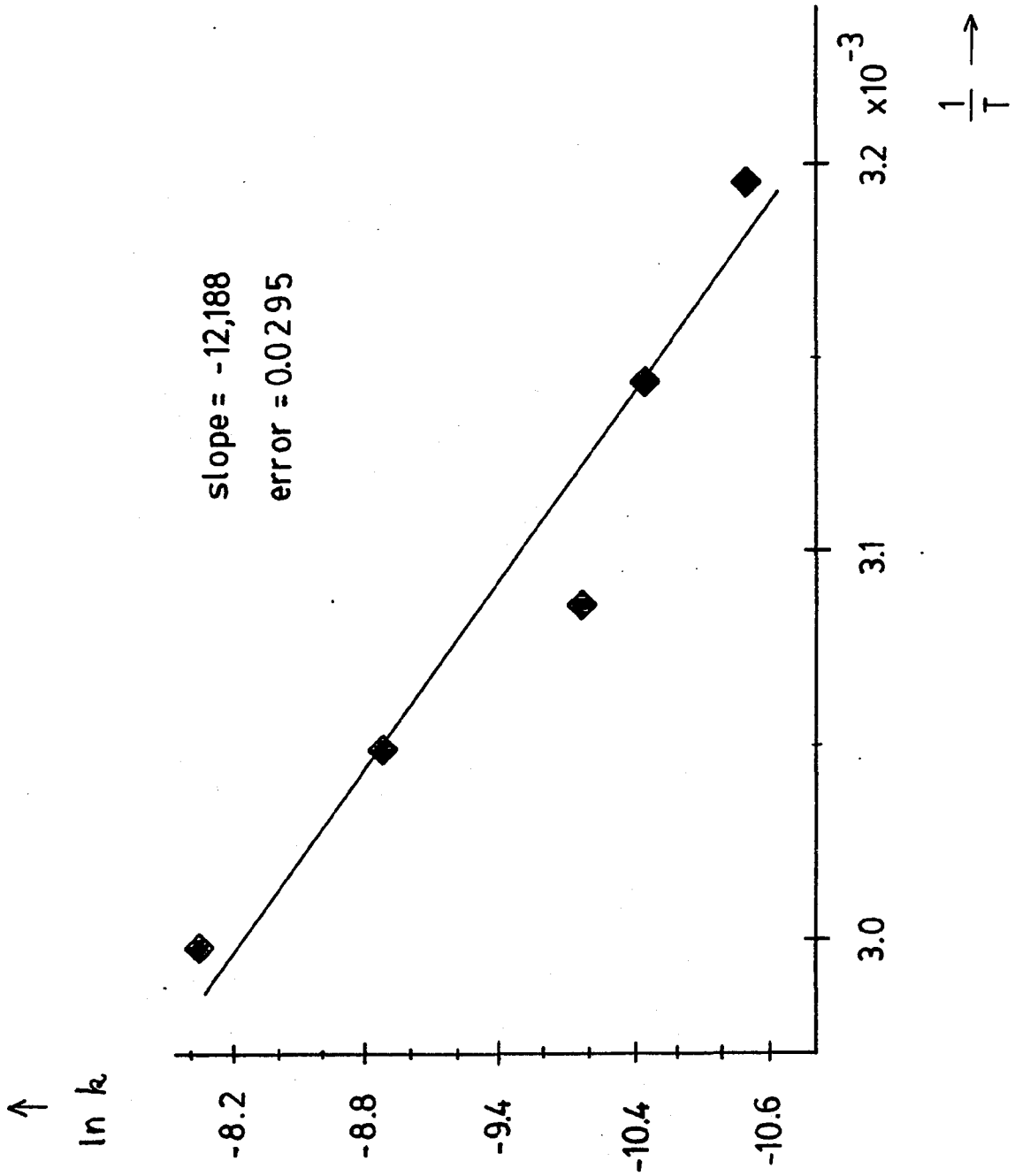

Fig. 36. Energy of activation for the substitution of tri-ruthenium carbonyl with PPh_3

produces a tri-substituted cluster which absorbs at 470 nm. No characteristic spectrum of this species was recorded in the infrared, however, which was attributed to the generally low band intensities found for phosphine-substituted ruthenium clusters.

Although stable at room temperature $Ru_3(CO)_{12}$ reacts thermally with chloroform, $CHCl_3$, and carbon tetrachloride, CCl_4. A loss of intensity in the optical spectrum and the gradual disappearance of the trimer absorptions in the infrared is observed. New absorptions that are independent of the type of chlorinated solvent appear at 2143 (m), 2132 (sh), 2085 (s), and 2027 cm^{-1} (m) (Figure 37). These observations demonstrate that chlorinated solvents are not necessarily inert towards the ruthenium trimer although they have been used as solvents of choice in several published studies.

3.2.2. PHOTOCHEMICAL REACTIONS IN SOLUTION

In the presence of a coordinating ligand, photolysis of the ruthenium trimer in hydrocarbon solution yields substituted monomeric complexes. Under 1 atm of CO, photolysis at 350 nm causes a decline in absorbance at 238 nm and 395 nm, characteristic of the trimer, and a concurrent growth in absorbance at 260 nm. The product spectrum indicates the formation of $Ru(CO)_5$ which, depending

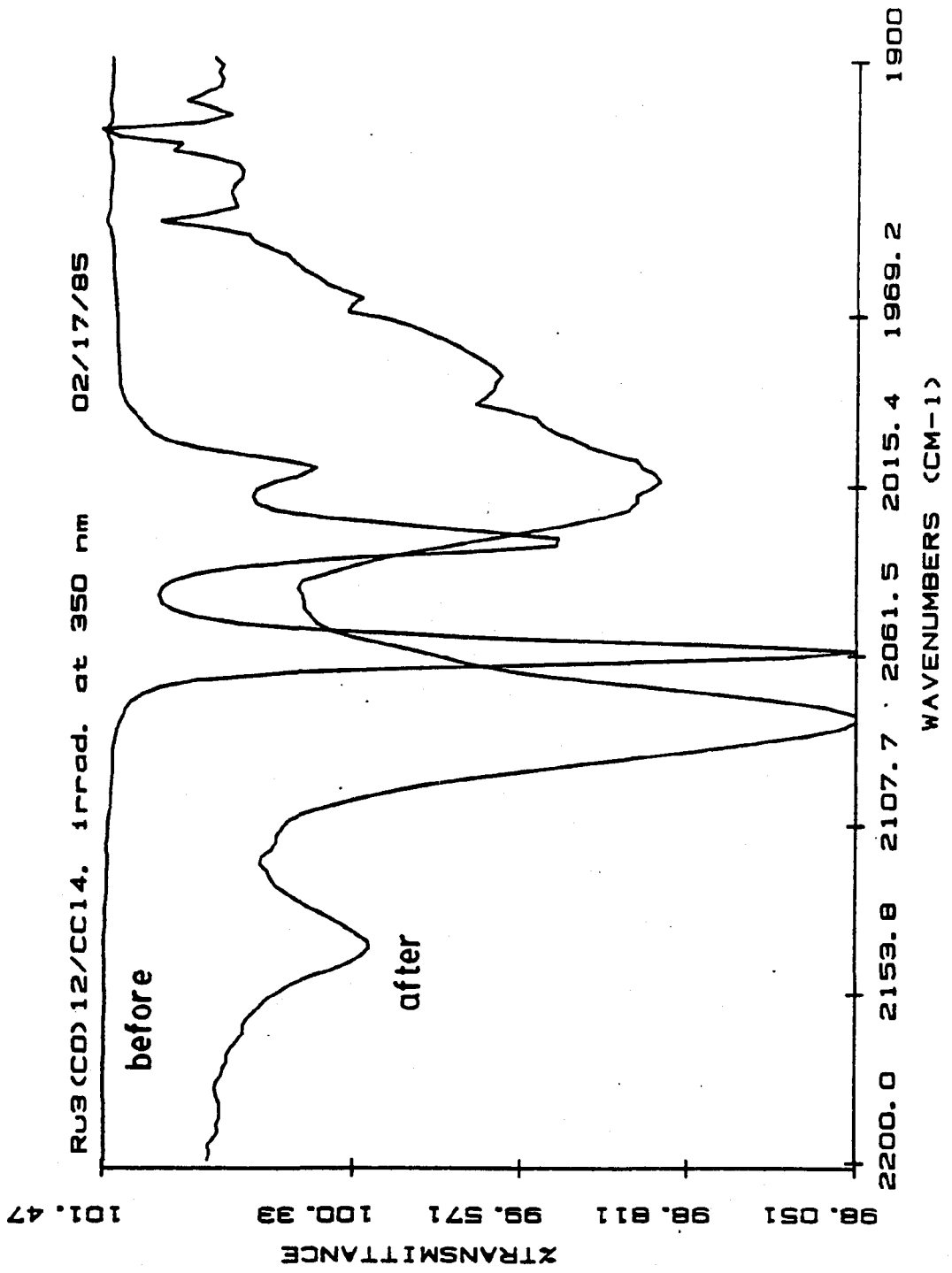

Fig. 37. Reaction of $Ru_3(CO)_{12}$ with chlorinated solvents

on the CO pressure, undergoes a thermal back-reaction, quantitatively regenerating the thermodynamically stable trimer.

Reaction with alkenes: Photolysis in the presence of 1-pentene causes a decline in the 395 nm absorption of the trimer with no apparent new features above 300 nm. Infrared spectra also show a decline in the trimer bands at 2061 (vs), 2031 (s), and 2012 cm^{-1} (m) and a growth of new absorptions at 2100 (w), 2018 (s), and 1992 cm^{-1} (m), which are in excellent agreement with the spectrum of $Ru(CO)_4$(1-pentene) (Figure 38) (Table V). The 1-pentene adduct is thermally labile and reacts quantitatively to regenerate the trimer within minutes after photolysis. Upon reaction of ruthenium carbonyl with diphenylacetylene, $C_{14}H_{10}$, the UV-visible spectrum shows a decrease of its 395 nm band with no apparent new features. IR spectra show that the trimer bands are replaced by five new absorptions at 2111 (vw), 2082 (w), 2039 (ms), 2031 (m), and 2002 cm^{-1} (m) (Figure 39). In contrast to its olefinic analogue, however, the acetylene adduct is stable under our experimental conditions and no backreaction to the ruthenium dodecacarbonyl could be detected.

Reaction with phosphines: Photolysis in the presence of triphenylphosphine, PPh_3, causes changes in the electronic spectrum indicative of fragmentation, and new IR bands at 2061 (m), 1988 (w), and 1955 cm^{-1} (s) confirm the

ISOMERATION OF OLEFINS

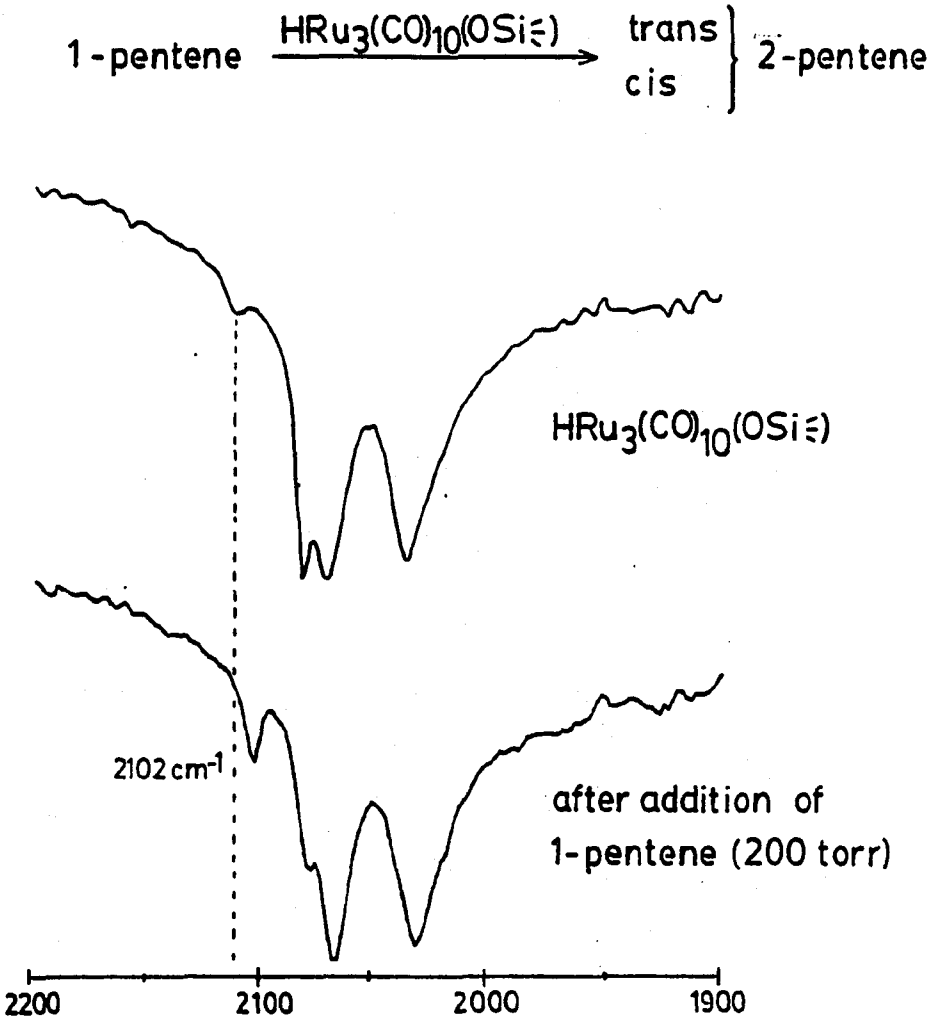

Fig. 38. Reaction of $HRu_3(CO)_{10}(OSi\equiv)$ with 1-pentene (IR)

Compound	cm^{-1}	ref.
$Ru(CO)_4$(1-pentene)[a]	2103 w, 2018 s, 1990 m	(53)
$Ru(CO)_4$(1-pentene)[a]	2100 w, 2018 s, 1992 m	t.w.
$Ru_3(CO)_{12}$/PhCCPh	2111 vw, 2082 w, 2039 ms, 2031 m, 2002 m	t.w.
$Ru_3(CO)_{12}/CCl_4$	2143 m, 2132 sh, 2085 s, 2027 m	t.w.
$Ru_3(CO)_{12}$/EtOH[f]	2125 w,br, 2089 w,br, 1973 vw,br	t.w.
$HRu_3(CO)_{10}SC_4H_9$[c]	2105 m, 2064 s, 2056 s, 2025 vs, 2012 m, 2007 s, 1994 m	(167)
$HRu_3(CO)_{10}NO$[c]	2109 w, 2064 s, 2033 vs, 2027 m, 2019 s, 1998 w	(165)
$HRu_3(CO)_{10}(OSi\equiv)$(1-pentene)	2102 m, 2069 s, 2034 s,br	t.w.
$[Ru(CO)_2(OSi\equiv)]_n$	2074 m,br, 2006 w,br[g]	t.w.
$[Ru(CO)_3(OSi\equiv)]_n$	2136 w,br, 2074 m,br, 2006 w,br[g]	t.w.
$[Ru(CO)_2(OSi\equiv)]_n$	2072 s, 2002 s[h]	(86)
$[Ru(CO)_3(OSi\equiv)]_n$	2138 m, 2073 s, 2014 s[h]	(86)
$(Ru(CO)_3SEt)_2$[d]	2080m, 2058 s, 2010 s, 2000 s	(176)
$Ru(CO)_4I_2$[e]	2160 m, 2106 s, 2097 s, 2069 s	(176)
$Ru_2(CO)_6Cl_4$[d]	2143 s, 2075 s, 2015 m	(176)
Ru_{metal}/CO[g]	2031 m	t.w.
Ru_{metal}/CO[h]	2080 br --> 1985 br	(86)

a = isooctane, b = heptane, c = cyclohexane, d = CCl_4
e = $CHCl_3$, f = pentane, g = PVG, h = silica gel

Table V. IR of ruthenium complexes

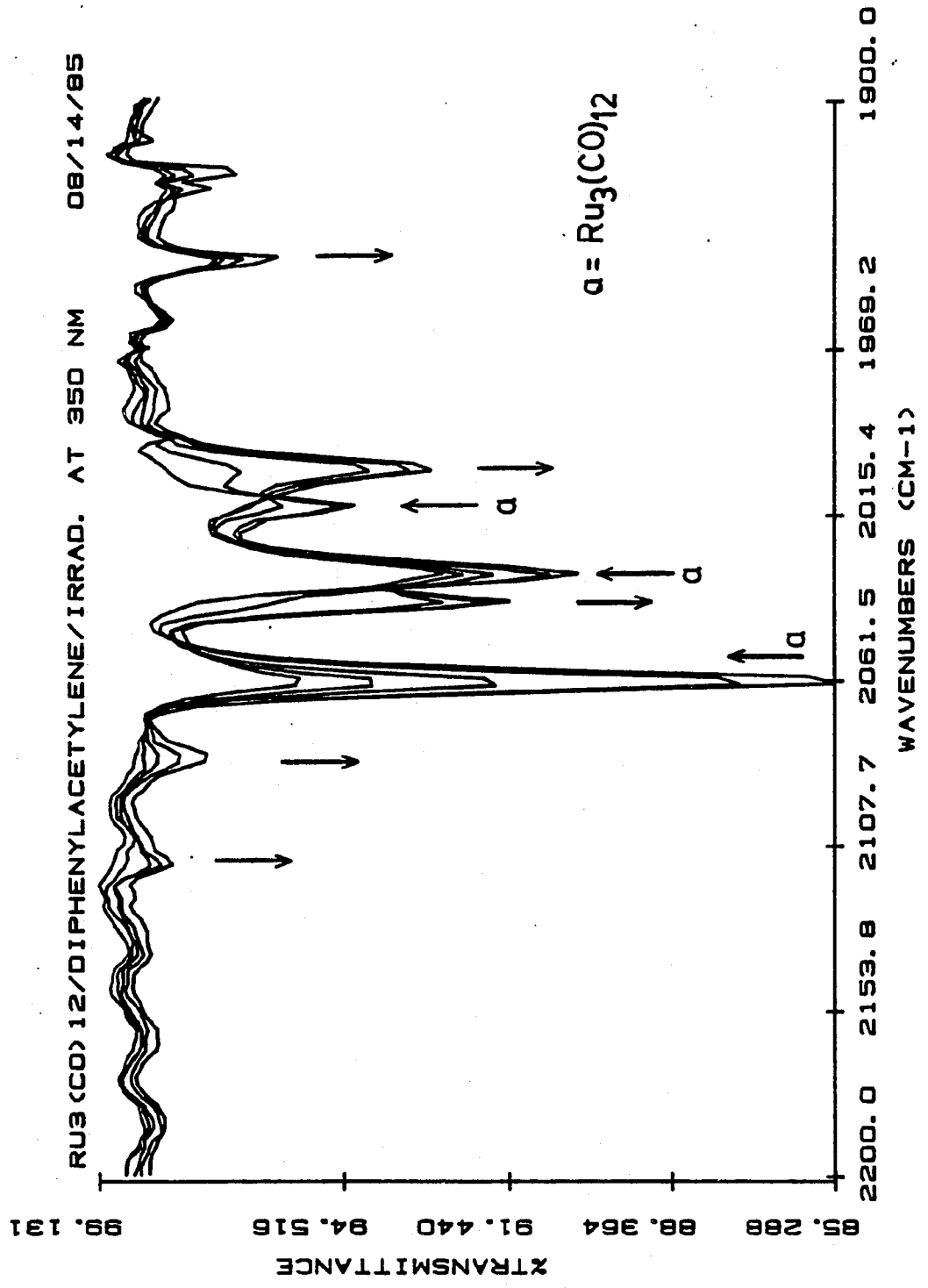

Fig. 39. Reaction of $Ru_3(CO)_{12}$ with PhC≡CPh (IR)

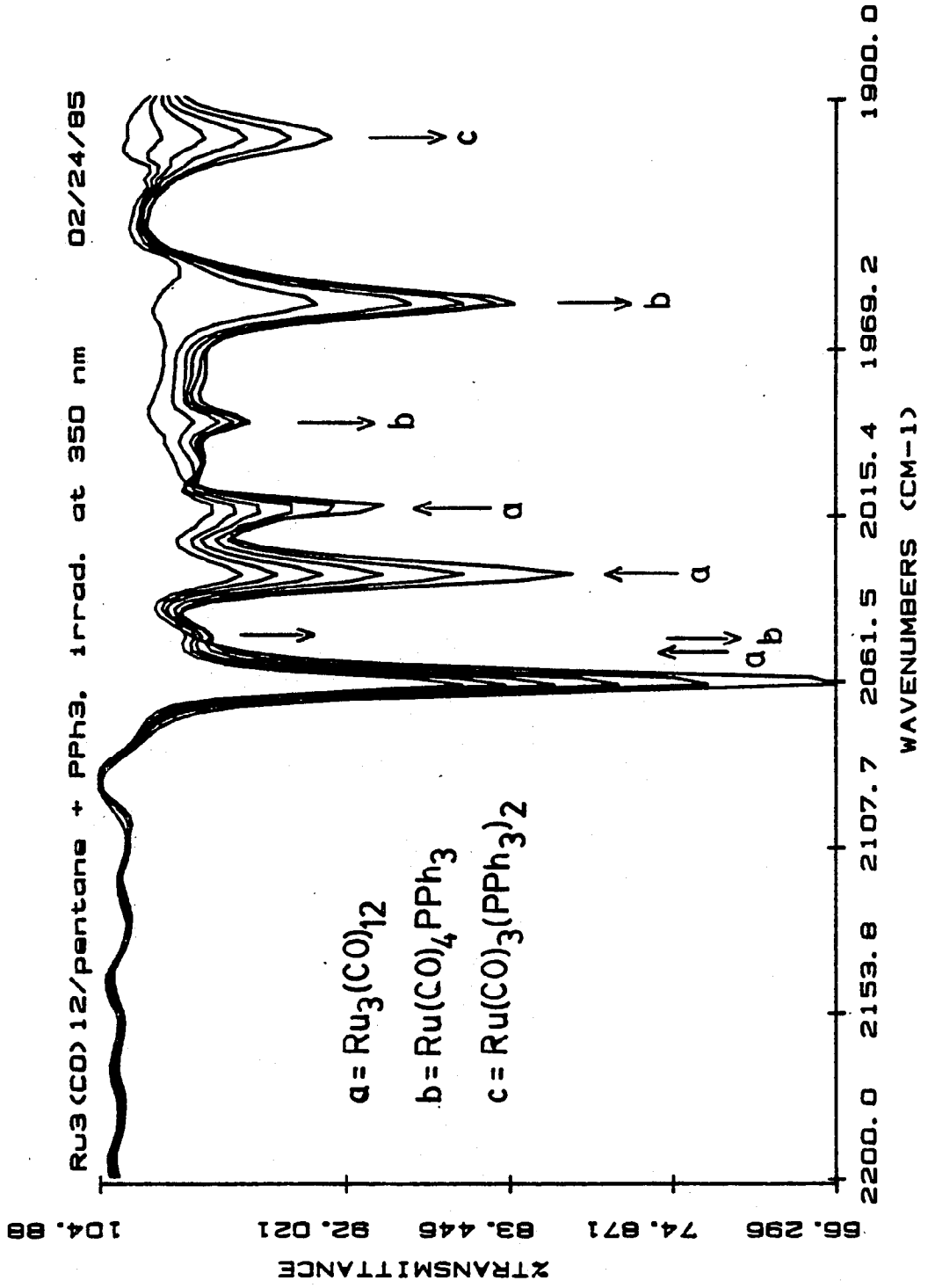

Fig. 40. Photochemical reaction of $Ru_3(CO)_{12}$ with PPh_3

formation of $Ru(CO)_4PPh_3$ (Figure 40,41). Upon continued photolysis the bands characteristic of the starting material and the growth rate of the 1955 cm^{-1} band diminish and a new absorption at 1909 cm^{-1} develops into the dominant feature of the IR spectrum (Figure 41). The location of this band corresponds to the reported spectrum of di-substituted ruthenium phosphine $Ru(CO)_3(PPh_3)_2$. In addition to the IR bands attributed to these monomeric species, weak absorptions at 2098, 2047, 2014, 1986, and 1974 cm^{-1} are observed until all of the ruthenium dodecacarbonyl has reacted. Over the course of the photolysis reaction the color of the solution slowly changes from yellow to transparent to pink. Long, red needles precipitate from the solution which can be dissolved in benzene to yield UV-visible maxima at 390 and 505 nm.

Under carbon monoxide, however, the monomers, mono- and disubstituted with phosphines, recombine in a thermal reaction to yield the original ruthenium dodecacarbonyl while experiencing a quantitative loss of their phosphine substitutents in the process. IR spectra recorded during this conversion clearly show the thermal reversibility of the photosubstitution reaction (Figure 42). The recovery of starting material after the first cycle was limited to less than 40% as determined by integration of the 2061 cm^{-1} band. A similar declusterification is observed for the substitution of the ruthenium trimer with butyl phosphine.

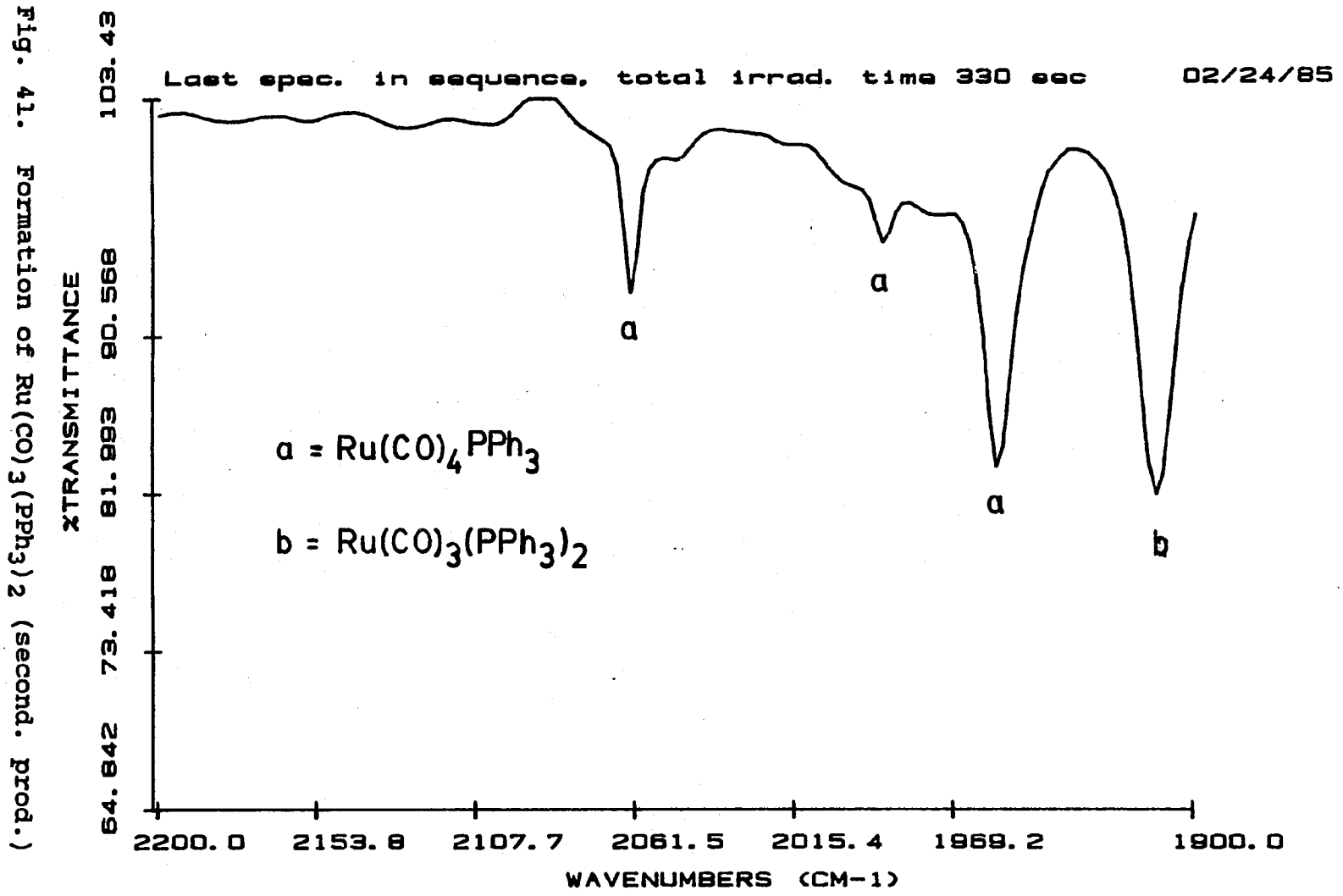

Fig. 41. Formation of $Ru(CO)_3(PPh_3)_2$ (second. prod.)

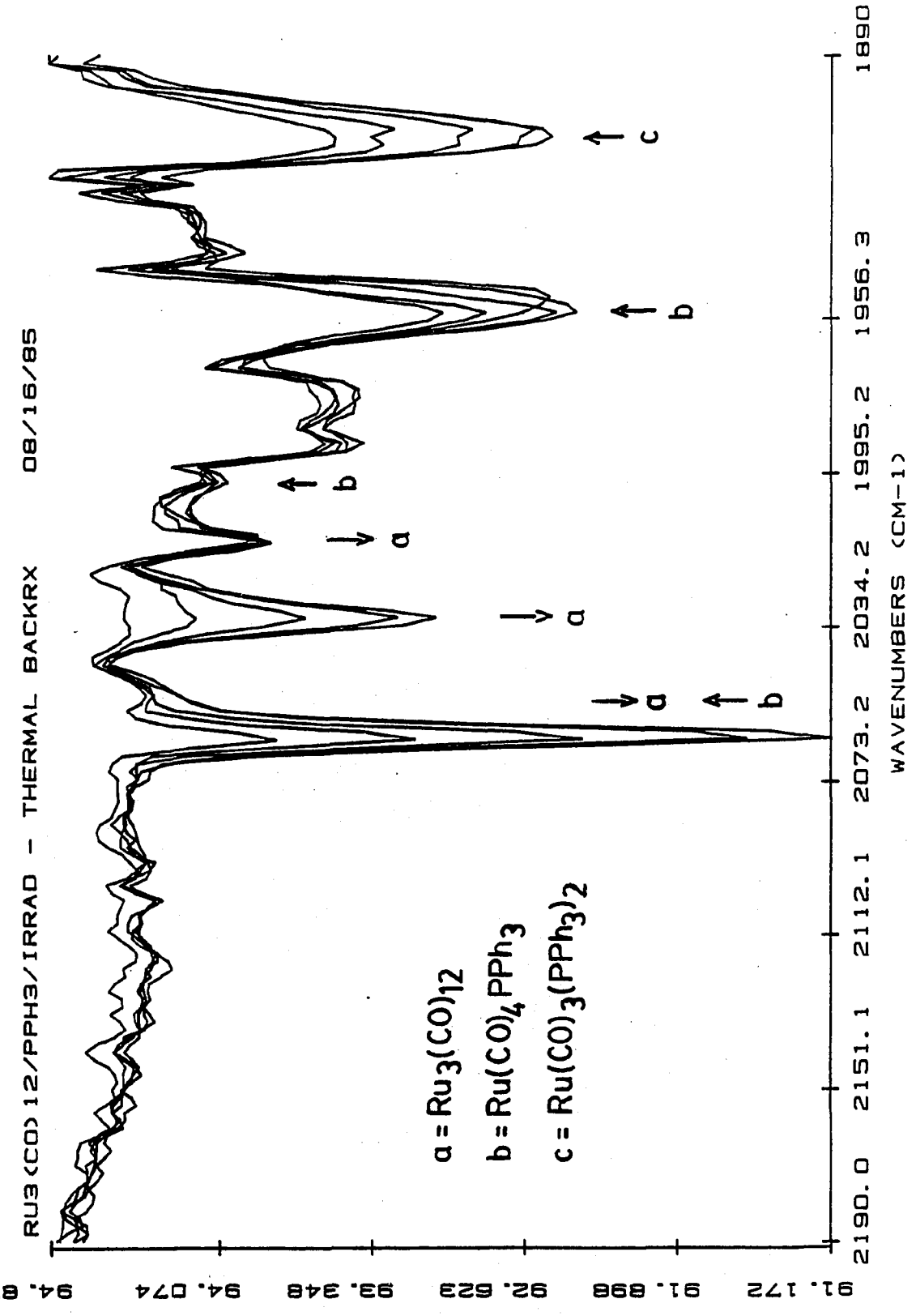

Fig. 42. Thermal recombination of phosphine substituted monomer to $Ru_3(CO)_{12}$

However, the pronounced changes in the UV region and IR bands at 2059, 1983, and 1945 cm^{-1} only indicate the formation of $Ru(CO)_4(P(t\text{-}Bu)_3)$. No absorptions could be attributed to a monosubstituted trimer, $Ru_3(CO)_{11}(PBu_3)$, or a disubstituted monomer, $Ru(CO)_3(PBu_3)_2$.

Quantum yield determination: For several ligands L (L = 1-pentene, diphenylacetylene, triphenylphosphine, and tributylphosphine), the quantum yield of declusterification has been determined (Table VI). The observed quantum yields, ϕ_{obs}, corrected for thermal reversibility by extrapolating the absorbance change after photolysis back to the end of photolysis, are independent of the excitation wavelengths, i.e., 350, 300, and 254 nm. As illustrated in Figure 43, however, ϕ_{obs} is a function of the ligand concentration, and plots of $1/\phi_{obs}$ vs. 1/[L], where L = 1-pentene, PPh_3, and tris(t-butyl)phosphine, $P(t\text{-}Bu)_3$, are linear. The extrapolated values, ϕ_{lim}, for $P(t\text{-}Bu)_3$ and 1-pentene, $8.4\pm0.5 \times 10^{-2}$ and $8.0\pm0.7 \times 10^{-2}$, respectively, are within experimental error, whereas that for PPh_3, $5.7\pm0.4 \times 10^{-2}$, is somewhat smaller. In spite of the difference, the quantum yield of $Ru_3(CO)_{12}$ - fragmentation is taken to be $7.3\pm1.1 \times 10^{-2}$, the mean of the above values, which is in reasonable agreement with the value of $10.5\pm2.2 \times 10^{-2}$ reported by Poe and coworkers (67).

Limiting Quantum Yields of Disappearance for the Reaction of $Ru_3(CO)_{12}$ with Ligands L

Ligand L	$\phi_{lim} \times 10^2$	reference
1-pentene	8.0 ± 0.7	t.w.
PPh_3	5.7 ± 0.4	t.w.
PPh_3	< 1	(57)
$P(t\text{-}Bu)_3$	8.4 ± 0.5	t.w.
CO	10.5 ± 2.2	(67)

Table VI. Quantum yield of declusterifcation

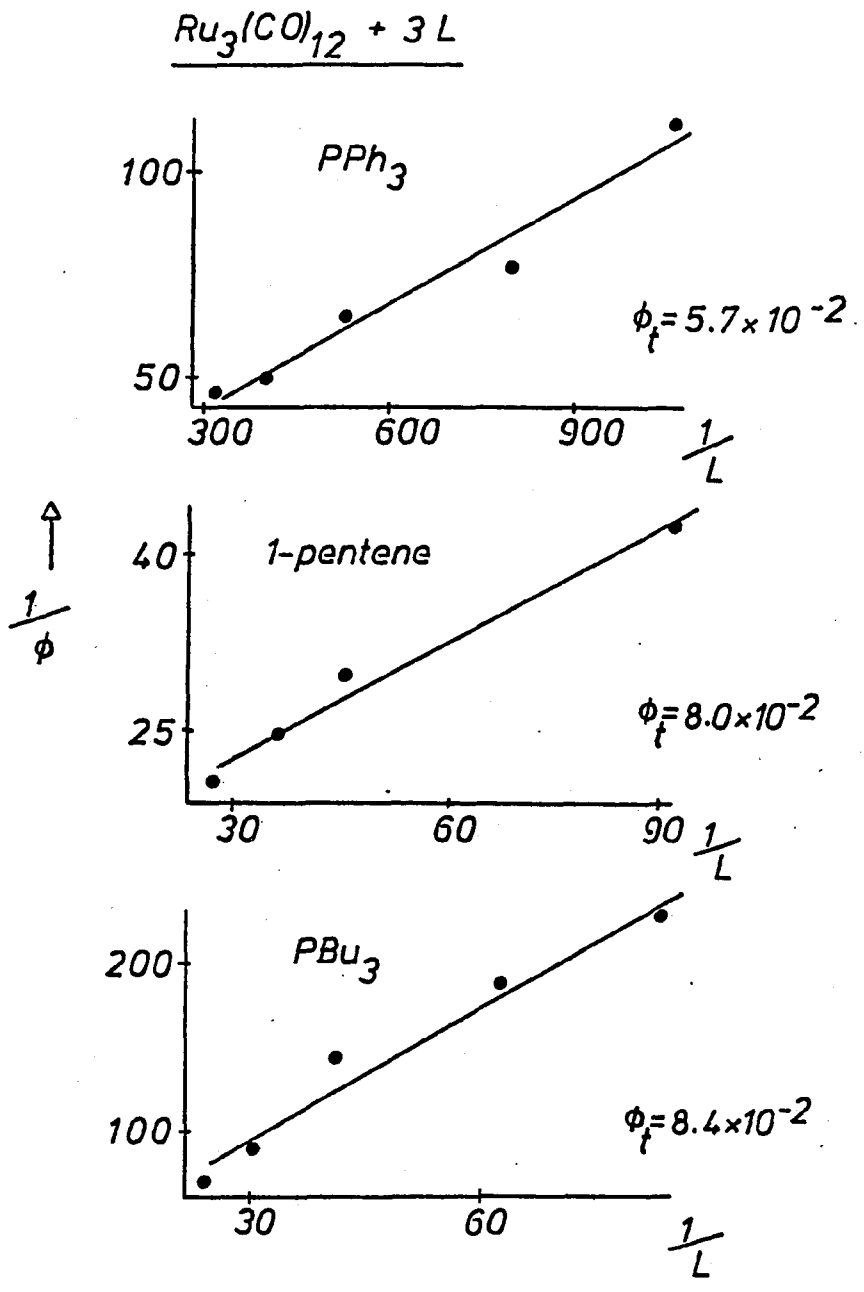

Fig. 43. Quantum yield of declusterification

3.3. SURFACE REACTIONS

Plate PVG samples were typically impregnated by adsorption from solution since this procedure enabled an absolute determination of the number of moles of complex per gram of glass. It was noted that highest surface concentrations were achieved when the support was impregnated at low temperatures (Figure 44). This effect can be explained with the temperature-dependence of the trimer concentration in solution. The solubility of $Ru_3(CO)_{12}$ in organic solvents is low and saturated solutions were used to impregnate PVG. Decreasing the temperature of such a solution by up to 35°C induces a condition termed supersaturation; seeding crystals will initiate an immediate precipitation of ruthenium carbonyl. We assume that the presence of porous Vycor glass in the solution prevents supersaturation. As the solution temperature and with it the solubility of $Ru_3(CO)_{12}$ decreases single cluster units are physically adsorbed onto the PVG surface. The amount of ruthenium carbonyl on the surface increases rapidly as an inverse function of the temperature.

3.3.1. PHYSISORBED SPECIES

Physisorbed trimer $Ru_3(CO)_{12}$: Regardless of whether the impregnation is by sublimation or by adsorption from

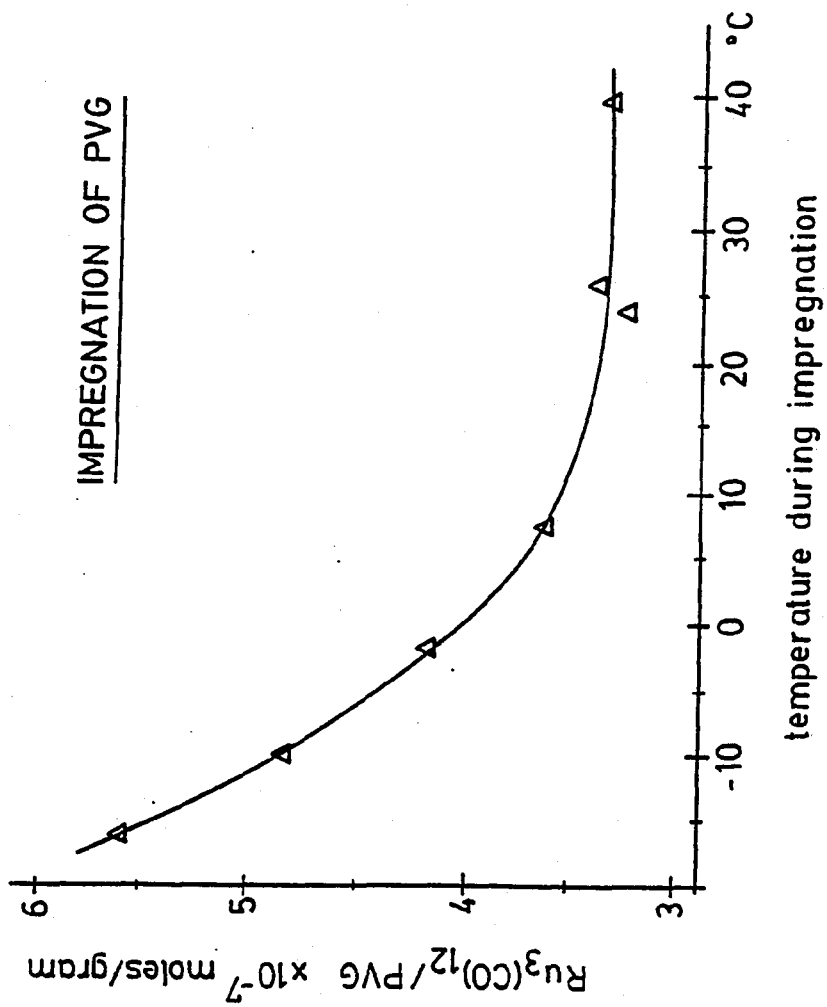

Fig. 44. Surface concentration of $Ru_3(CO)_{12}$ on PVG vs. temperature of impregnation

solution, UV-visible spectra recorded at different locations on the same sample are within experimental error, and GC analysis of the vapor phase after subliming the complex onto PVG give no indication of CO, CO_2, or H_2 evolution. In the 230 to 500 nm region, the UV-visible spectrum of $Ru_3(CO)_{12}$.ads, is within experimental error in band maximum, band halfwidth, and relative extinction coefficient of the spectrum of the complex in isooctane. However, the intensity ratio of the metal-to-ligand charge transfer band, MLCT, at 238 nm to that of the ligand field band at 395 nm is constant at 5.0±0.4 to 1.0 only if the PVG plate has been rigorously dehydrated before impregnation and if the impregnating solution is free of moisture. Exposure of the PVG plate to room air for several minutes effects a disproportionate increase in absorbance for wavelengths < 250 nm, ultimately reducing the strong MLCT band to a shoulder. The IR spectrum of the adsorbed trimer consists of bands at 2064 (s), 2035 (m), and 2018 cm^{-1} (sh) (Figure 45). No additional bands that might correspond to the vibrations of perturbed CO groups are observed in the spectrum. Broadening or splitting of the bands, characteristic of polycrystalline $Ru_3(CO)_{12}$ (Figure 46) is not detected, and, although shifted to higher wavenumbers by 2-6 cm^{-1}, the bands retain the relative intensity pattern found in fluid solution. Examination of the hydroxyl stretching region of the support upon adsorption of

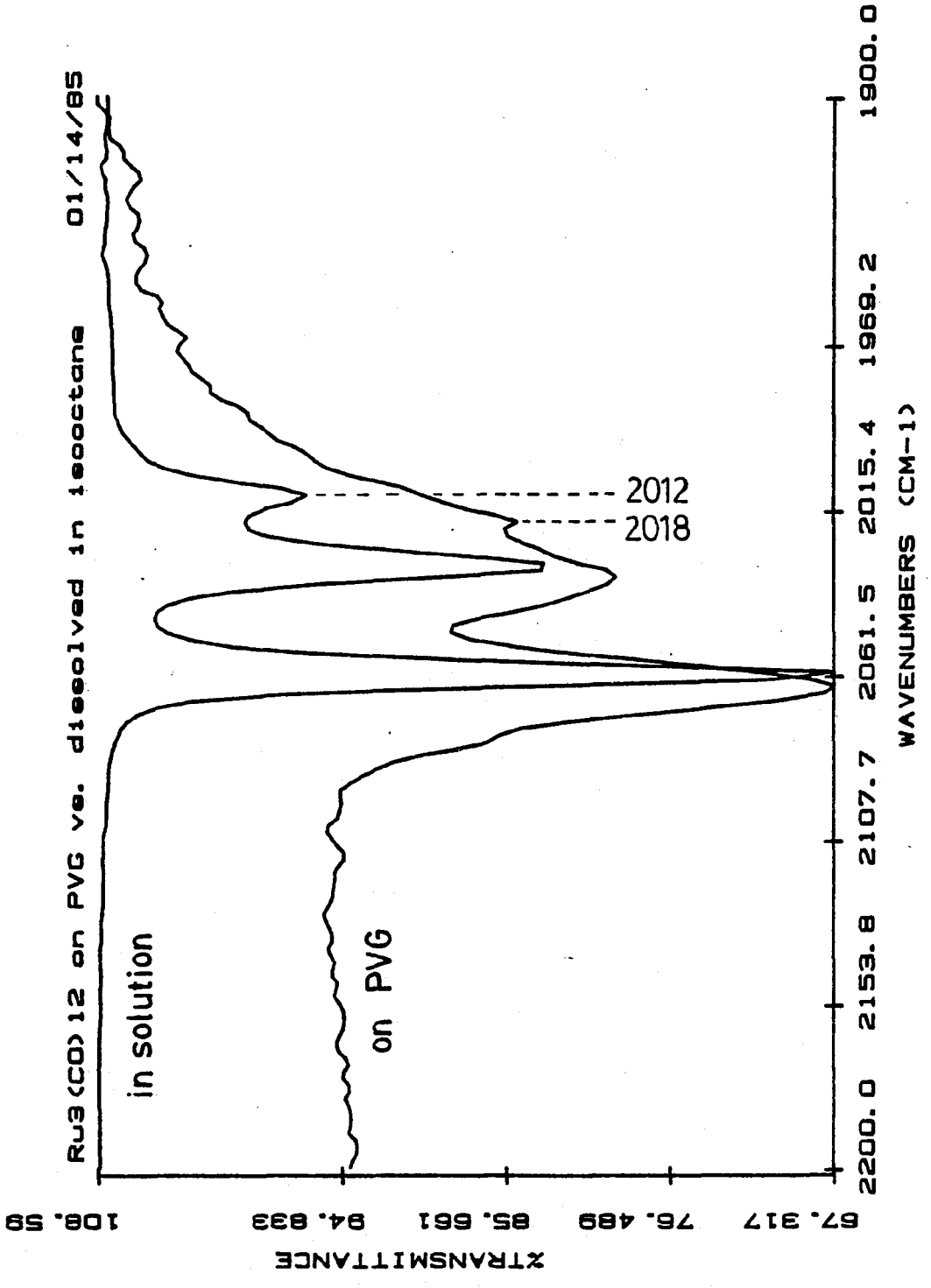

Fig. 45. FTIR spectrum of $Ru_3(CO)_{12}$ on PVG

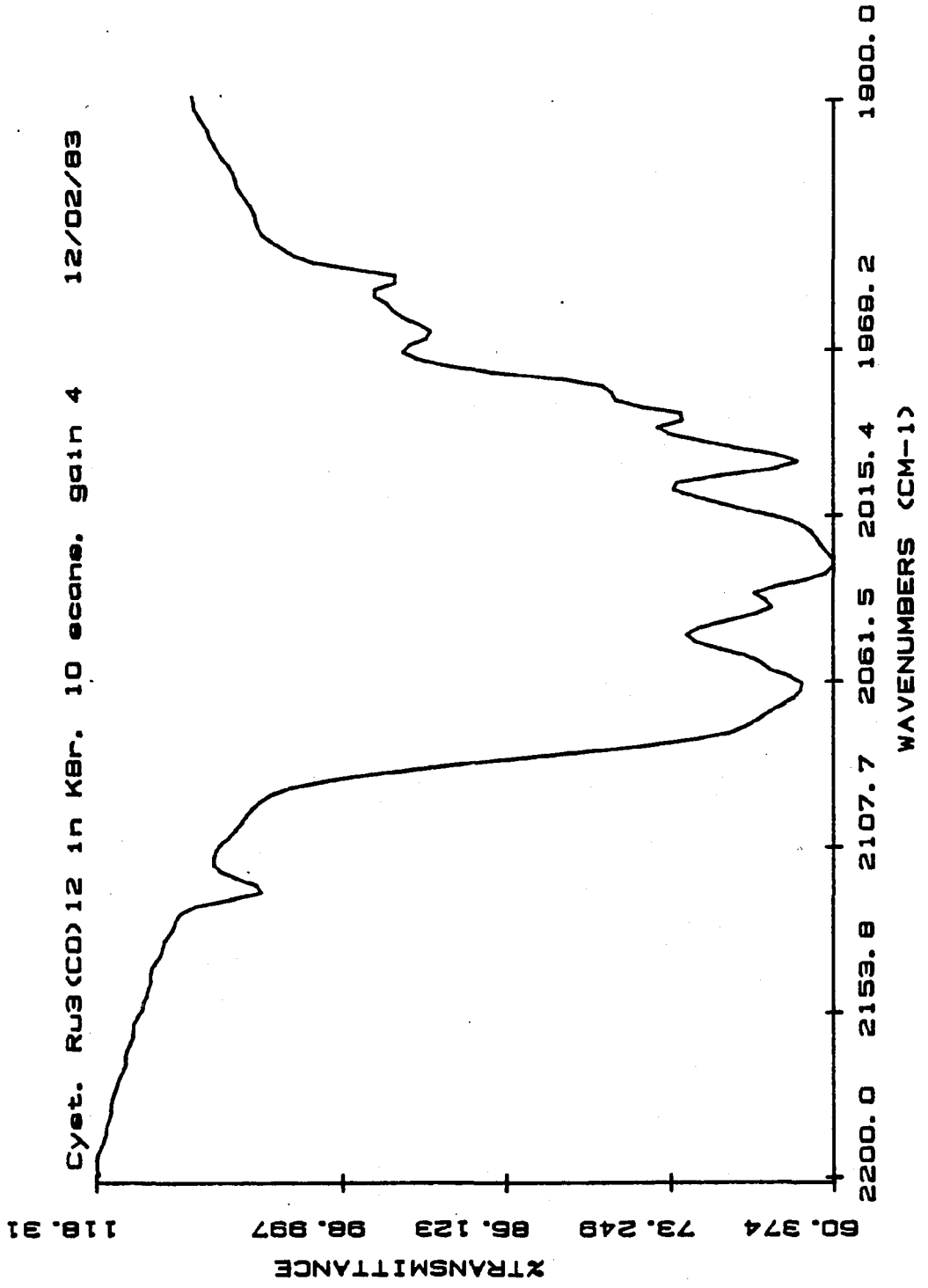

Fig. 46. Polycrystalline $Ru_3(CO)_{12}$ in KBr

$Ru_3(CO)_{12}$ shows no reproducible decrease in the intensity of the intense free silanol vibration at 3745 cm^{-1}.

Physisorbed monomer $Ru(CO)_5$: UV photolysis (wavelength > 254 nm) of $Ru_3(CO)_{12}$.adsorbed (.ads) under 1 atm of CO causes no significant decline in absorbance at 238 and 395 nm and no bands characteristic of the formation of $Ru(CO)_5$ are observed. This finding is in sharp contrast to the reaction found in fluid solution where the trimer is photochemically decomposes to the monomeric species. In an alternate experiment $Ru(CO)_5$ was photochemically prepared in pentane and adsorbed onto PVG. A weak shoulder at 260 nm establishes the presence of pentacarbonyl on the surface of the glass. However, no thermal recombination of the supported monomeric units to $Ru_3(CO)_{12}$ is observed. This again is in contrast to the behavior in fluid solution and suggests a low mobiltity of the transition metal complex on the surface of the glass.

Supported $Ru_3(CO)_9(PPh_3)_3$: Initial attempts to adsorb thermally prepared $Ru_3(CO)_9(PPh_3)_3$ onto the PVG were unsuccessful; the red color of the trimer bleached without any sign of adsorption. However, if the glass is impregnated with PPh_3 prior to adsorption of $Ru_3(CO)_{12}$ the substituted trimer can be generated in-situ. An alternate route is the co-sublimation of ruthenium carbonyl and phosphine yielding a sample with an intense red color. The optical spectrum of the trisubstituted ruthenium cluster is identical to its corresponding spectrum in fluid solution

and in the absence of light and moisture the surface species is stable in air. Repeated attempts to record the IR spectrum by diffuse reflectance techniques were unsuccessful. However, the difficulties were not unexpected since the cluster also resists IR characterization in hydrocarbon solution. Photolysis of the substituted trimer in vacuum or under CO cause a rapid decrease of the absorbance at 505 nm without the appearance of distinct features. The IR spectrum is equally inconclusive and does not show any bands which could be compared to absorption spectra, recorded in fluid solution.

3.3.2. CHEMISORBED SPECIES

Chemisorbed trimer $HRu_3(CO)_{10}(OSi\equiv)$: Photolysis of $Ru_3(CO)_{12}$.ads in vacuo causes the spectral changes illustrated in Figure 47. Excitation with either 350, 300, or 254 nm light results in a decline at 395 nm and in the UV and a concurrent increase of absorbance at 330 nm. The spectral changes are independent of the amount of $Ru_3(CO)_{12}$.ads present on the surface of the Vycor glass and will be assigned to a conversion of the physisorbed trimer to a chemisorbed species with the formula $HRu_3(CO)_{10}(OSi\equiv)$. The conversion was found to be quantitative under our experimental conditions which allowed for a maximum surface loading of *ca.* 1×10^{-5} moles/gm for powder samples,

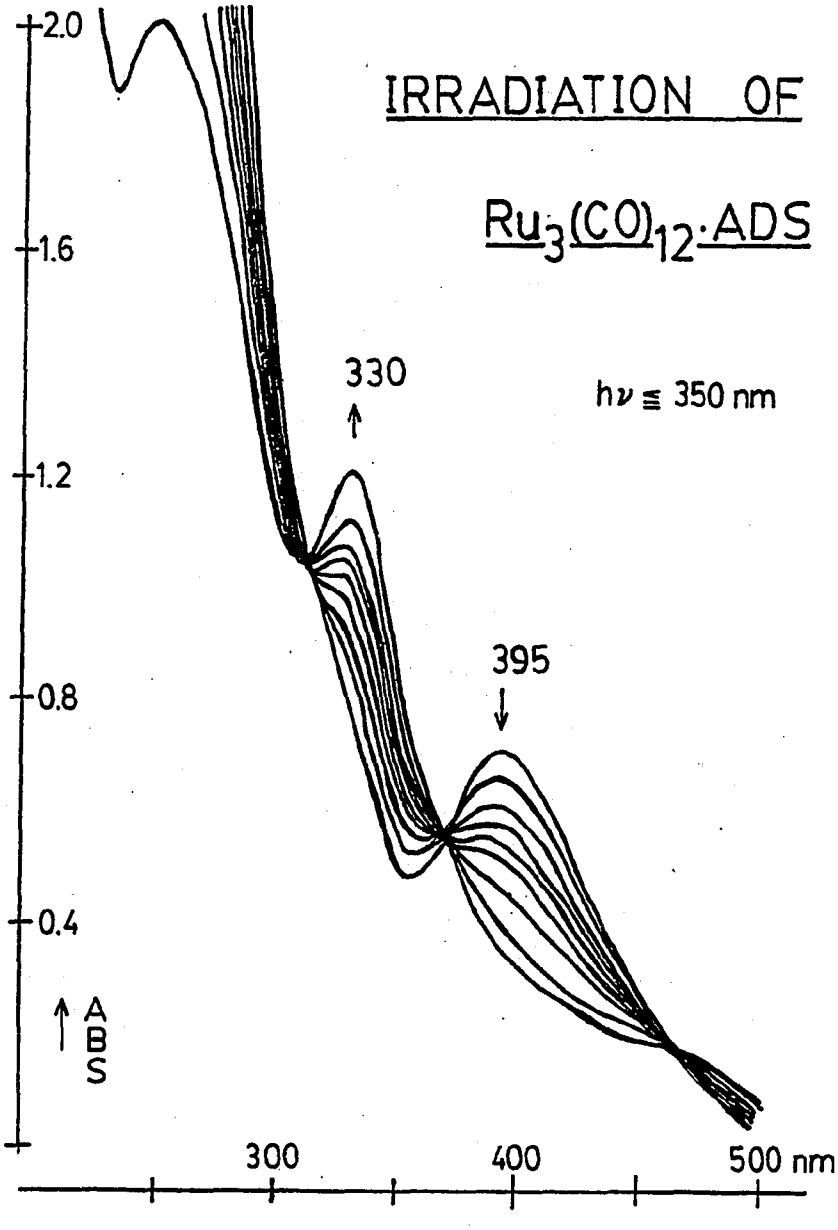

Fig. 47. Conversion of $Ru_3(CO)_{12}$.ads to $HRu_3(CO)_{10}(OSi\equiv)$

1×10^{-6} moles/gm for 1 mm plate PVG, and 3×10^{-7} moles/gm for 4 mm plate PVG. The surface loading achieved for PVG powder corresponds to a surface coverage of ca. 4% whereas the maximal surface concenatrations on plate samples translate into a coverage of < 1% (Figure 48). This discrepancy must be attributed to our assumption that the cluster is uniformly distributed throughout the impregnation depth a. Especially in view of brief impregation times and cluster size it appears more likely that even on plate PVG the coverage on the outer surface approaches or exceeds the 4% found on powder samples, but drops off rapidly with increasing impregnation depth. GC analysis of the vapor phase at various degrees of conversion indicates the evolution of 1.8±0.3 moles of CO per mole of $Ru_3(CO)_{12}$.ads reacted; the latter is determined from the decline in absorbance at 395 nm. Neither H_2 evolution, which is indicative of metal oxidation, nor CO_2 evolution is detected. IR spectra show a decline in the bands characteristic of the trimer, and as illustrated in Figure 49, the appearance of bands at 2109 cm^{-1} and two relatively intense bands at 2078 and 2069 cm^{-1}, and a broad band at 2034 cm^{-1} with shoulders at 2017 and 1999 cm^{-1}. Bands in the bridging CO region, indicative of dimeric, CO-bridged complexes, or bands indicative of monomeric complexes are not detected. Provided the photodissociated CO is continuously removed, the photogeneration is quantitative as indicated by a loss

CALCULATION OF SUPPORT LOADING

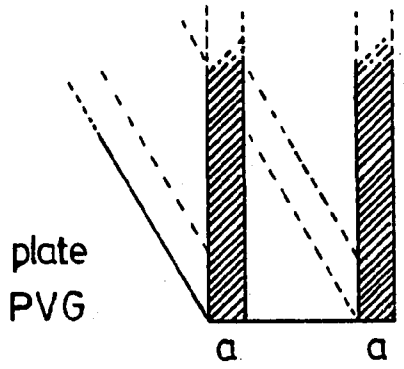

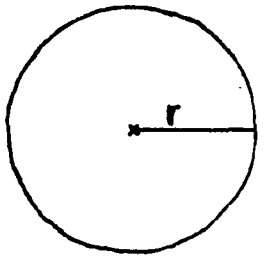

area covered by $Ru_3(CO)_{12}$

Impregnation depth: $a = 0.3$ mm

PVG surface area: $S = 130\ m^2/gm$

Radius of Ru cluster: $r = 5 \times 10^{-8}$ cm

Area covered by Ru cluster $A = \pi r^2$
$= 7.85 \times 10^{-15}\ cm^2/molec.$

Loading of $Ru_3(CO)_{12}$ per gram of PVG calculated under the assumption: impregnation depth >> PVG thickness

$1.3 \times 10^6 / 7.85 \times 10^{-15}$ molec./gm
$= 1.66 \times 10^{20}$ molec./gm
$= 2.75 \times 10^{-4}$ moles $Ru_3(CO)_{12}$/gm

Max. cluster loading as a function of sample type:

A] < 630 mesh powder: 100 wt% can be impregnated
max. loading: 2.75×10^{-4} moles/gm

B] 1 mm PVG plate: 60 wt% can be impregnated
max. loading: 1.65×10^{-4} moles/gm

C] 4 mm PVG plate: 15 wt% can be impregnated
max. loading: 4.13×10^{-5} moles/gm

Fig. 48. Calculation of surface coverage

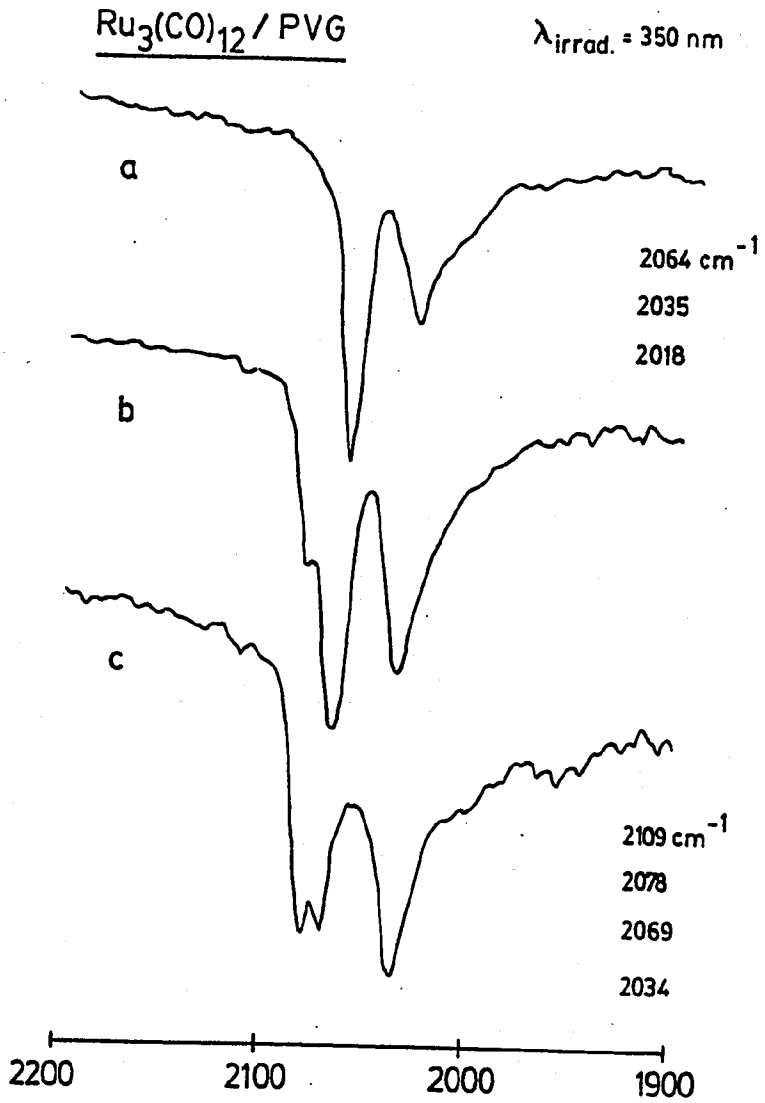

Fig. 49. IR analysis of chemisorption reaction

of absorbance at 395 nm with the maintenance of the isosbestic points at 365 and 290 nm through 80% of the reaction (Figure 47). On thin PVG, where the surface is flat and light intensity losses due to reflection are minimized, the quantum yield for the photoreaction is $1.4\pm0.6 \times 10^{-2}$ for an irradiation wavelength of 254 nm and $3.0\pm0.4 \times 10^{-2}$ for a wavelength of 350 nm. In a closed cell of small volume, evacuated or under 1 atm of N_2, the conversion is not quantitative. The initial spectral changes are identical to those in Figure 47 but the reaction achieves a photostationary state. Periodic removal of the liberated carbon monoxide increases the product/reactant ratio. Chemisorption of ruthenium dodecacarbonyl on PVG can also be achieved by means of a thermal reaction, albeit at a much slower rate. The rate constants, measured at temperatures between 15 and 60°C, are summarized in Table IV. The activation energy of the process, as determined from the slope of the Arrhenius plot (Figure 50), has been calculated to 6.2±0.4 kcal/mole.

Reaction with CO: Addition of CO during the reaction quenches the formation of the chemisorbed product. The 330 nm absorption remains unchanged and continued 300 or 350 nm photolysis causes no significant spectral changes. Exposing the $HRu_3(CO)_{10}(OSi\equiv)$ photoproduct to 1 atm of CO at room temperature causes a decline in absorbance at 330 nm and a concurrent growth at 395 nm, indicative of a regenera-

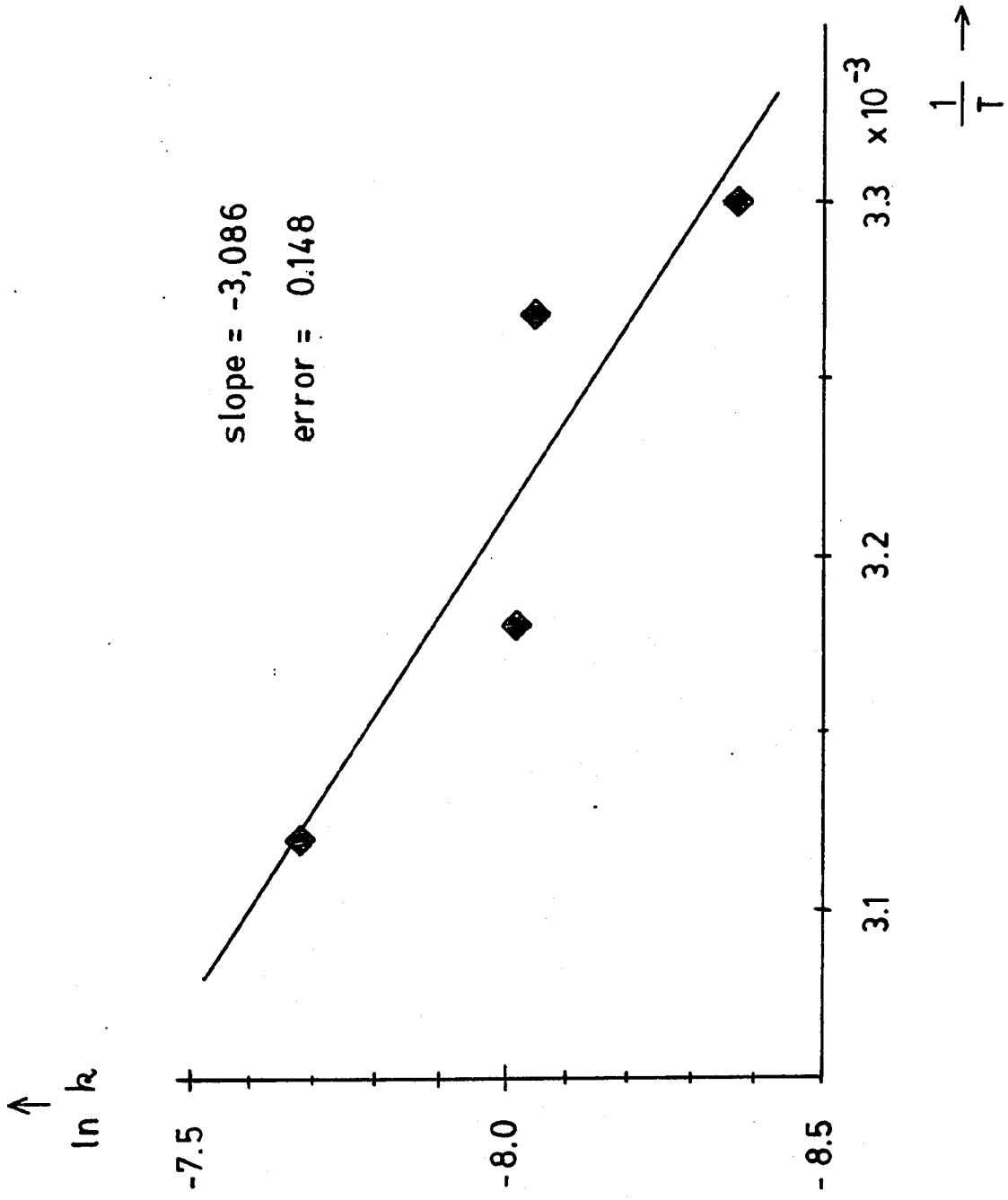

Fig. 50. Energy of activation for the oxidative addition reaction

tion of the physisorbed trimer. Surprisingly the 330 nm species is photochemically inert; 300 or 350 nm photolysis in vacuo causes no detectable spectral change. Although photochemically inert, the reaction product is kinetically labile and thermally reacts with a variety of ligands. As mentioned above, exposure to 1 atm of CO at room temperature regenerates the adsorbed trimer in >90% yield. The reaction, monitored by the increase in absorbance at 395 nm, follows pseudo-first order kinetics, and the rate constants measured at various temperatures are listed in Table IV. An Arrhenius plot (Figure 51) yields an activation energy of 5.1±0.2 kcal/mole.

Reaction with phosphines: Exposure of the chemisorbed trimer on the surface of PVG to 50 torr of $P(t\text{-}Bu)_3$ causes an immediate loss of the 330 nm absorption. Lower energy visible absorptions at 470 nm, indicative of equatorially tri-substituted phosphine adducts which can be obtained from the thermal reaction of $Ru_3(CO)_{12}$ and $P(t\text{-}Bu)_3$, are not detected (Figure 52b). Pronounced changes in the UV domain of the spectrum imply the formation of substituted ruthenium monomers although this could not be confirmed by IR spectroscopy.

Reaction with olefins: Exposure of the 330 nm species to 160 torr of 1-pentene at various temperatures between 25 and 65°C causes an immediate decrease of the intensity of the 330 nm band concommitant with an increase

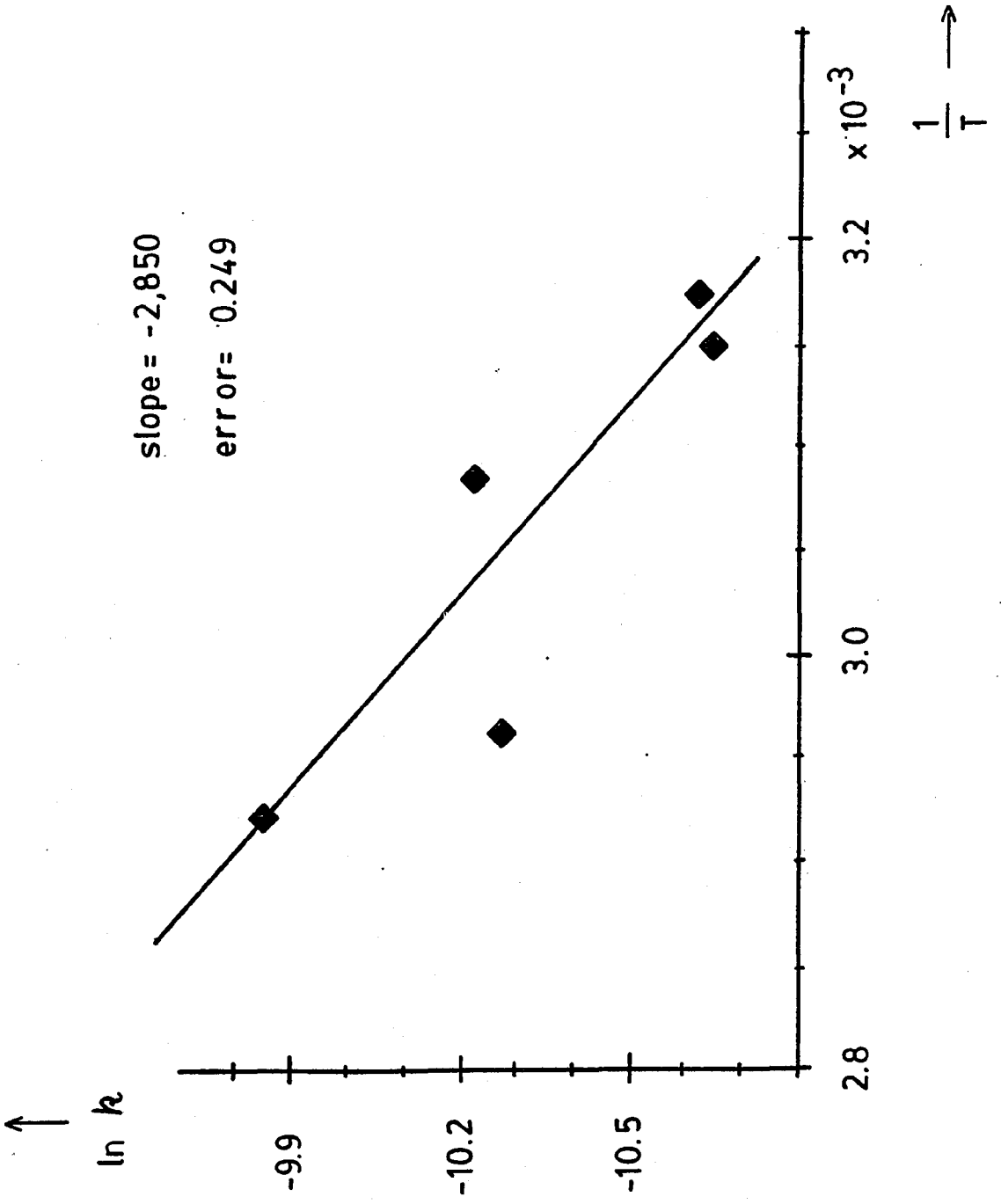

Fig. 51. Energy of activation for the reverse oxidative addition reaction

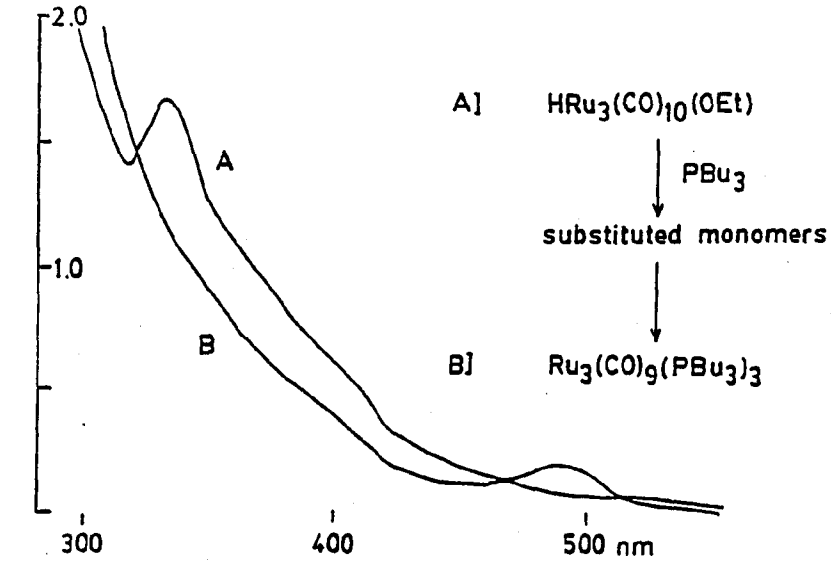

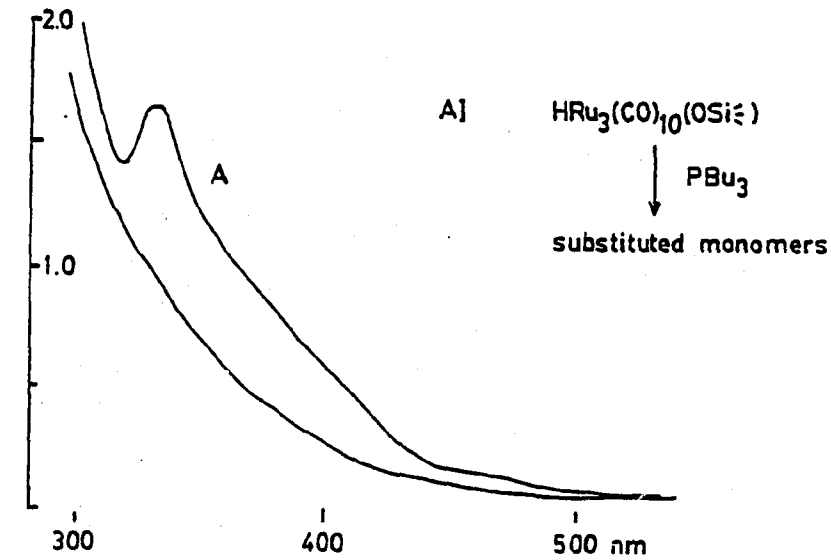

Fig. 52a. Reaction of $Ru_3(CO)_{12}$/EtOH with $P(t\text{-}Bu)_3$

Fig. 52b. Reaction of $HRu_3(CO)_{10}(OSi\equiv)$ with $P(t\text{-}Bu)_3$

in intensity in the UV range. However, no new bands are observed in the optical spectrum. The initial rapid thermal reaction is followed by a slower, temperature-dependent conversion indicated by a general decrease of UV-visible intensity and yielding one or more products that have no detectable bands above 300 nm. Infrared spectra recorded during the reaction show a modification of the spectrum of the chemisorbed starting material; the intensities of the 2109 cm^{-1} and 2078 cm^{-1} absorptions decrease and a new medium strong absorption at 2102 cm^{-1} is observed (Figure 53).

3.3.3. MODEL REACTIONS IN FLUID SOLUTION

A series of attempts were undertaken to model the reactions of the adsorbed trimer, which are occuring on a hydroxylated silica surface, by examining its thermal and photochemical reactions in homogeneous fluid solution. Ligands, containing hydroxyl or oxygen functions such as triphenylsilanol, ethanol, THF,and 1,4-dioxane, were used to model surface silanol groups. However, the reactions in fluid solution proved to be complex and did not exhibit the specificity found for the adsorbed trimer. For example, refluxing a deaerated $CHCl_3$ solution containing stoichiometric amounts of $Ru_3(CO)_{12}$ and triphenylsilanol causes a rapid decline in the bands characteristic of the trimer.

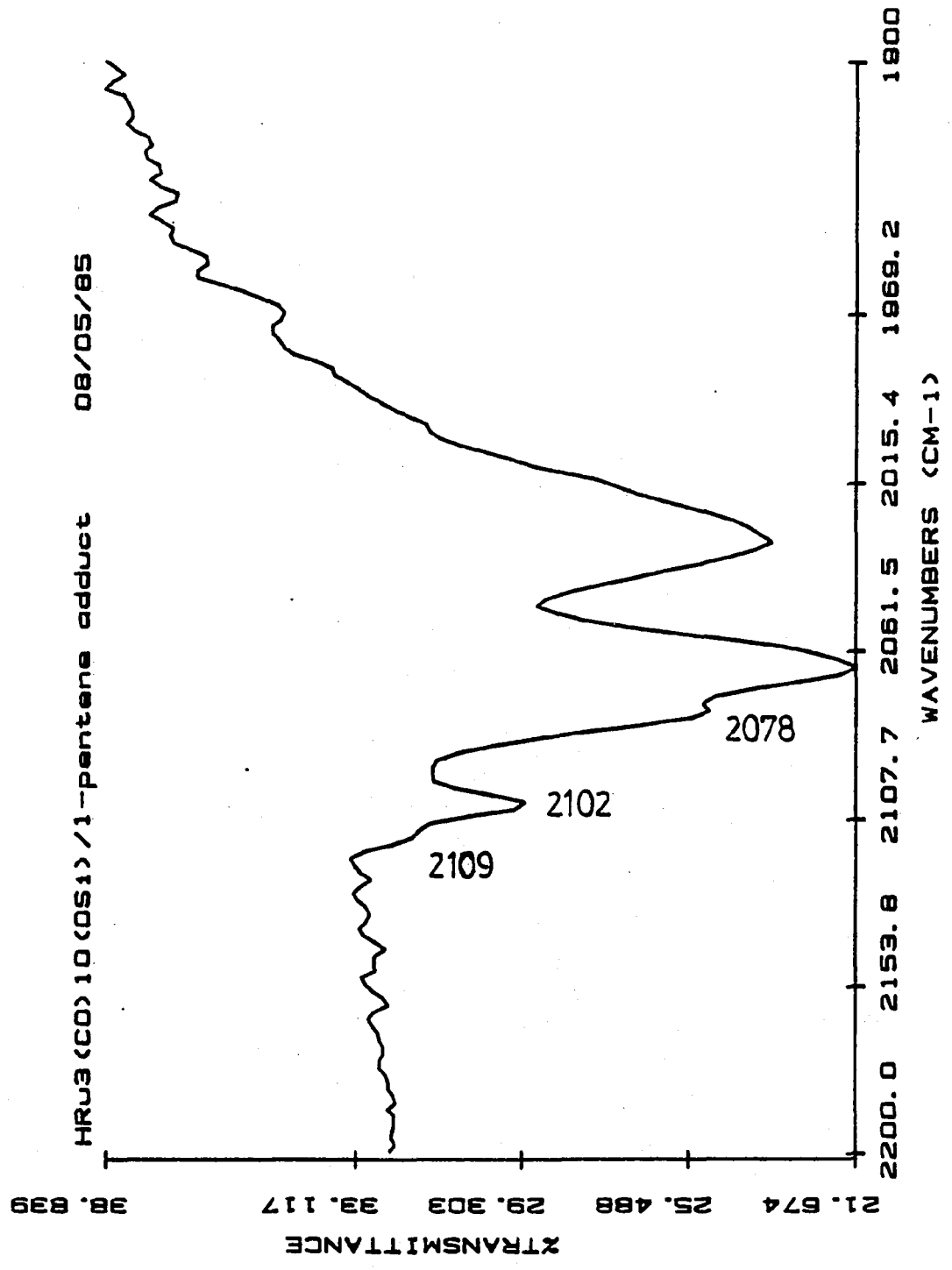

Fig. 53. Reaction of chemisorbed ruthenium trimer with 1-pentene (IR)

However, the complexity of the product IR spectrum and the different rates of growth of the IR bands suggest the formation of a number of substituted product. A 350 nm photolysis of the deaerated pentane solution containing equimolar amounts of the trimer and phenylsilanol cause a rapid loss of the 395 nm absorption of the starting material. IR spectra show a decline of trimer bands and formation of weak bands at 2140, 2071, and 2003 cm^{-1}. No bands indicative of the 330 nm species are observed either in the IR or the UV-visible. A continued photolysis results in the development of an intense absorption at 440 nm without the appearance of any new features in the infrared, which eventually becomes featureless in the CO region (Figure 54). Tetrahydrofuran, THF, and 1,4-dioxane were two other ligands used in the attempt to gain insight into the formation of the oxidative addition species. If THF is reacted with $Ru_3(CO)_{12}$ at temperature up to 50°C a rapid loss of intensity at 395 nm is observed. The baseline in the visible region of the spectrum increases linearly with reaction time but without the appearance of any prominent features. A well defined isosbestic point at 470 nm is maintained through > 50% of the reaction (Figure 55). In the infrared a general decline of the bands in the carbonyl region is observed. The rate of disappearance for the trimer bands approximates the rate of appearance of the broad $Ru_3(CO)_{12}$/THF feature at 1978 cm^{-1} (Figure 56). For

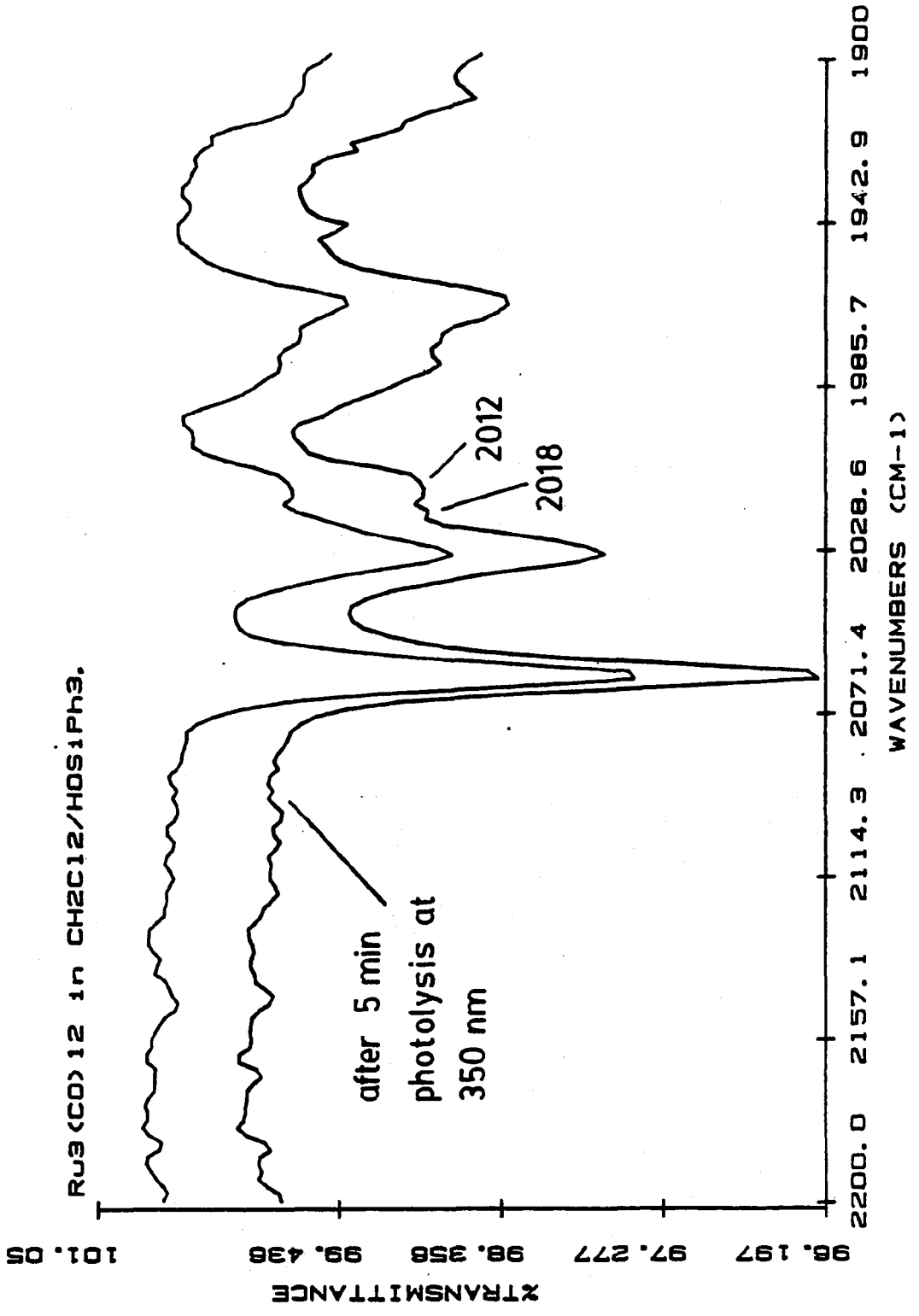

Fig. 54. Reaction of $Ru_3(CO)_{12}$ with $HOSiPh_3$ (IR)

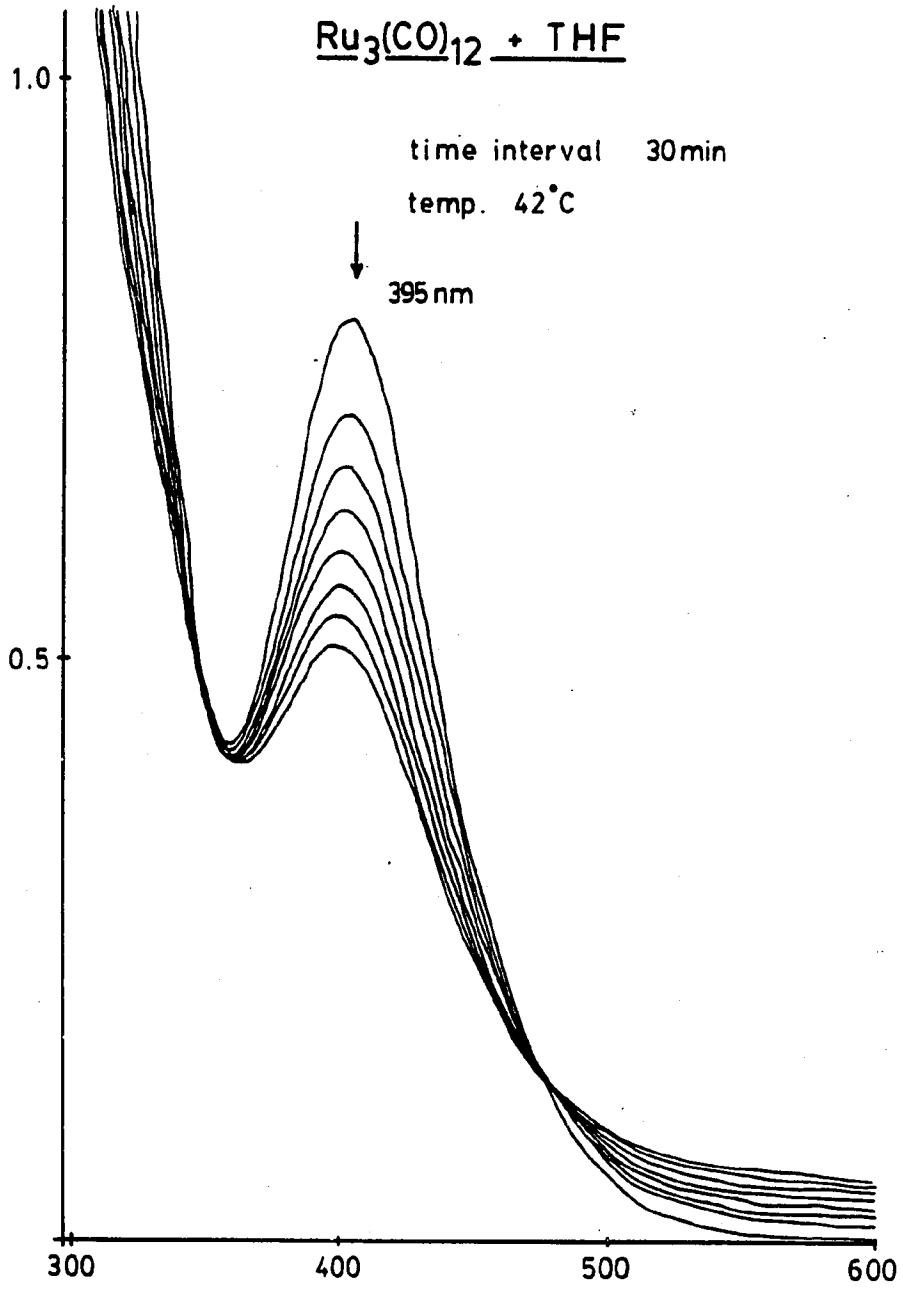

Fig. 55. Reaction of $Ru_3(CO)_{12}$ with THF (UV-vis)

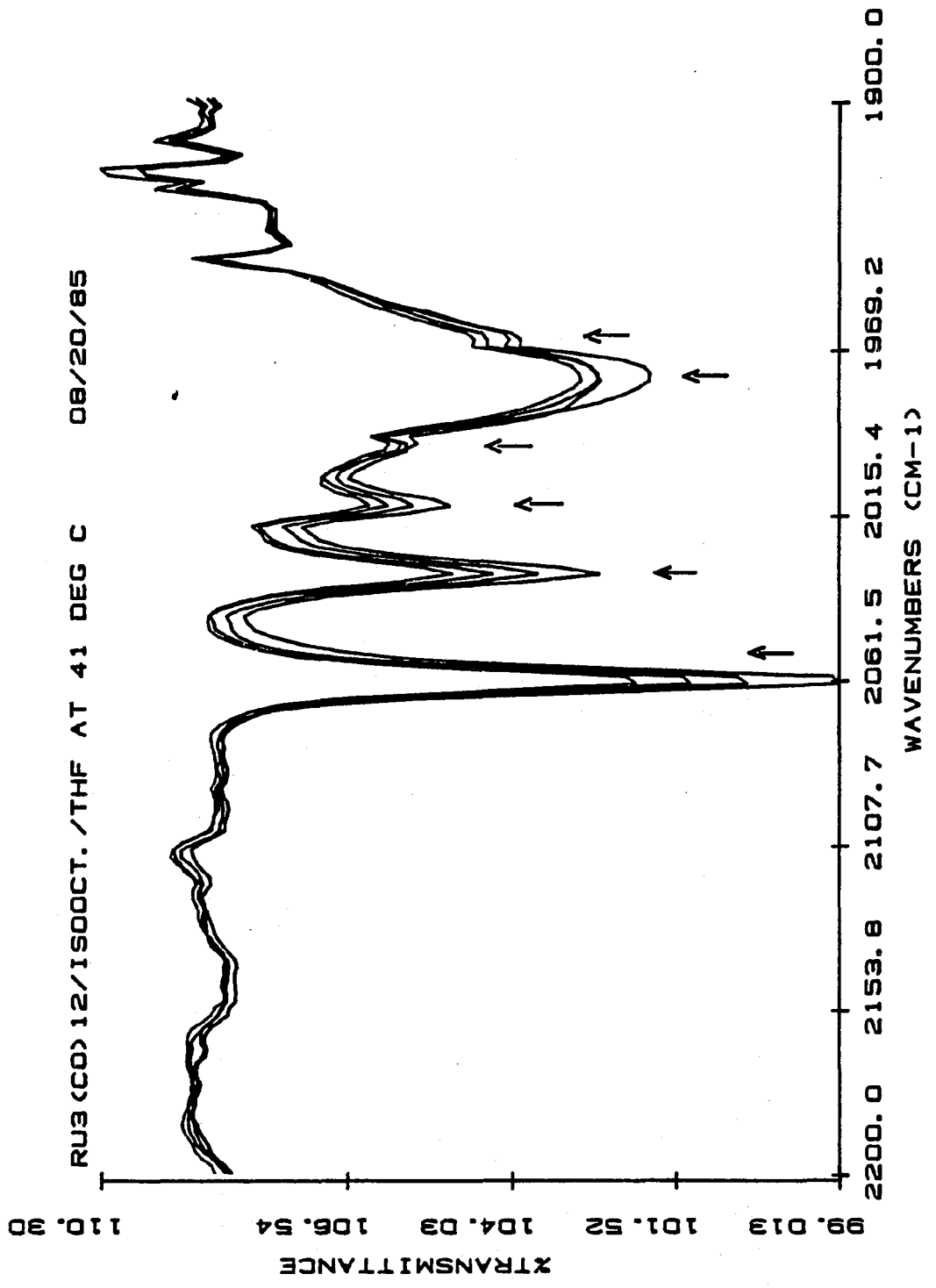

Fig. 56. Reaction of $Ru_3(CO)_{12}$ with THF (IR)

L = 1,4-dioxane the 395 absorption, characteristic of $Ru_3(CO)_{12}$, also diminishes but no increase in absorbance is observed in the UV or visible region of the spectrum (Figure 57). The IR spectrum shows a decline of the trimer bands and new absorptions at 2135 (w,br), 2089 (w), 1988 (s), 1960 (ms), and 1899 cm^{-1} (m) (Figure 58).

Significant similarities, however, exist between the reaction of $Ru_3(CO)_{12}$ on the surface of PVG and its reaction with ethanol in homogeneous fluid solution. Photolysis of a pentane solution, 10^{-4} M in ruthenium cluster and 10^{-1} M in EtOH, in a Rayonet reactor with UV light (wavelength $\leq$ 350 nm) shifts the lowest energy absorption of the trimer from 395 nm to 330 nm (Figure 59). New IR bands appear at 2125 (w,br), 2089 (w,br), and 1973 cm^{-1} (vw,br) but cannot be assigned to a single species with a sufficient degree of certainty. The quantum efficiency of the reaction is extremely low ($<<10^{-2}$) and the conversion appears to consist of several steps, the first being characterized by a decrease in absorbance at 395 nm without development of the 330 nm feature. If $P(t\text{-}Bu)_3$ is added to a solution which contains the 330 nm product from ethanol, an immediate color change from light yellow to orange red is observed. UV visible spectroscopy reveals the presence of a new band at 470 nm, known from the spectrum of $Ru_3(CO)_9(P(t\text{-}Bu)_3)_3$ (Figure 52a). This spectroscopic result differs from the spectrum obtained after addition of butyl

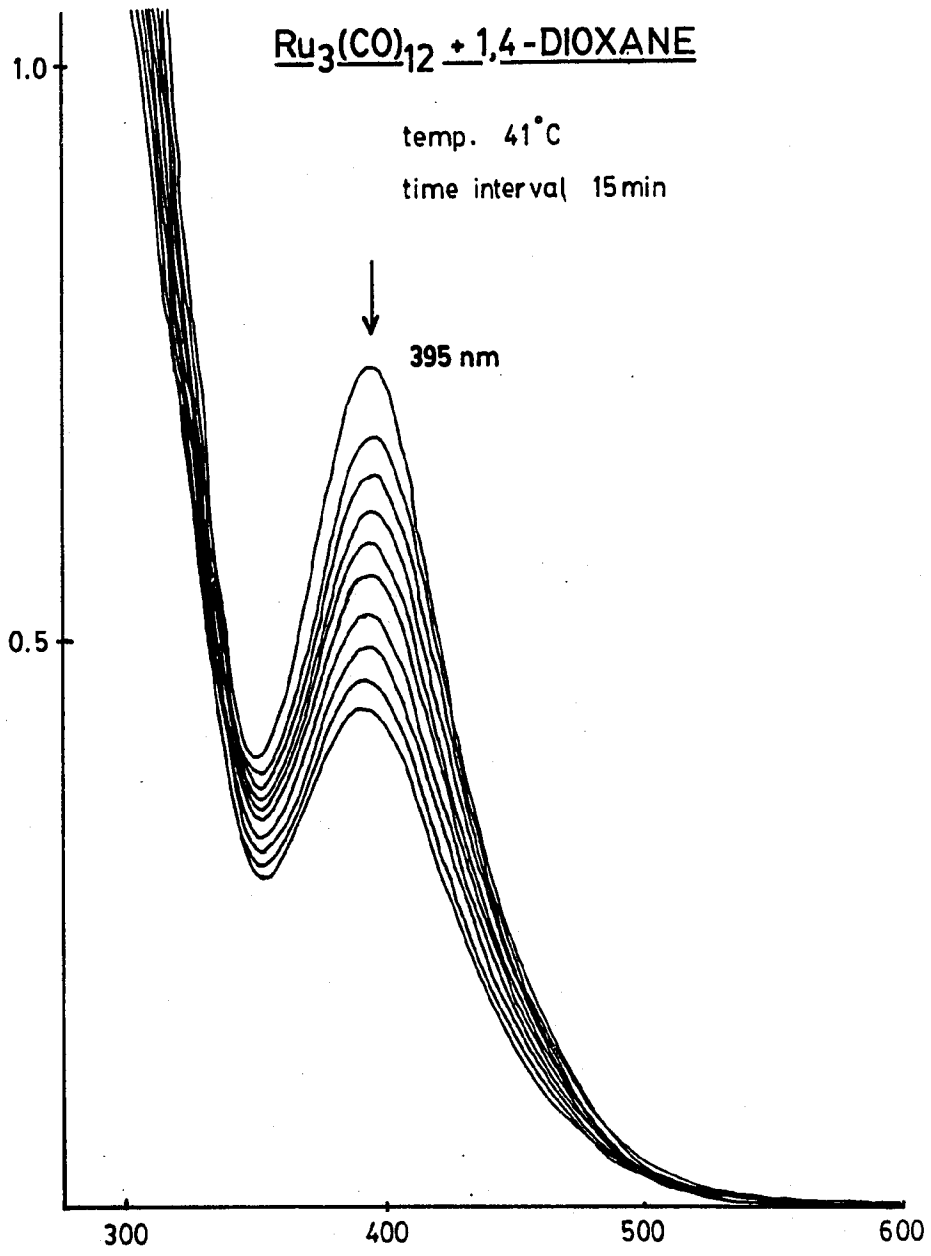

Fig. 57. Reaction of $Ru_3(CO)_{12}$ with dioxane (UV-vis)

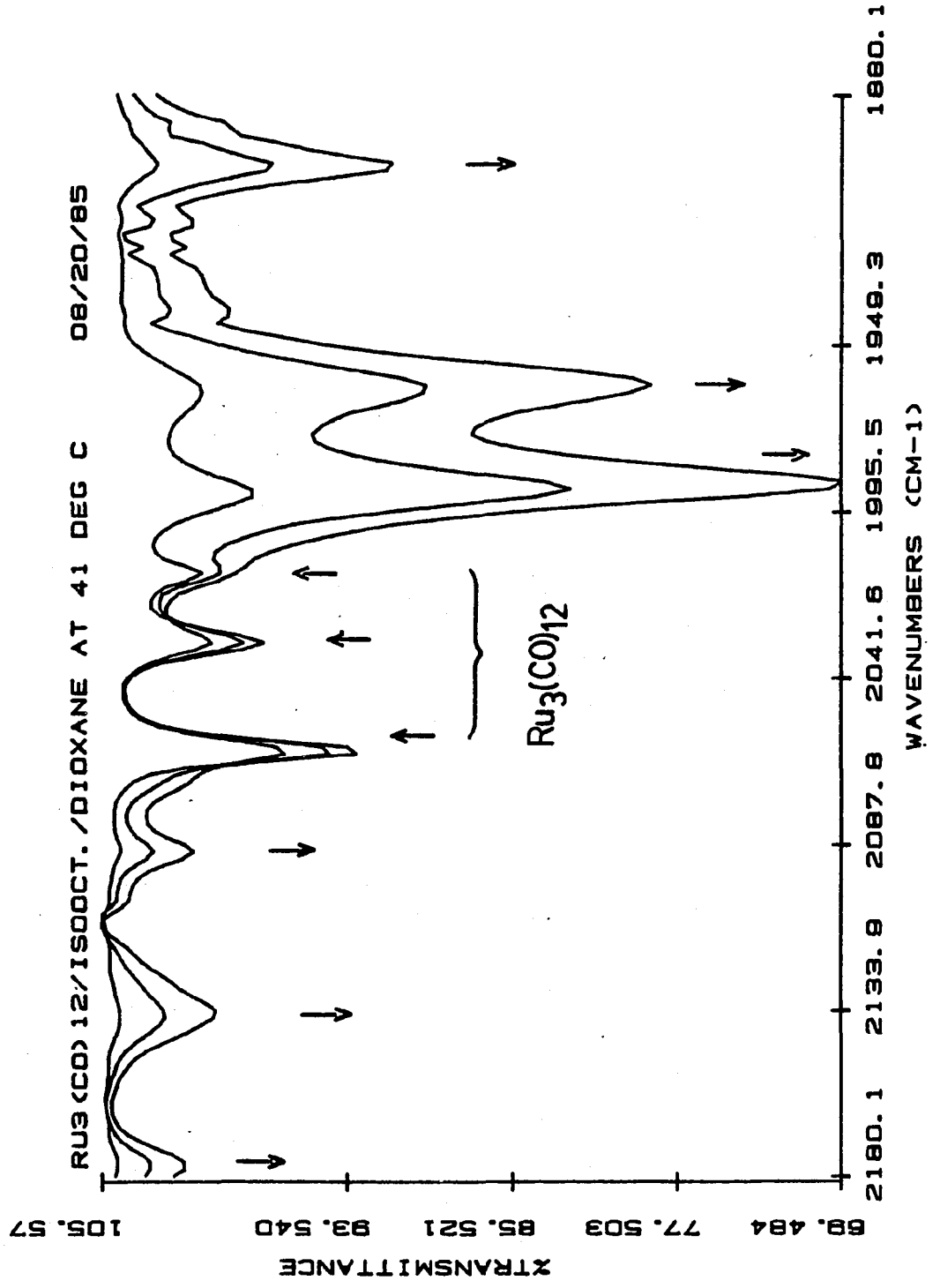

Fig. 58. Reaction of $Ru_3(CO)_{12}$ with dioxane (IR)

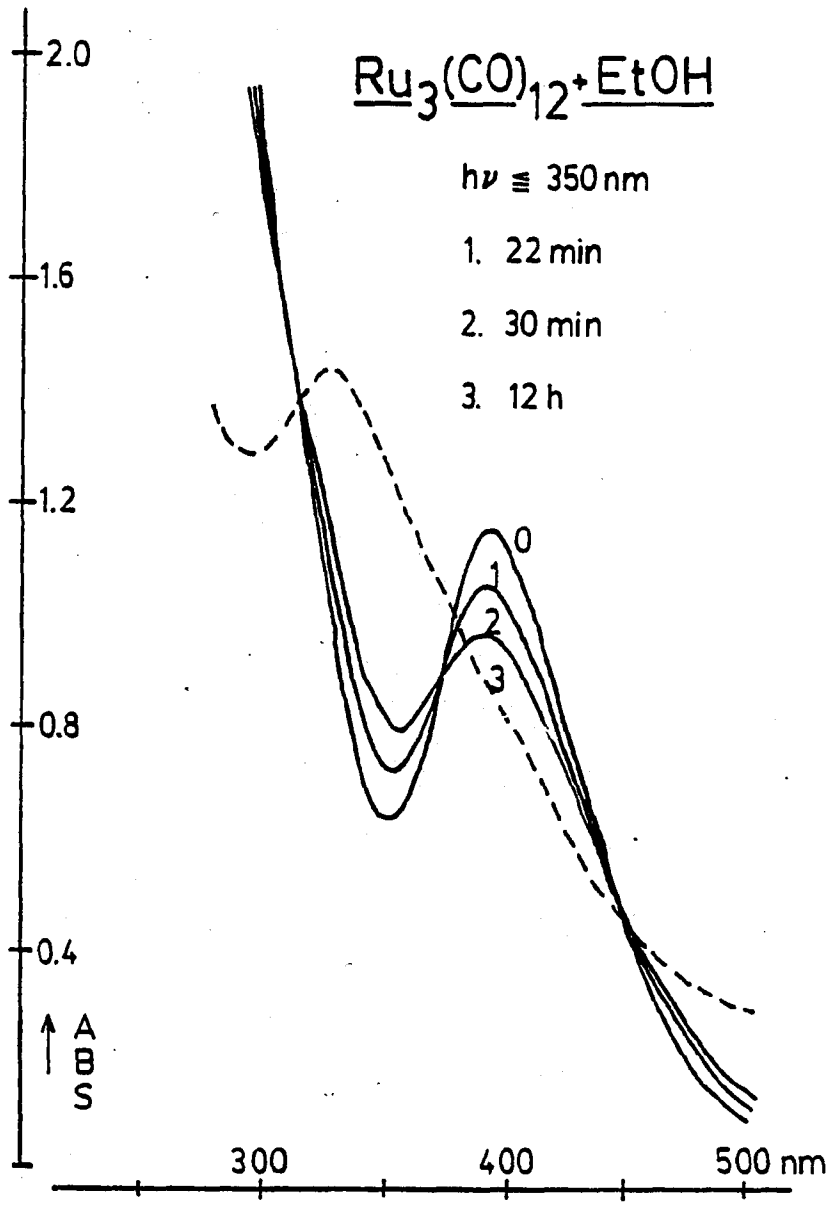

Fig. 59. Reaction of $Ru_3(CO)_{12}$ with EtOH (UV-vis)

phosphine to $HRu_3(CO)_{10}(OSi\equiv)$/PVG (Figure 52b).

3.4. SUPPORTED SUBCARBONYLS / Ru-OXIDES

If $Ru_3(CO)_{12}$ or $HRu_3(CO)_{10}(OSi\equiv)$ under vacuum (10^{-3} torr or better) is photolyzed with 254 nm light for a prolonged period of time (> 12 hours) all IR bands indicative of ruthenium cluster species disappear from the spectrum. Two new bands are observed in the 1900 to 2200 cm^{-1} region at 2074 (m,br) and 2006 cm^{-1} (w,br) (Figure 60). Upon admission of oxygen a third weak band appears at 2136 cm^{-1}. If the ruthenium trimer is photolyzed

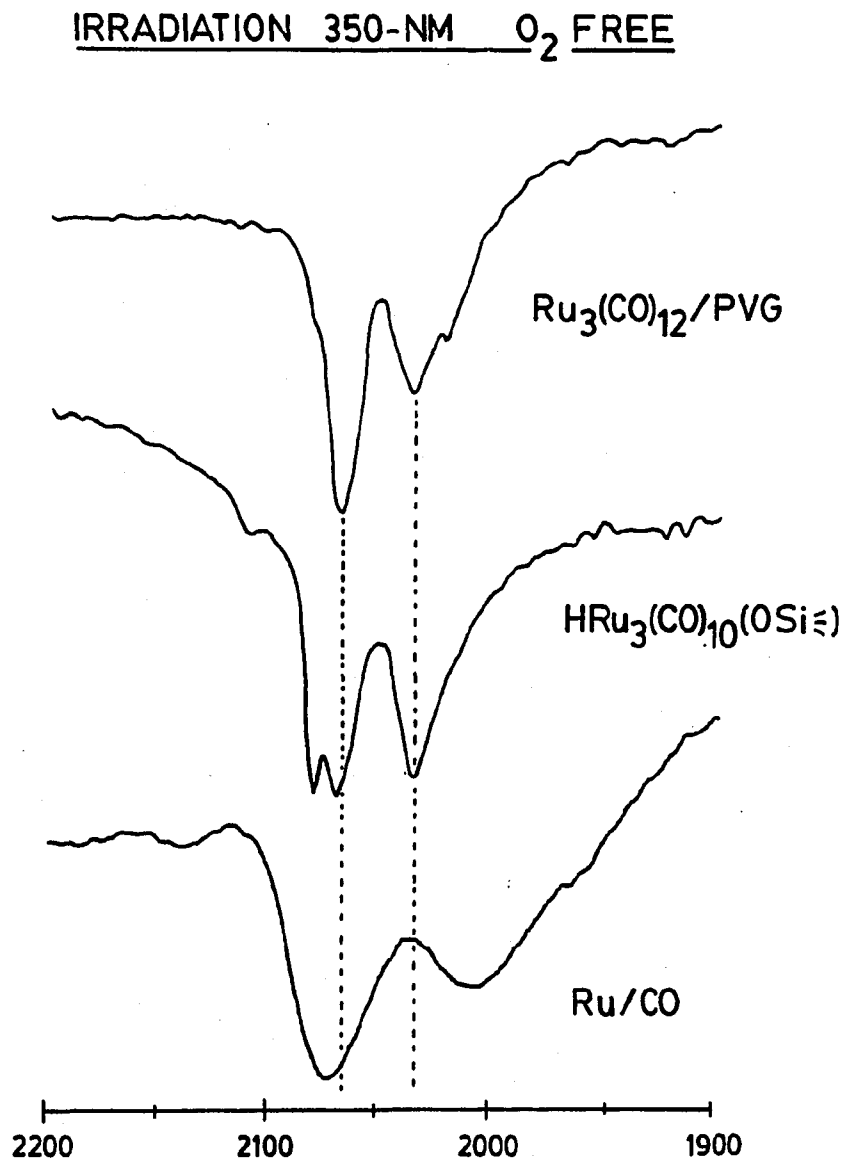

Fig. 60. Photolysis of $Ru_3(CO)_{12}$.ads in vacuum

in the direct presence of 50 torr of O_2, a broad band at 2136 cm^{-1} is formed in addition to the known bands of the chemisorbed ruthenium trimer (Figure 61).

3.5. REDUCTION OF SUPPORTED RUTHENIUM SPECIES

PVG-supported ruthenium dodecacarbonyl was reduced in the high vacuum chamber of the FTIR with a hydrogen flow of 10 ml/min at 200°C. A continuous loss of intensity is observed for the three IR bands of the trimer until they totally disappear from the spectrum. Re-admission of carbon monoxide generates a single band at 2031 cm^{-1} whereas after admission of a CO/O_2 mixture four bands can be observed at 2136 (w), 2074 (w-m,br), 2031 (m), and 2006 cm^{-1} (sh). A comparable result is obtained if either $HRu_3(CO)_{10}(OSi\equiv)$ or the Ru/CO oxide species are use as starting material for the reduction (Figure 62).

3.6. ADDITIONAL SPECTROSCOPIC TECHNIQUES

Ruthenium NMR is a viable tool for probing structural characteristics of ruthenium compounds (159,160). ^{99}Ru, natural abundancy 12.72%, is preferably selected as target nucleus since it has a lower quadrupole moment than ^{101}Ru with a natural abundancy of 17.07%. The resonance of $Ru_3(CO)_{12}$, reported at -1208 ppm vs. RuO_4 (160), is expected

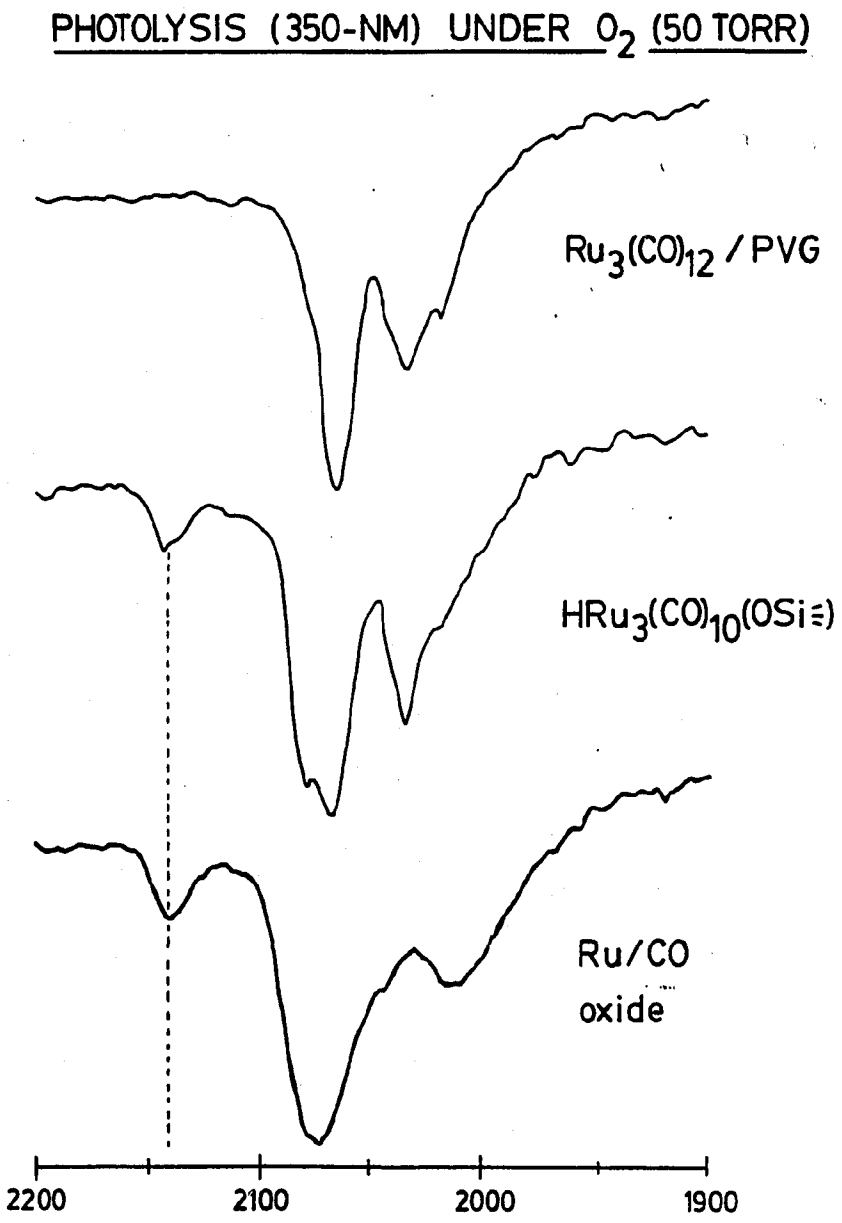

Fig. 61. Photolysis of $Ru_3(CO)_{12}$.ads under O_2

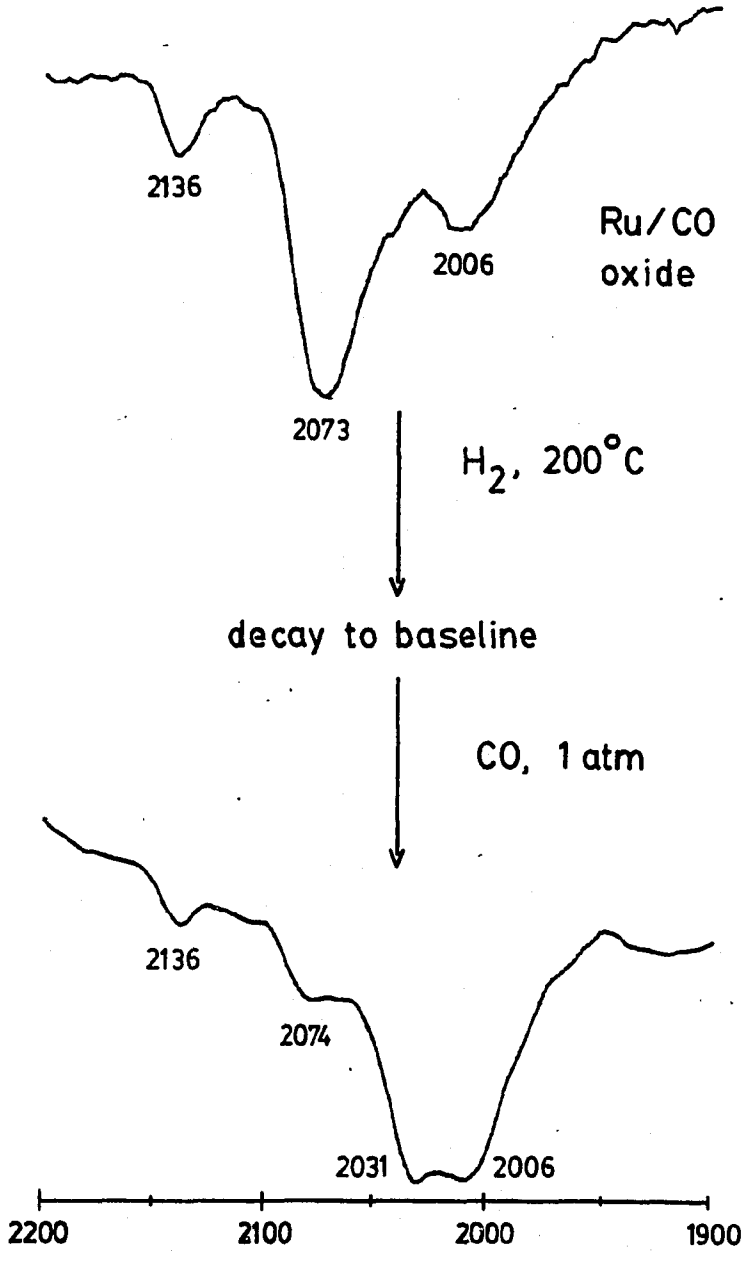

Fig. 62. Admission of CO/O_2 to reduced Ru/PVG

to shift to higher frequencies as the oxidation state of the metal atom increases during the course of an oxidative addition reaction. In order to observe ^{99}Ru or ^{101}Ru on a 200 MHz NMR instrument the spectrometer must be tuned to 6.78 MHz or 9.8 MHz respectively. Unfortunately only a 8 - 29 MHz broad band probe was available for this low frequency region. No characteristic spectrum could be measured at 9.8 MHz and attempts to re-tune the probe to 6.78 MHz were unsuccessful. The use of ^{13}C NMR allows the direct observation of the carbon in $Ru_3(CO)_{12}$ (161,162). As a consequence of the low solubility of the ruthenium trimer in hydrocarbons even the average of several thousand scans does not produce a clear signal. Chlorinated solvents offer a higher solubility but lack the required inertness towards the cluster. The use of ruthenium carbonyl with isotopically labelled carbon might have solved the sensitivity problem but was not attempted at this time.

3.7. REACTIONS OF $RuHCl(CO)(PPh_3)_3$

$RuHCl(CO)(PPh_3)_3$ is obtained in form of a beige, air-stable powder. It is insoluble in aliphatic hydrocarbons but readily dissolves in benzene yielding a deep yellow and very air sensitive solution. Photolysis of phosphine monomer in benzene with 350 nm light causes the expected color change to violet and produces to new maxima in the visible region of the spectrum at 470 nm and 520 nm,

indicative of the formation of $RuHCl(PPh_3)_3$. Attempts to impregnated porous Vycor glass with the complex from deaerated benzene solution were unsuccessful. Over a periode of several hours the solution darkened and a tinted PVG plate without any characteristic UV-vis absorptions was recovered after impregnation. Shorter impregnation times and the sublimation of the complex onto powdered PVG at 80°C did not produce any features in the optical or vibrational spectrum which could be attributed to an adsorbed metal complex.

3.8. CATALYTIC REACTIONS

Dehydrated porous Vycor glass promotes the isomerization of 1-pentene to cis- and trans-2-pentene at elevated temperatures and with a low rate constant. At 60°C and over a period of 3 hours, 300 mg of PVG convert 4.1±0.3% of a 10 ml mixture of 160 torr 1-pentene in N_2 to the 2-pentene isomers. The observed cis- to trans-isomer ratio is 1 : 1.3 and thus lower than the thermodynamic ratio of 1 : 3.2. At room temperature no activity is observed for blank PVG or for $Ru_3(CO)_{12}$ physisorbed on PVG. However, if the chemisorbed trimer, $HRu_3(CO)_{10}(OSi\equiv)$, is photochemically generated from its $Ru_3(CO)_{12}$.ads precursor and then charged with 1-pentene, the system catalytically converts the substrate to cis- and trans-2-pentene. GC analysis of the gas phase above the supported catalyst again shows a

deviation from the expected thermodynamic ratio of 3% 1-pentene, 23% cis-2-pentene, and 74% trans-2-pentene. For photochemically catalyzed reactions a cis- to trans-2-pentene ratio in the order of 1 : 5 is observed whereas the ratio for thermally catalyzed reactions stays within the thermodynamic limits of 1 : 3.

3.8.1. IN SITU INFRARED ANALYSIS

If 1-pentene is admitted at room temperature into an evacuated cell containing porous Vycor glass a disappearance of the free silanol band at 3745 cm^{-1} is observed and new IR bands due to the olefin are identical to those found in fluid solution. The admission of 1-pentene has no apparent effect on the IR spectrum of the physisorbed ruthenium trimer, $Ru_3(CO)_{12}$.ads, on the surface of the glass. However, if the 330 nm species is generated prior to the addition of olefin, its characteristic IR pattern with a weak band at 2109 cm^{-1}, two relatively intense bands at 2078 and 2069 cm^{-1}, and a broad band at 2034 cm^{-1} changes immediately (Figure 53). The intensity of the two high frequency bands decreases, the band at 2069 cm^{-1} shifts to 2066 cm^{-1} and the 2034 cm^{-1} band shifts to 2028 cm^{-1}. In addition a new IR absorption is observed at 2102 cm^{-1} and its intensity increases from weak to medium as the 2078 cm^{-1} band of the 330 nm species is progressively reduced in size. Gas chromatographic analysis of the vapor

phase does not indicate any ejection of CO from the cluster and removal of 1-pentene by evacuation quantitatively regenerates the bands characteristic of the 330 nm species. At room temperature the ruthenium cluster/olefin adduct is stable and no change in the IR spectrum is observed over a periode of several days. Optical analysis of PVG supported $HRu_3(CO)_{10}(OSi\equiv)$ after admission of 160 torr 1-pentene shows that no new features develop in the visible or UV range although the 330 nm band is reduced to ca. 50% of its initial intensity.

Thermal activation: Thermal activation of the adduct at temperatures between 40 and 150°C partially regenerates the 330 nm species as characterized by the IR-spectrum; however, side-reactions ultimately lead to a poorly resolved spectrum with an intense broad band at 2068 cm^{-1} and a broad feature centered at 2004 cm^{-1} (Figure 63).

Photochemical activation: UV photolysis with a 254 nm penlamp reduces within minutes the amount of olefin adduct by approx. 20% and regenerates an equal amount of 330 nm species. Continued photolysis causes a complete loss of the band at 2102 cm^{-1} and formation of a new broad feature centered at 2000 cm^{-1} in addition to the bands characteristic of the 330 nm species. Photolysis of the adduct with 350 nm light also regenerates 10-20% of the starting material but does not induce any further decomposition of the olefin adduct or the chemisorbed ruthenium

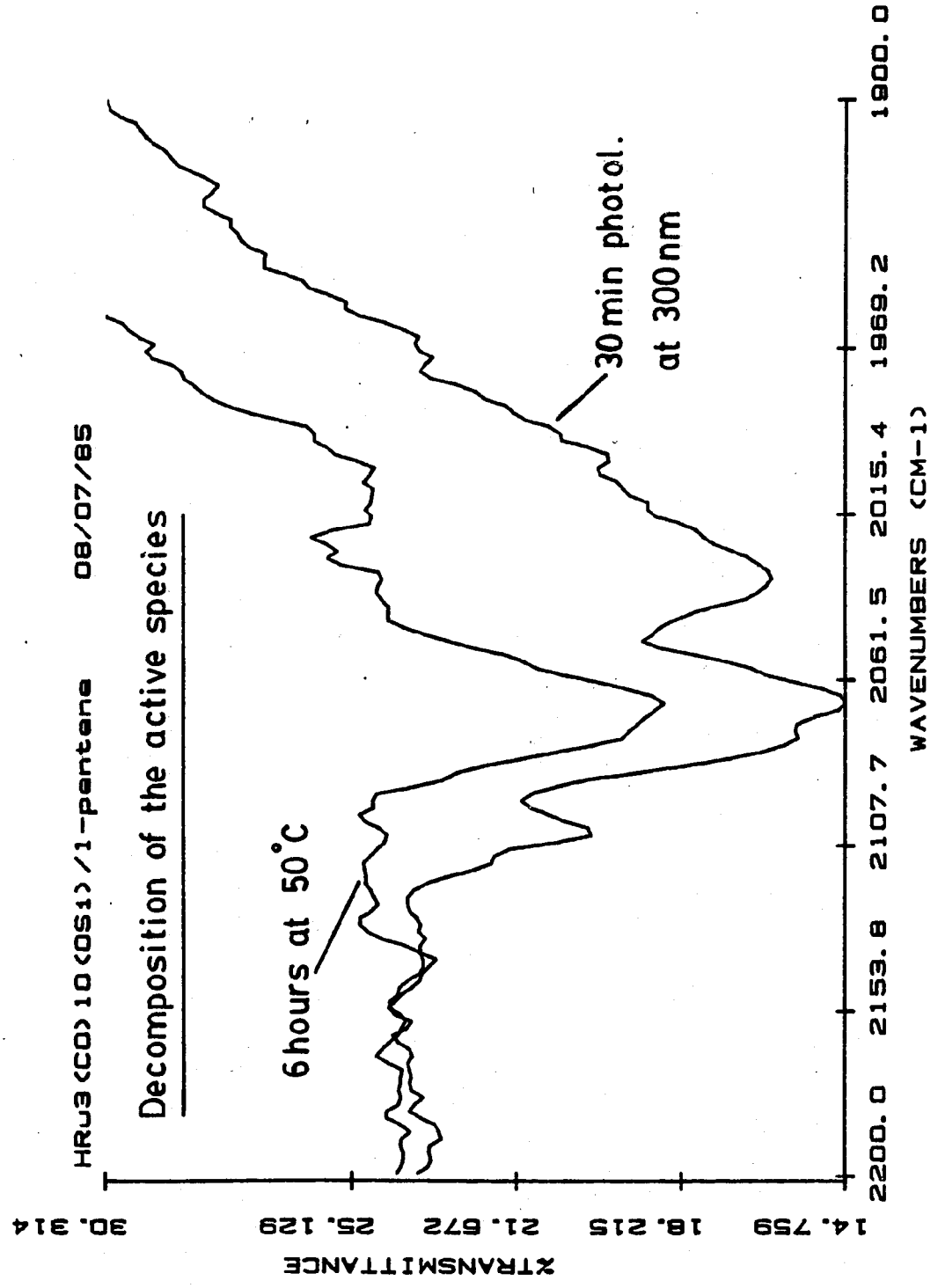

Fig. 63. IR spectrum after thermal activation of the $HRu_3(CO)_{10}(OSi\equiv)$/1-pentene adduct

cluster, characterized by its 330 nm absorption.

3.8.2. GAS CHROMATOGRAPHIC ANALYSIS

Gas chromatography was used to assess whether a supported ruthenium species was catalytically active and to determine the turnover number (Figure 64). In this context the turnover number denotes the number of isomerized substrate molecules divided by the number of ruthenium clusters per unit time. 1-Pentene in contact with powdered or plate PVG at temperatures up to 60°C or under photolytic conditions was isomerized to less than 2%. At room temperature $Ru_3(CO)_{12}$.ads on PVG did not catalyze any detectable isomerization over 4 hours and the isomerization due to $HRu_3(CO)_{10}(OSi\equiv)$ was limited to 1-2% over the first 30 minutes and 40% over a period of 7 days. The ratio of cis-2-pentene to trans-2-pentene, hereafter called c:t, for thermal isomerizations varied from 1:1.2 in the early stages to 1:2.5 for 40% conversions. As expected, heating the $HRu_3(CO)_{10}(OSi\equiv)$ / 1-pentene starting material to 50°C significantly improved the conversion rate with c:t appearing close to the thermodynamic ratio of 1:3. Photolysis of the reaction system with 254 nm light in the HVC of the IR instrument yielded a conversion of 0.6% with a c:t ratio of 1:5.2±0.3 after 30 minutes. If an excitation wavelength of 350 nm is used, 20% of the olefin molecules are isomerized

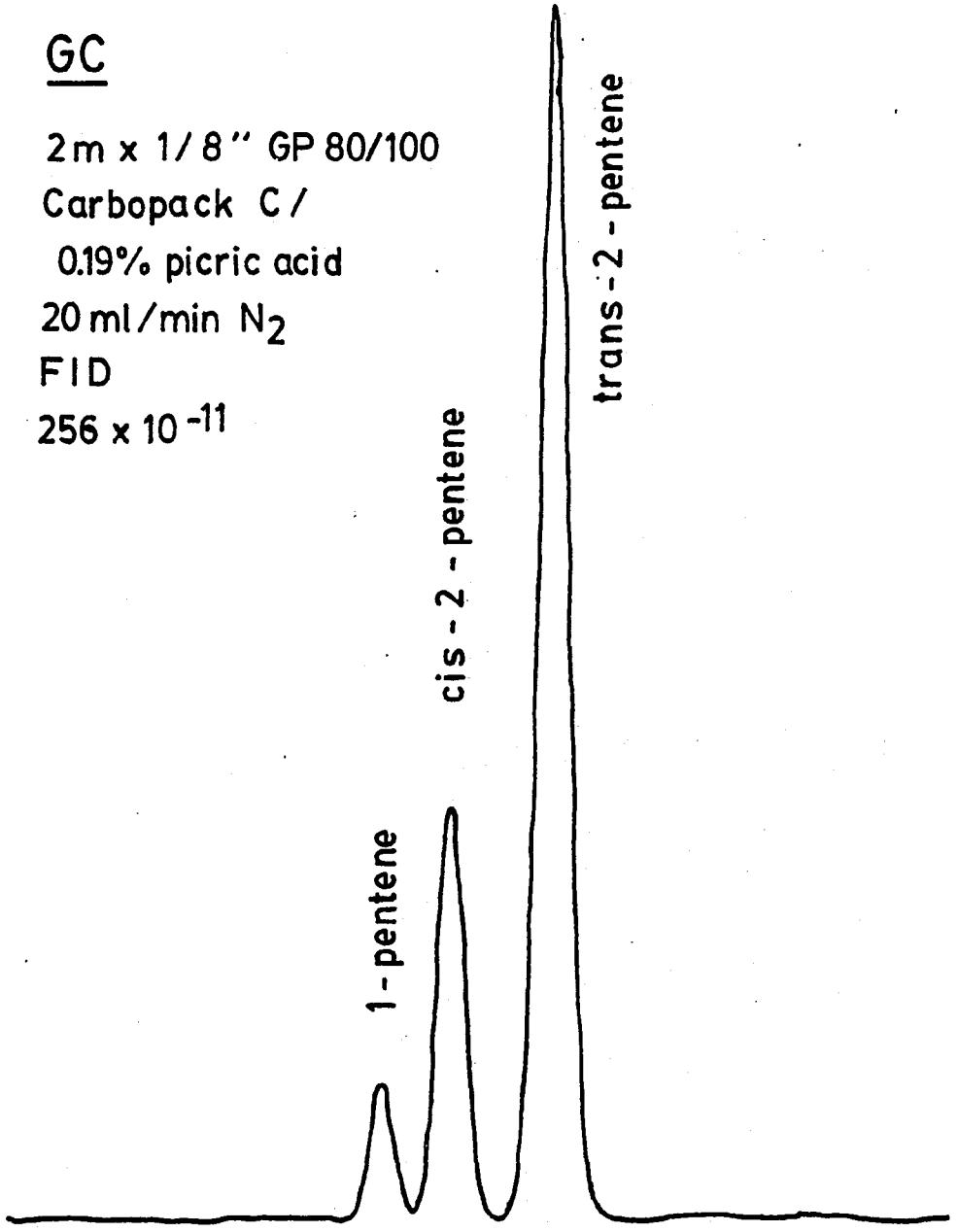

Fig. 64. Gas chromatogram of pentene after isomerization

within 30 minutes and 60% over a total photolysis time of 16 hours, yielding a turnover number in excess of 400. Removing the olefin by evacuation and recharging the reaction cell with fresh 1-pentene restores the catalytic activity of the supported species. The reaction system can be cycled between the two clearly defined molecular states which are characterized by their respective IR spectrum.

4. DISCUSSION

In the introduction to this thesis I pointed out that the primary focus of this work was the thermochemistry and the photochemical behavior of PVG-supported $Ru_3(CO)_{12}$ and its derivatives. Because of conflicting experimental results and interpretations reported in the literature regarding silica-supported ruthenium carbonyls (78,85,86, 163) and through inital reproducibility problems with results obtained in this laboratory, we became quickly aware of the need to improve our understanding of the chemical and spectroscopic properties of the support and to develop a standardized and non-destructive sample handling procedure. It also became apparent that we had to study the reactions of $Ru_3(CO)_{12}$ in fluid solution and obtain quantitative data such as quantum yields, rate constants, and energies of activation in order to realize differences between the chemistry of the cluster in homogeneous solution and supported on PVG. Special emphasis was placed on reactions of the ruthenium trimer with ligands having oxo- or hydroxo-group-coordinating moieties for their capability to model the interactions with the surface of the porous glass. Finally we used a typical isomerization reaction to discover the catalytic activity of the adsorbed species and to characterize its active form. Here it was not our goal to develop an industrially viable process or even to optimize a specific catalytic reaction but rather to locate possible

differences between the thermally activated catalysis and the photoinduced catalysis by PVG-supported ruthenium carbonyl.

4.1. REACTIONS IN FLUID SOLUTION

Thermal reactions: It is well known that the stability of the metal-to-metal bond in transition metal clusters increases with the period number. Whereas at 25°C $Fe(CO)_5$ is stable in liquid form, $Ru(CO)_5$ readily reacts to regenerate the trimeric species. Correspondingly, the phosphine substituted monomer $Ru(CO)_4PPh_3$ is thermally labile towards formation of $Ru_3(CO)_9(PPh_3)_3$ (Figure 5).

The reactivity of $Ru_3(CO)_{12}$ towards photosubstitution with PPh_3 has been known for several years and the photoinert character of the Ru-PPh_3 bond has been reported. In contrast to previous studies (62), which report the formation of mono and disubsituted ruthenium phosphines in the approximate ratio of 1 to 2, Figure 40 clearly shows that the monosubstituted monomer is the principal photolysis product in pentane.

$$Ru_3(CO)_{12} + 3PPh_3 \xrightarrow[\leq 400\ nm]{h\nu} 3Ru(CO)4PPh_3 + 3CO \quad (4)$$

The weak absorptions that are observed at 2098, 2047, 2014, 1986, and 1974 cm^{-1} during the photofragmentation of the ruthenium trimer closely match frequencies reported for

$Ru_3(CO)_{11}PPh_3$ and indicate the presence of small amounts of this monosubstituted trimer. We conclude that $Ru_3(CO)_{11}PPh_3$ serves as an intermediated between the trimer and the monosubstituted $Ru(CO)_4PPh_3$. As the solution concentration of $Ru(CO)_4PPh_3$ increases the disubstituted monomer, characterized by its strong IR absorptions at 1909 cm^{-1}, is produced according to the equation

$$Ru(CO)_4PPh_3 + PPh_3 \xrightarrow[\leq 400\ nm]{h\nu} Ru(CO)_3(PPh_3)_2 + CO \quad (5)$$

The color change observed during the photolysis reaction confirms the disappearance of the ruthenium cluster and the formation of mononuclear species which generally do not absorb in the visible region of the spectrum. Finally, the development of a pink solution color and a red precipitate point to the formation of $Ru_3(CO)_9(PPh_3)_3$, identified by its characteristic optical spectrum, which crystallizes as its concentration surpasses its low solubility in hydrocarbon solvents. The low reaction temperature of 25°C and the apparent induction period for the formation of the substituted ruthenium cluster, $Ru_3(CO)_9(PPh_3)_3$, are clear indications that the substituted trimer is generated from monomeric ruthenium species rather than by direct substitution of $Ru_3(CO)_{12}$ with PPh_3. We thus can formulate a thermal reaction, which is concurrent with the room temperature photodeclusterification and combines monomeric

units to the trisubstituted trimer $Ru_3(CO)_9(PPh_3)_3$ at a low rate.

$$3Ru(CO)_4PPh_3 \xrightarrow[25°C]{\Delta} Ru_3(CO)_9(PPh_3)_3 + 3CO \qquad (6)$$

If, however, the photoejected or thermally liberated CO is not purged from solution or if a solution containing $Ru(CO)_4PPh_3$ is saturated with carbon monoxide, a second thermal process competes successfully with the formation of $Ru_3(CO)_9(PPh_3)_3$. This new process regenerates the $Ru_3(CO)_{12}$ starting material as evidenced by the reappearance of its characteristic IR bands at 2061, 2031, and 2012 cm^{-1}. Since the rate constant for the second process, i.e. regeneration of $Ru_3(CO)_{12}$, is strongly dependent on the concentration of CO in solution, no $Ru_3(CO)_{12}$ was observed when CO was removed from the system, we must assume that the cluster formation occurs from a $Ru(CO)_5$ intermediate. This conclusion is supported by a control experiment where, under our experimental conditions and 1 atm of CO, $Ru_3(CO)_9(PPh_3)_3$ remained stabil towards substitution.

$$3Ru(CO)_4PPh_3 + 3CO \xrightarrow[> 30°C]{\Delta} 3[Ru(CO)_5] + 3PPh_3 \qquad (7)$$

$$3[Ru(CO)_5] \xrightarrow[-\ 3\ CO]{\Delta} Ru_3(CO)_{12}$$

The concentration of the $Ru(CO)_5$ intermediate is expected to be low since its absorptions do not appear in the infrared spectra. A thermal substitution of phosphine ligands in $Ru(CO)_4PPh_3$ complexes by CO has not been reported before and allows the entire reaction sequence to be cycled with a recovery rate of > 40%. The recovery of starting material is a function of the concentration of CO and is limited by the precipitation of $Ru_3(CO)_9(PPh_3)_3$ (Figure 65).

Quantum yield determination: In deaerated fluid solution, photoactivation of $Ru_3(CO)_{12}$ with light of ≤ 400 nm leads to population of a metal-metal σ^* orbital and fission of a Ru-Ru bond (65). In the presence of a ligand, L, the primary photoproduct, a cleaved trinuclear species, is scavenged to form monomeric, substituted complexes of the type $Ru(CO)_4L$. For all examined reactions, the quantum yield, ϕ_{obs}, depends strongly on the concentration of the scavenging ligand. This suggests that at sufficiently high ligand concentrations every primary photoproduct will be scavenged and ϕ_{obs} will approach a limiting value, the true quantum yield ϕ_t. Plots of $1/\phi_{obs}$ against $1/[L]$ are indeed closely linear and extrapolate to a value that places the quantum efficiency of metal-metal bond cleavage in $Ru_3(CO)_{12}$ at $> 7.3 \pm 1.1 \times 10^{-2}$ (Figure 43). The limiting yield in our experiment is independent of the reacting ligand and within experimental error of that reported by Poe and coworkers (67) using CO as the scavenging ligand. This lack of

Reactions of $Ru_3(CO)_{12}$ with PPh_3

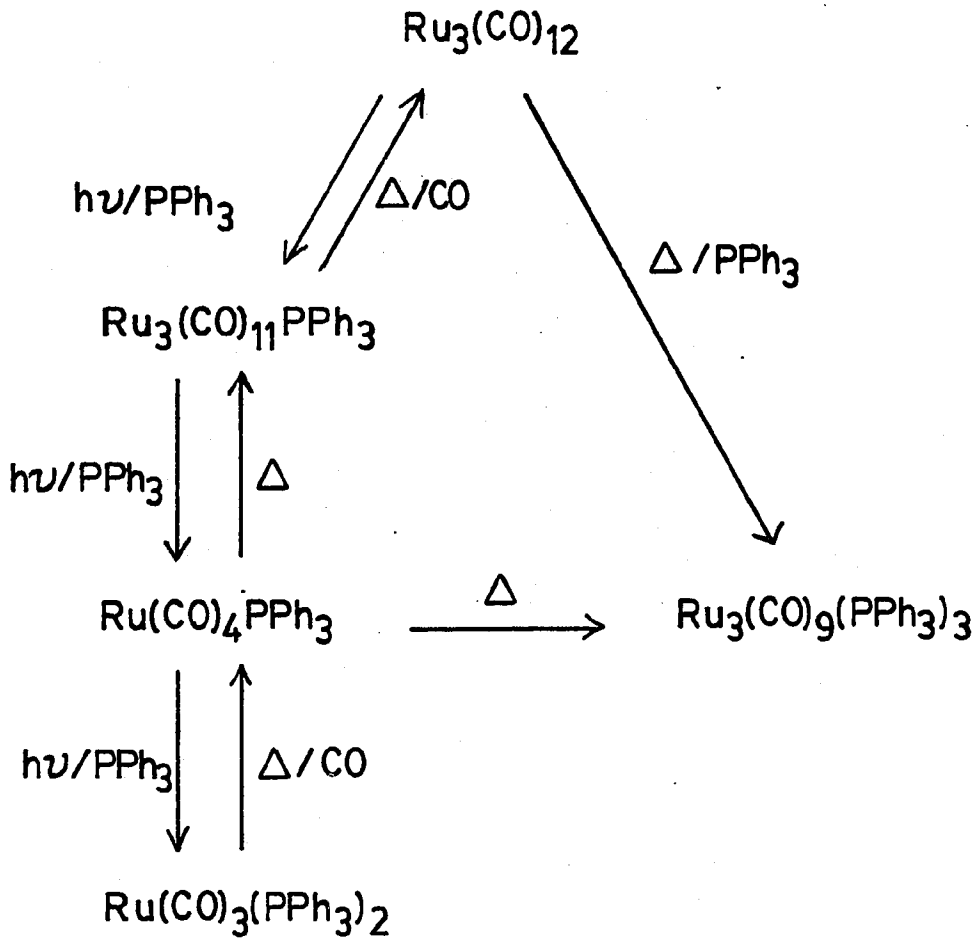

Fig. 65. Reactions of $Ru_3(CO)_{12}$ with PPh_3 in solution

dependence on the nature of the reacting ligand suggests that the relative inefficiency of product formation does not solely reflect a competition between scavenging and ring reclosure. Rather, the primary photochemical process is per se relatively inefficient, and for comparison with the adsorbed molecule, we place the quantum efficiency of Ru-Ru bond rupture following 350 nm excitation of the trimer in fluid solution at $\phi = 0.09 \pm 0.03$.

4.2. REACTIONS OF SUPPORTED $Ru_3(CO)_{12}$

The photoreactivity of $Ru_3(CO)_{12}$.ads reflects the chemical nature of the PVG surface and its dimensionality. The DRIFT spectrum of calcined PVG (Figure 30) indicates a surface consisting of individual silanol groups, a 3745 cm^{-1} band, and associated or hydrogen bonded groups, a shoulder at 3570 cm^{-1}. The presence of oxo functionalities on the surface of silica gels and PVG is known from the literature and accounts for the anionic character of these materials. Adsorption of $Ru_3(CO)_{12}$ onto PVG occurs without significant change in the electronic spectrum of the trimer (Figure 15). The vibrational bands resemble the absorptions found in fluid solution but show a shift of 2 to 6 wavenumbers to higher frequency (Figure 45). This similarity to UV-visible and IR spectra of the complex in solution as well as the absence of detectable decomposition products, such as CO, H_2, and CO_2, establish that absorption onto PVG

does not disrupt the metal triangle or the coordination about the metal atoms. Since the ruthenium atoms in the cluster are coordinatively saturated and well shielded by two axial and two radial CO's, one might infer that it adsorbs onto the support without any preferential orientation. A hydrogen bond-type interaction between surface silanol groups and one or more of the trimer carbonyls would polarize the carbon-oxygen bond in the ligand and account for the observed IR shift. However, close examination of the vibrational spectrum shows that the radial e'(b_1) vibration, which is a distinct, albeit a medium intensity band in fluid solution, is most affected by the interaction with the support. At low surface coverage the band is not noticeable in the spectrum, whereas at high cluster concentrations a weak absorption appears at 2018 cm^{-1}, the location of the radial e'(a_1) band in solution. In view of the anionic nature of the PVG surface, this may be due to a polarization within the cluster which reduces backbonding and electron density in the carbonyl π antibonding orbitals. It seems unlikely, however, that the polarization occurs through the metal triangle as proposed for the interaction of $Ru_3(CO)_{12}$ with thiol. This interaction would require an opening of the coordination sphere around the ruthenium atoms and affect the UV-visible spectrum. We summarize that, on the basis of infrared evidence alone it is not possible to pinpoint a specific interaction or to deduce a preferential orientation of the physisorbed

ruthenium cluster on the surface. Nevertheless, the close resemblance of the IR spectrum of PVG-supported ruthenium timer to spectra reported for $Ru_3(CO)_{12}$ on silica (86) and to the observed spectrum in $HOSiPh_3$-containing solutions (Figure 54) (Table V) lead us to conclude that this interaction must occur between cluster carbonyls and silanol functionalities which are common to both support materials and dissolved triphenylsilanol. However, any polarization of the cluster must be reversible since adsorbed $Ru_3(CO)_{12}$ can be extracted from the surface with chlorinated solvents, yielding the original spectrum with three distinct carbonyl bands.

It has been claimed in several reports that the adsorption of $Ru_3(CO)_{12}$ does not affect the intensity of the surface silanol vibration at 3745 cm^{-1}. Although we found similar results in the IR spectrum of PVG supported ruthenium trimer, these findings alone do not suffice to exclude an interaction of the adsorbed metal cluster with the surface hydroxyls. Assuming an average of 5 silanol hydroxyls per 100$Å^2$ for dehydrated PVG, a cluster radius of 5Å, and a surface coverage of 10% a calculation reveals that only 2% of all hydroxyls would be involved in an interaction with the metal species. For reasons of geometry it appears unlikely that more than two hydroxyls can be perturbed by a single cluster, limiting the decrease of the 3745 cm^{-1} band to < 4%. Changes of this magnitude, however, are difficult to detect since the intensity of the silanol band of the

sample is ratioed against a previously prepared reference that has not been subjected to the impregnation procedure.

The spectrum of $Ru_3(CO)_{12}$ on PVG does not show any correlation field splitting (intermolecular coupling (164)) which complicates the solid state spectrum of polycrystalline ruthenium dodecacarbonyl (Figure 46), and absorption spectra recorded at different locations on the same sample are within experimental error. We conclude that the trimer physisorbs onto porous Vycor glass and exists as individual molecular entities uniformly distributed over the support surface. Thus, changes in quantum efficiency or reaction pathway are not a consequence of molecular changes or distortions caused by adsorption.

Reactions of adsorbed $Ru_3(CO)_{12}$: In contrast to the reactions observed in fluid homogeneous solution, UV photolysis of $Ru_3(CO)_{12}$(adsorbed) under pressures of a scavenging ligand L does not produce monomeric, substituted complexes, i.e. $Ru(CO)_4L$. The trimer is stable under 1 atm of carbon monoxide and several hours of photolysis with 300 and 350 nm light as determined by UV-visible spectroscopy. We attribute this stability of the trimer to the restrictive environment that the cluster experiences on the surface. It is known from our investigation of the photoreactivity of $Ru_3(CO)_{12}$ in fluid solution, that the quantum efficiency of the metal to metal bond breakage is relatively low, $\phi = 0.09 \pm 0.03$. Bond reformation will be favoured for cluster species that are immobilized on rigid surfaces since

the free access of a coordinating ligand to the broken metal-metal bond is limited. More importantly, the surface support does not allow the cluster to twist or to open the metal triangle following the bond breakage. Thus the metal orbitals remain in a position which is favourable to ring reclosure and which will result in a decrease of the lifetime of the activated bond. An equal degree of photochemical stability for the physisorbed trimer is found towards L = phosphine or 1-pentene where the infrared spectrum shows no significant change under our experimental conditions.

Different observations were encountered for the substituted trimer $Ru_3(CO)_9(PPh_3)_3$.PVG. We were unable to achieve a significant surface concentration of ruthenium nonacarbonyl tris-triphenylphospine by impregnation from solution and had to resort to successive adsorption of PPh_3 and $Ru_3(CO)_{12}$ and to co-sublimation. Since both compounds are easily adsorbed on an individual basis we conclude that the lack of interaction of the bulky substituted trimer with surface silanol groups is caused by steric hindrance. In addition to their size, the cone angle of the three PPh_3 groups is 145° and much larger than the 95° cone angle of the carbonyl groups (Figure 66). An adsorbed phosphinated trimer will therefore experience a weaker interaction with surface silanol groups than the unsubstituted $Ru_3(CO)_{12}$ and will also be subject to bond strain in order to maintain

$Ru_3(CO)_9(PPh_3)_3$

EFFECT OF PHOSPINE CONE ANGLE

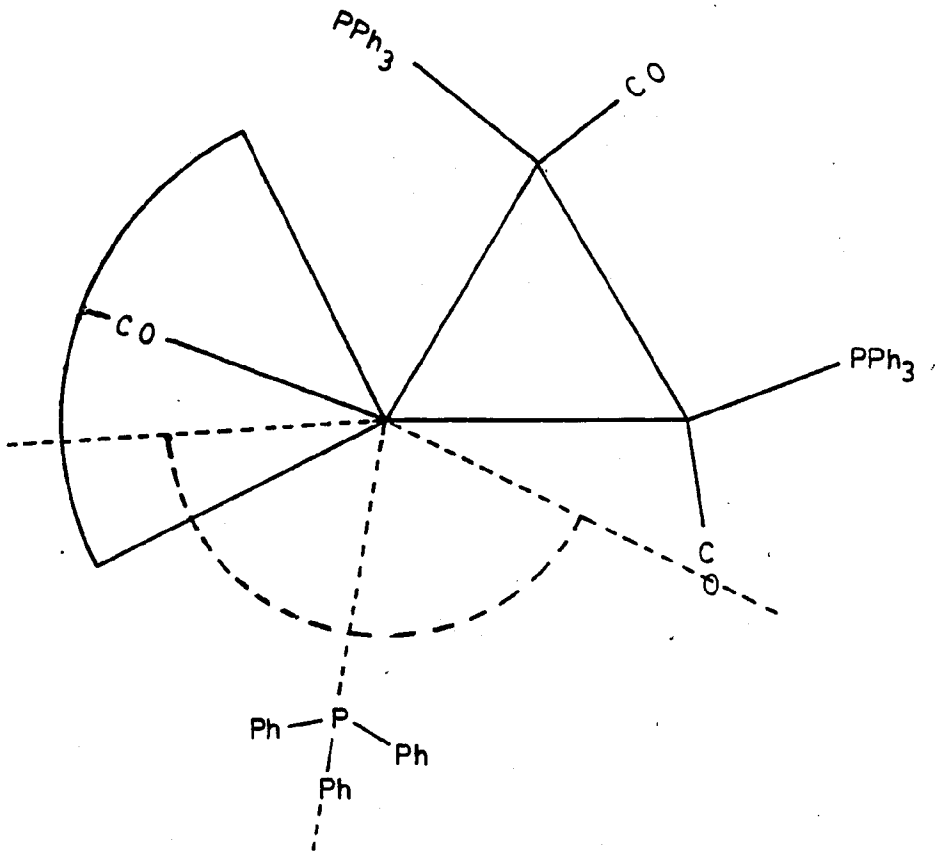

Fig. 66. Cone angles of phosphine substituted ruthenium carbonyl

this interaction. The energy required to introduce a strain into the cluster effectively precludes an adsorption from solution which is the observed experimental result. Co-sublimation and, to a much lesser degree, successive adsorption does yield the supported substituted trimer. In the latter case adsorption can be explained by the favourable energetics of phosphine substitution; the anchored phosphine replaces one or more carbonyl groups and curtails desorption of the substituted trimer into the solution phase. In the case of co-sublimation it is not possible to determine from our results whether the substitution occurs in the gas phase or whether successive sublimation of phosphine and cluster are responsible for the presence of $Ru_3(CO)_9(PPh_3)_3$ on the surface of PVG. Also, the formation of phosphinated ruthenium carbonyl crystals on the glass surface cannot be excluded since after several hours of sublimation at 60°C crystals of this red species are formed even on the surface of the quartz sublimation flask. Figure 67 clearly shows that the IR spectrum of the substituted cluster on PVG is very similar, albeit broadened, when compared to the spectrum of the species in fluid solution. The only striking difference is the narrow band at 2067 cm^{-1} in the spectrum of the supported trimer for which we have no explanation at this time. PVG-supported $Ru_3(CO)_9(PPh_3)_3$ does not show the same stability as supported $Ru_3(CO)_{12}$, since the intense red color fades in vacuum and the adsorbed

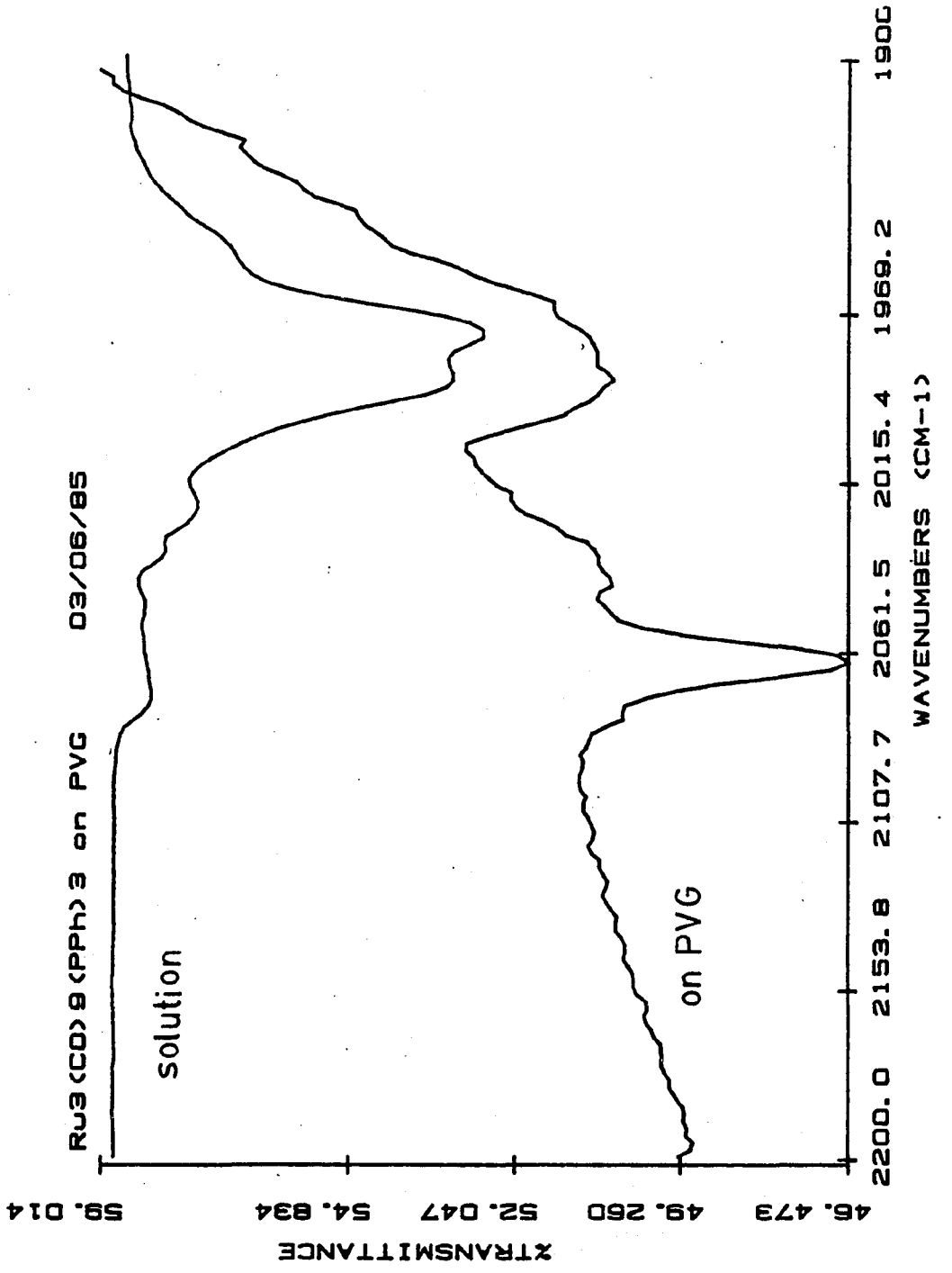

Fig. 67. $Ru_3(CO)_9(PPh_3)_3$ in solution vs. on PVG

cluster undergoes a photochemical reaction with carbon monoxide. The lack of new characteristic bands in the vibrational spectrum should be attributed to the formation of several products, but can also be explained with the poor infrared response of phosphine-substituted clusters. On the basis of the preceding discussion it is therefore reasonable to deduce the presence of strained $Ru_3(CO)_9(PPh_3)_3$ on the surface of PVG, evidenced by the broadened IR features. In contrast to the supported $Ru_3(CO)_{12}$, the strained, phosphine substituted cluster readily reacts with ligands to form monomeric and/or dimeric subcarbonyls.

Chemisorbed ruthenium trimer: In the absence of an external ligand such as CO, olefin, or phosphine, the photochemically-activated physisorbed $Ru_3(CO)_{12}$.PVG undergoes a reaction with the surface of the porous Vycor glass resulting in the disappearance of the 395 nm band and the development of an absorption at 330 nm (Figure 47). This modification of the optical spectrum is indicative of a chemisorption of the trimer on the surface since it signals intrusion into the primary coordination sphere of the metal. Two isosbestic points at 295 and 365 nm are present through > 80% of the reaction and indicate the absence of a significant amount of stable intermediates. The photoreaction occurs with the evolution of 1.8±0.3 moles of CO per mole of $Ru_3(CO)_{12}$ reacted, and the electronic and IR spectra of the photoproduct (Table II and V) are identical to those reported by Basset and coworkers (86) for the

thermal activation of $Ru_3(CO)_{12}$ adsorbed onto silica gel. The IR spectrum of the product (Figure 49c) exhibits a band at 2109 cm^{-1} that can be assigned to the symmetric A_1 CO vibration of the ruthenium trimer. Although forbidden under D_{3h} symmetry, a comparable band is observed at 2117 cm^{-1} in the spectrum of crystalline $Ru_3(CO)_{12}$. The occurrence of this band suggests a degradation of the D_{3h} symmetry of the photoproduct to ca. C_{2v}. Although fully-allowed under C_{2v}, the intensity of this high frequency band typically remains low which is the observed experimental result for $Ru_3(CO)_{12}$.cryst and our photoproduct on the surface of PVG. Since an oxidative addition of Si-OH either to an individual Ru atom or across a Ru-Ru bond reduces the D_{3h} symmetry of the physisorbed cluster, we conclude that $Ru_3(CO)_{12}$ is chemisorbed on the surface by reaction with one or more surface silanol groups (Figure 68). The reaction results in a complex with an approximate symmetry of C_{2v}. The question of whether the addition occurs across a metal-to-metal bond or at a metal atom can be answered by comparison with known species. The IR spectrum of the photoproduct is equivalent to spectra of a series of Ru and Os oxidative addition products, $HM_3(CO)_{10}L$ (L = SR, OH, NO, and OSi≡), where addition across the metal-metal bond has been established by X-ray diffraction and other techniques (165,166,167) (Table V). Also, no indication was found for a terminal Ru-H vibration which is expected to have a significantly

OXIDATIVE ADDITION REACTION

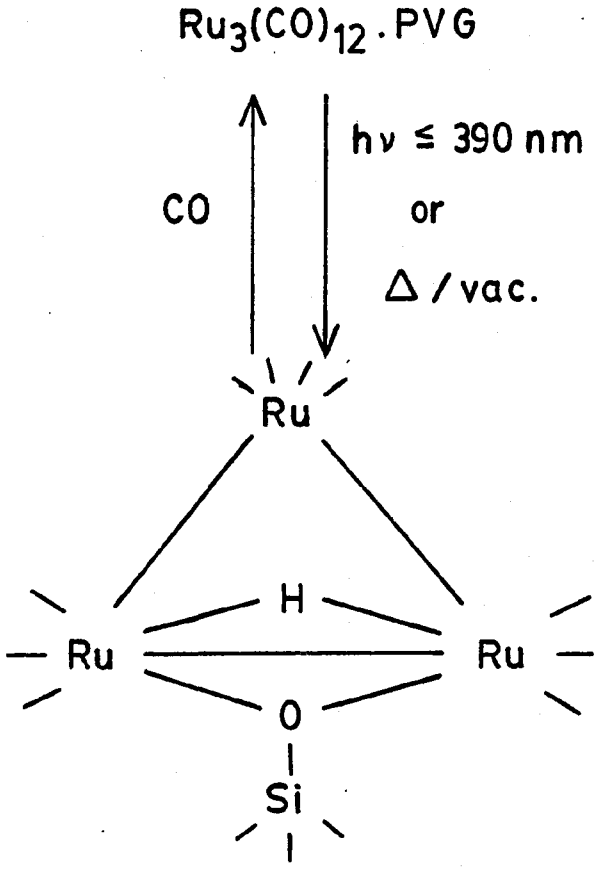

UV: 330 nm

IR : 2109 w, 2078 s, 2069 s, 2034 m

Fig. 68. Oxidative addition of $Ru_3(CO)_{12}$.ads

higher intensity than the vibration due to bridged hydrogen which is normally not detected in the IR spectrum of transition metal clusters (168). We conclude that the primary photochemical reaction of $Ru_3(CO)_{12}$ supported on porous Vycor glass in vacuo is a quantitative oxidative addition across a Ru-Ru bond yielding the chemisorbed surface species $(\mu\text{-H})Ru_3(CO)_{10}(\mu\text{-OSi}\equiv)$. In this complex oxygen acts as a three electron donor and the hydrogen connects to the cluster frame with a two electron three center bond. Many neutral complexes with the formula $(\mu_2\text{-H})M_3(CO)_{10}(\mu_2\text{-X})$ with M = Ru, Os and X = CO, NO, OR, SEt, PHPh, $CNMe_2$ (169,170,171,172) are similar to $HOs_3(CO)_{10}(SEt)$. In all of them X formally acts as three e^- donor (173).

The quantum yield of formation of the oxidative addition product, $1.6\pm0.4 \times 10^{-2}$, is approximately an order of magnitude less than the quantum yield of Ru-Ru bond breaking found in fluid solution. Although dependent on previous heatings, studies of a variety of hydroxylated silicas indicate 4 to 7 silanol groups per 100 $Å^2$. Relative to the molecular dimension of $Ru_3(CO)_{12}$.ads, this high surface density of ≥Si-OH units suggests that the reduction in quantum yield can not be attributed to the inefficiency of scavenging. Rather, we believe that the reduction reflects constraints imposed by the low dimensionality of the surface. As mentioned earlier, the Hausdorff or fractal dimension of PVG, 1.74±0.12, indicates a restrictive

environment where the excited adsorbate has essentially two degrees of freedom. Unlike fluid solution, where the fluidity of the solvent cage offers the excited complex greater distortional flexibility, the rigidity of the support and its constraining dimensionality enhances ring closure or the nonradiative processes which deactivate the excited state. Either possibility or some combination of both reduces the quantum yield of formation of the oxidative addition product.

Reduction of $Ru_3(CO)_{12}$.ads with hydrogen: Under our experimental conditions we were not able to photochemically decarbonylate the ruthenium trimer to ruthenium metal. Photolysis with $\leq$350 nm light for > 24 hours did cause the expected rapid conversion to $HRu_3(CO)_{10}(OSi\leq)$ which then slowly decomposed to yield a grey-coloured sample. Considering the high photon flux through the PVG plate the quantum efficiency of a photochemical reaction would have to be $<< 10^{-6}$ and we therefore attribute the decompositon, shown in Figure 60.and 61, to a slow thermal reaction caused by local heating. This interpretation is supported by experimental evidence obtained from the thermal decomposition ($T \leq 100°C$) of $Ru_3(CO)_{12}$ under vacuum which results in reaction products with an identical set of IR vibrations. If the decomposition occurs in an environment free of molecular oxygen, an IR spectrum with two broad bands at 2073 (m) and 2006 cm^{-1} (w) is observed. Based on the work of Brown and Gonzales (90) we assign the 2073 cm^{-1}

band to carbon monoxide linearly adsorbed on ruthenium and the 2006 cm^{-1} vibration to CO adsorbed on Ru perturbed by neighboring oxygen atoms, probably oxo and hydroxo functionalities on the surface of the glass. The additional band that appears at 2136 cm^{-1} after decomposition of the trimer under O_2 (Figure 61) is caused by CO adsorbed on oxidized or partially oxidized ruthenium. The frequency of this band is close to the frequency of free carbon monoxide since there is very little π-backbonding from an oxidized metal to the antibonding π^* orbital of the carbonyl group. Therefore the bond between the PVG-supported ruthenium oxide and the carbonyl group will have a sigma character. Ruthenium oxides and zerovalent ruthenium carbonyls can be reduced to the metallic state as shown in Figure 62. The total disappearance of the carbonyl vibrations clearly indicates that all ruthenium species are reduced under our experimental conditions. Recarbonylation yields a medium intensity band at 2031 cm^{-1} in addition to the three bands known from the Ru/Ru-oxide moiety which is found to be in excellent agreement with the band at 2030 cm^{-1} observed or 6% Ru on SiO_2. This latter band has been reported by Gonzales and Brown and assigned to CO adsorbed on ruthenium crystallites. We conclude that reduction of Ru-species on PVG with H_2 leads to an agglomeration of larger metal particles in addition to smaller particles whose carbonyl bands are perturbed by neighboring oxygen atoms (Figure 69).

DECARBONYLATION OF $Ru_3(CO)_{12}$.PVG

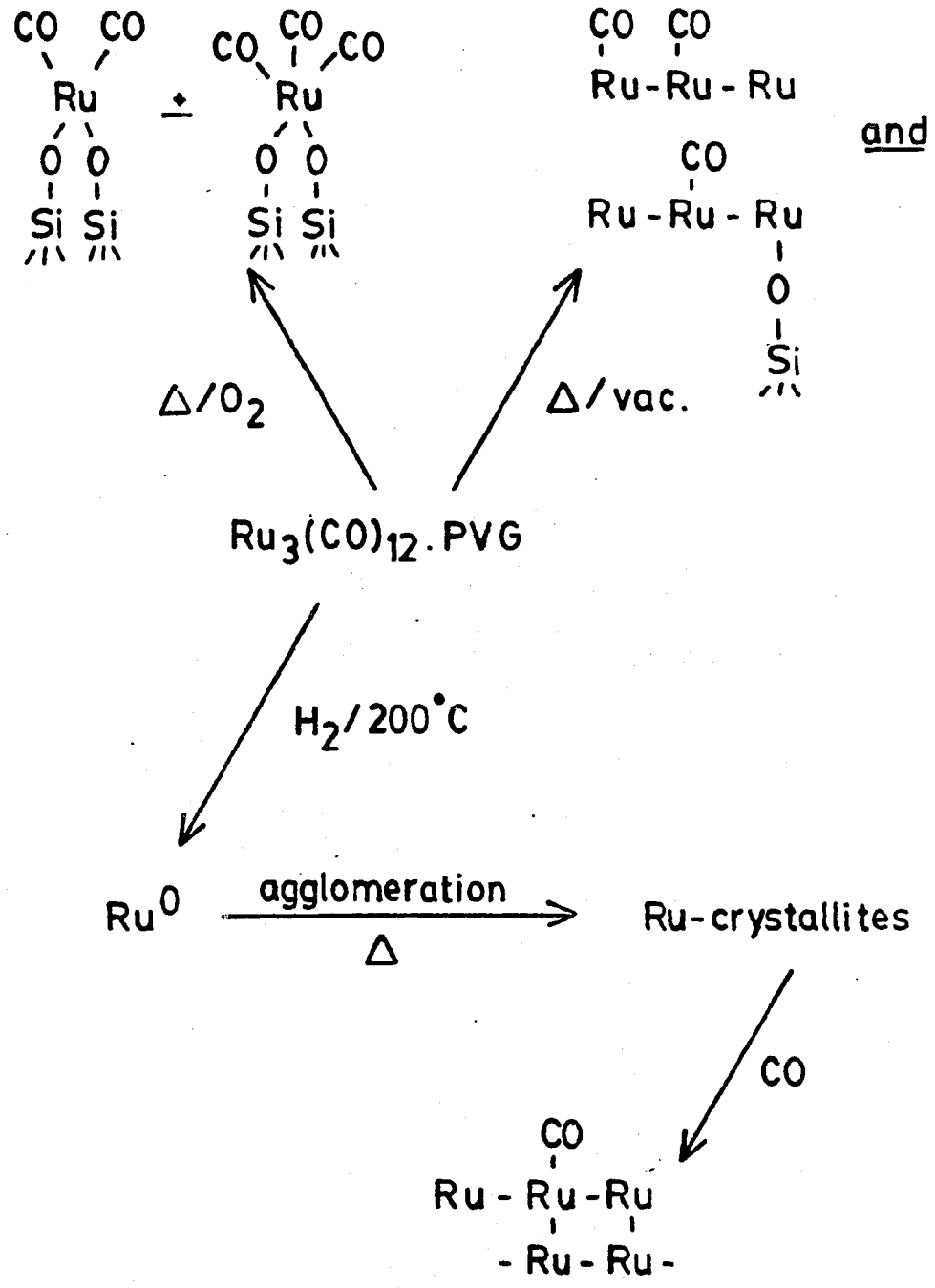

Fig. 69. Reaction of $Ru_3(CO)_{12}$.adsorbed

4.3. HYBRID CATALYSIS REACTIONS

The immediate and quantitative disappearance of the free silanol IR vibration which occurs upon addition of 1-pentene to PVG points to an interaction between the olefin, probably its double bond, and the silanol group. However, since no modification of the vibrational spectrum of the pentene species is observed, a weak physisorption of the hydrocarbon onto the support must be inferred. Under vacuum the olefin can be quantitatively removed from the surface. The low catalytic activity of the physisorbed $Ru_3(CO)_{12}$ is not surprising since, as a coordinatively saturated species, the trimer lacks the active sites which are required for a coordinative bond between the substrate and the metal cluster. A coordination of the substrate to the catalytic species, however, is a prerequisite for catalysis and the unperturbed IR spectrum of the supported cluster conclusively shows the lack of such an interaction. In contrast to the physisorbed species the chemisorbed cluster, $HRu_3(CO)_{10}(OSi\equiv)$, was shown to be active at room temperature towards ligands such as CO and $P(t\text{-}Bu)_3$. Addition of 1-pentene to the reaction system effects an immediate change in the IR spectrum of $HRu_3(CO)_{10}(OSi\equiv)$ and leads to the development of a new band at 2102 cm^{-1} which is found in many transition metal carbonyls coordinated to olefins. Gas chromatographic analysis of the effluent from the reactor shows that the

formation of the pentene-adduct does not cause the ejection of carbon monoxide from $HRu_3(CO)_{10}(OSi\equiv)$. Before the olefin can bind to the ruthenium species, however, a coordinative unsaturation must be introduced into the cluster by rupturing either a Ru-oxygen or a Ru-H bond. In the latter case a terminal Ru-H is produced which should appear in the vibrational spectrum. However, no such band is observed in the IR spectrum of the ruthenium cluster / pentene adduct and we conclude instead that the electron donation from the silanol oxygen to the chemisorbed cluster is reduced from three electrons to one (Figure 70). The newly created lone electron pair on the silanol oxygen probably remains in close proximitry to the unsaturated Ru-atom, assisting in its stabilization (174). Upon coordination with 1-pentene, a low catalytic activity is recorded for the adduct by means of gas chromatographic analysis of the reactor effluent. As the temperature is increased, however, there is a marked increase in the conversion of 1-pentene to cis- and trans-2-pentene. This observation points to a relatively strong metal to olefin bond which requires thermal energy in form of elevated temperatures to rupture and to release the isomerized molecule. IR data obtained during the reaction supports this conclusion; an increase in temperature recovers approx. 20% of the high frequency bands of the chemisorbed trimer which serves as evidence that some olefin is lost from the adduct. Fresh 1-pentene can coordi-

ISOMERIZATION OF 1-PENTENE

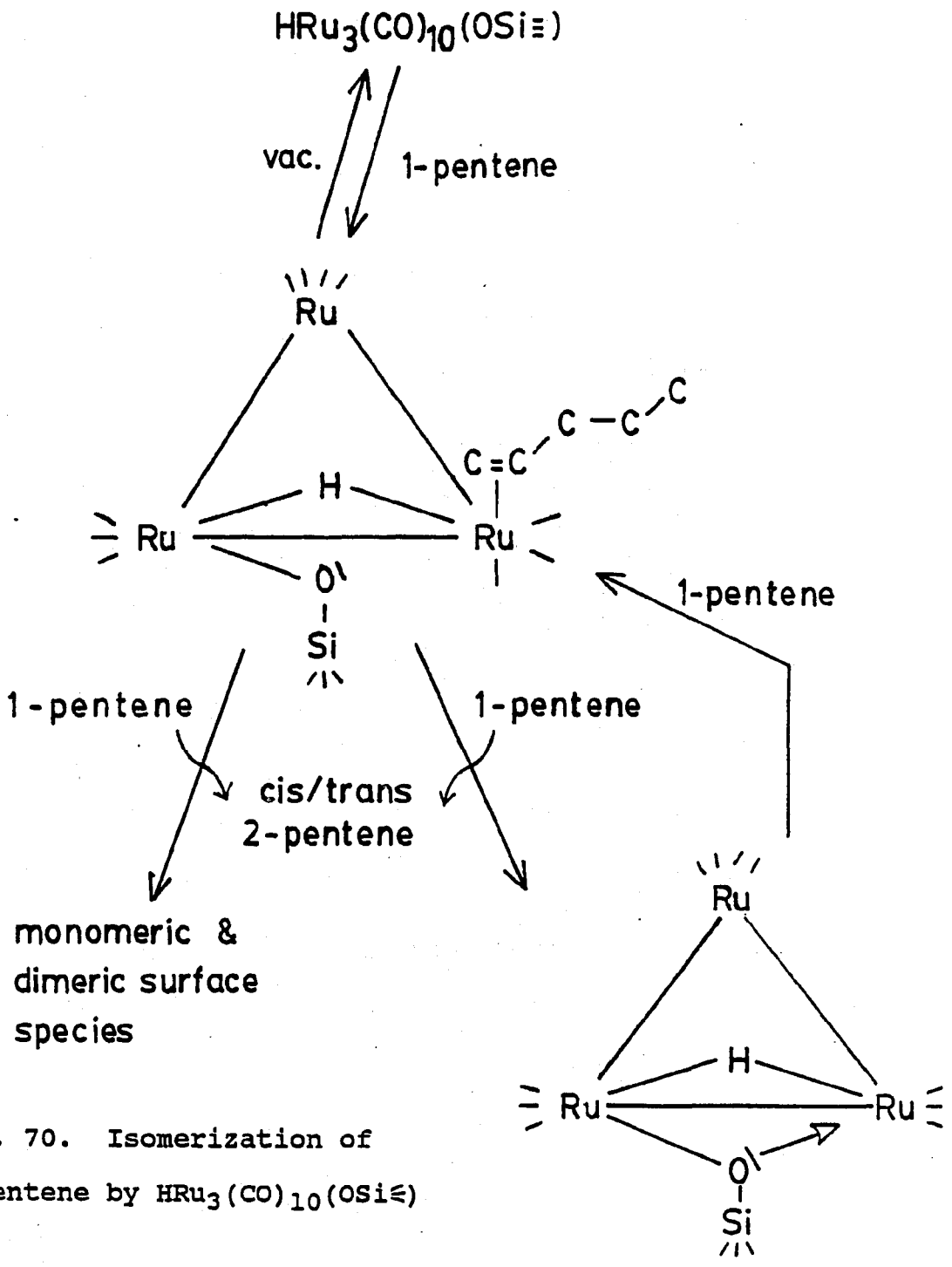

Fig. 70. Isomerization of 1-pentene by $HRu_3(CO)_{10}(OSi\equiv)$

nate with the cluster and an increase in the observed reaction rate is the consequence. At reaction temperatures of 40°C and more, however, IR spectra recorded over the course of the reaction indicate a progressive degradation of the original active species. At temperatures of 100°C and above these side-reactions occur very rapidly and poorly resolved spectra with broad bands at 2080 cm^{-1} and 2000 cm^{-1} result after several minutes.

4.4. SUGGESTIONS FOR FUTURE PROJECTS

In the conception stage of this thesis work, we set out to characterize catalytic processes based on the reaction of a substrate with a PVG-supported ruthenium carbonyl complex. We are now able to characterize the interactions of the ruthenium cluster with the support and its reaction pathways on the surface. The viability of catalysis was shown by using the isomerization of 1-pentene as an example and the catalytically-active species for this reaction has been identified. It would now be very interesting to further characterize the differences found between thermal catalysis and photoinitiated catalysis on PVG. Reactions between the supported cluster and a mixture of CO and H_2 will certainly be rewarding since ruthenium is a known catalyst for the synthesis gas reaction. With the help of impregnation techniques developed in this dissertation other metal complexes, especially $RuHCl(CO)(PPh_3)_3$,

should be supported on the glass and evaluated with respect to their stability and thermal and photochemical activity. Finally the use of ^{13}C NMR on ^{13}C-enriched ruthenium carbonyls would shine light on the reactions of those compounds with EtOH, THF, 1,4-dioxane, and $HOSiPh_3$ and help to further characterize the reactions occuring on the surface of porous Vycor glass. Studies using ^{99}Ru NMR in solution and possibly magic angle spinning (MAS) ^{99}Ru NMR for heterogeneous systems would provide us with information about the interaction of the metal atoms with each other and with their respective ligands. To our knowledge this latter technique has not yet been employed in the investigation of catalytic systems and catalytic active intermediates.

5. REFERENCES

1. Schrauzer,G.N. "Transition Metals in Homogeneous Catalysis"; Dekker: New York, 1971; p 10.

2. Satterfield,C.N. "Heterogeneous Catalysis in Practice"; McGraw-Hill: New York, 1980, p 1.

3. Thomas,J.M.; Thomas,W.J. "Introduction to the Principles of Heterogeneous Catalysis"; Academic Press: London-New York, 1967; p 8.

4. Chalk,A.J. The Spex Speaker 1983, 28/1.

5. Rard,J.A. Chem. Rev. 1985, 85, 1.

6. Dry,M.E. In "CATALYSIS - Science and Technology"; Anderson,J.R.; Boudart,M., Ed.; Springer: Berlin, 1981; Vol.I, Chapter 4.

7. King,D.L. J. Catal. 1978, 51, 386.

8. Everson,R.C.; Woodburn,E.T. and Kirk,A.R.M. J. Catal. 1978, 53, 186.

9. Dalla Betta,R.A. and Shelef,M. J. Catal. 1977, 48, 111.

10. Vannis,M.A. J. Catal. 1977, 50, 228.

11. Cotton,F.A. and Wilkinson,G. "Advanced Inorganic Chemistry", 3rd ed.; Interscience: New York, 1972; Chapter 24, p 770.

12. Nakamura,A. and Tsutsui M. "Principles and Applications of Homogeneous Catalysis"; Wiley: New York, 1980.

13. Parshall G.W. "Heterogeneous Catalysis, Homogeneous Catalysis"; Wiley: New York, 1980.

14. Wender,I. and Pino,P. "Organic Synthesis Via Metal Carbonyls"; Interscience: New York, 1968.

15. "Transition Metal Mediated Organic Synthesis"; Slocum, D.W. and Hughes,O.R., Eds.; Ann. N.Y. Acad. Sci. 1980, Vol. 333.

16. Muetterties,E.L. J. Organomet. Chem. 1977, 200, 177.

17. Muetterties,E.L. Catal. Rev.-Sci. Eng. 1981, 23, 69.

18. Muetterties,E.L. Bull. Soc. Belg. 1975, 84, 959.

19. Ugo,R. Catal.Rev. 1975, 11, 225.

20. Lewis,J. and Johnson,B.F.G. Pure Appl. Chem. 1975, 44, 43.

21. Laine,R.M.; Thomas,D.W. and Cary,L.W. J. Am. Chem. Soc. 1982, 104, 1763.

22. Laine,R.M. J. Mol. Catal. 1983, 21, 119.

23. Halpern,J. Science 1982, 217, 401.

24. Masters,C. "Homogeneous Transitionmetal Catalysis"; Chapman & Hall: New York, 1981.

25. Markó,L.; Heil,B.; Vastag,S. Adv. Chem. Ser. 1974, 132, 27.

26. Mond,L. et al. Proc. Chem. Soc. (London) 1910, 26, 67.

27. Mond,L. et al. Z. anorg. allg. Chem. 1910, 68, 207.

28. Corey,E.R. and Dahl,L.F. J. Am. Chem. Soc. 1961, 83, 2203.

29. Corey,E.R. and Dahl,L.F. Inorg. Chem. 1962, 1, 521.

30. Mason,R. and Rae A.I.M. J. Chem. Soc. A 1968, 778.

31. Churchill,M.R.; Hollander,F.J. and Hutchinson,J.P. Inorg. Chem. 1977, 16, 2655.

32. Poliakoff,M. and Turner,J.J. J. Chem. Soc. A 1971, 654.

33. Quicksall,C.O.; Spiro,T.G. Inorg. Chem. 1968, 7, 2365.

34. Huggins,D.K.; Flitcroft,N. and Kaesz,H.D. Inorg. Chem. 1965, 4, 166.

35. Battiston,G.A.; Bor,G.; Dietler,U.K.; Kettle,S.F.A. Rossetti,R.; Sbrignadello,G. and Stanghellini,P.L. Inorg. Chem. 1980, 19, 1961.

36. Adams,D.M. and Tyler,I.D. J. Chem. Soc. Faraday Trans 2, 1982, 78, 1561.

37. Ago,D; Ganozzi,A.D.; Tondello,E. and Fragala,I. Inorg. Chim. Acta 1979, 37, 191.

38. Tyler,D.R.; Levenson,R.A. and Gray,H.B. J. Am. Chem. Soc. 1978, 100, 7888.

39. Strohmeier,W. and Weigelt,L. J. Organomet. Chem. 1978, 145, 189.

40. Sanchez-Delgado,R.A.; de Ochoa,O.L. J. Mol. Catal. 1979, 6,303.

41. Pino,P.; Braca,G; Sbrana,G. and Cuccuru,A. Chem. & Ind. 1968, 1732.

42. Castiglioni,M.; Milone,L.; Osella,D.; Vagilio,G.A. and Valle,M. Inorg. Chem. 1976, 15, 394.

43. Knifton,J.F. J. Mol. Catal. 1980, 11, 91.

44. King,R.B.; King Jr.,A.D. and Tanaka,K. J. Mol. Catal. 1981, 10, 75.

45. Johnson,T.H.; Siegle,L.A. and Chaffin,J.K. J. Mol. Catal. 1980, 9, 307.

46. Geoffroy,G.L. and Wrighton,M.S. "Organometallic Photochemistry"; Academic Press: New York, 1979.

47. Wrighton,M.S. Chem. Revs. 1974, 74, 401.

48. Balzani,V. and Carassiti,V. "Photochemistry of Coordination Compounds"; Academic Press: New York, 1970; Chapter 17.

49. Koerner v. Gustorf,E. and Grevels,F.W. Fortschr. Chem. Forsch. 1979, 13, 366.

50. Porter,G.B. J. Chem. Educ. 1983, 60, 785.

51. Malouf,G. and Ford,P.C. J. Am. Chem. Soc. 1974, 96, 601.

52. Giordano,P.J. and Wrighton,M.S. Inorg. Chem. 1977, 16, 160.

53. Austin,R.G.; Paonena,R.I.; Giordano,P.J.; Wrighton,M.S. Adv. Chem. Ser. 1978, 168, 189 and reference therein.

54. Wubbles,G.G. Acc. Chem. Res. 1983, 16, 285.

55. reference 46, p 324.

56. Wrighton,M.S. and Schroeder,M.A. J. Am. Chem. Soc. 1976, 98, 551.

57. Graff,J.L.; Sanner,R.D. and Wrighton,M.S. ibid. 1979, 101, 273.

58. Sanner,R.D.; Austin,R.G.; Wrighton,M.S.; Honnick,W.D. and Pittman,C.U. Inorg. Chem. 1979, 18, 928.

59. Krausz,P.; Carnier,F. and Debois,J.E. J. Am. Chem. Soc. 1975, 97, 437.

60. Hill,B. et al. Mol. Photochem. 1975, 5, 195.

61. Graff,J.L.; Sanner,R.L. and Wrighton,M.S. Organomet. 1982, 1, 837.

62. Johnson,B.F.G.; Lewis,J. and Twigg,M.V. J. Organomet. Chem. 1974, 67, C75.

63. Johnson,B.F.G.; Lewis,J. and Twigg,M.V. J. Chem. Soc. Dalton 1975, 1876.

64. Stone,F.G.A. et al. J. Chem. Soc. Dalton 1972, 2094.

65. Graff,J.L.; Sanner,R.D. and Wrighton,M.S. J. Am. Chem. Soc. 1979, 101, 273.

66. Wrighton,M.S. et al. in reference 15, p 188.

67. Malito,J.; Markiewicz,S. and Poe,A. Inorg. Chem. 1982, 21, 4335.

68. Desrosiers,M.F.; Wink,D.A. and Ford,P.C. Inorg. Chem. 1985, 24, 2.

69. Strohmeier,W.; Hitzel,E. and Kraft,B. J. Mol. Catal. 1977, 3, 61.

70. Smith,A.K. and Basset,J.M. J. Mol. Catal. 1977, 2, 229.

71. Yermakov,Y.I. J. Mol. Catal. 1983, 21, 35.

72. Ciardelli,F.; et al. J. Mol. Catal. 1982, 14, 1.

73. Vol'pin,M.E. paper presented at IVth International Symposium on Relations between Homogeneous and Heterogeneous Catalysis, Asilomar, CA, U.S.A., 1983.

74. Basset,J.M. and Choplin,A. J. Mol. Catal. 1983, 21, 95.

75. Basset,J.M. J. Am. Chem. Soc. 1978, 100, 2590.

76. Verdonck,J.J.; Jacobs,P.A. and Uytterhoven,J.B. J. Chem. Soc. Chem. Commun. 1979, 181.

77. Goodwin,J.G. and Naccache,C. J. Mol. Catal. 1982, 14, 259.

78. Sanchez-Delgado,R.A. et al. J. Mol. Catal. 1981, 11, 193

79. Kuznetsov,V.L.; Bell,A.T. and Yermakov,Y.I. J. Catal. 1980, 65, 374.

80. Zecchina,A.; Guglielminotti,E; Bossi,A and Camia,M. J. Catal. 1982, 74, 225.

81. Guglielminotti,E.; Zecchina,A.; Bossi,A. and Camia,M. J. Catal. 1982, 74, 240.

82. Guglielminotti,E.; Zecchina,A.; Bossi,A. and Camia,M. J. Catal. 1982, 74, 266.

83. Gallezot,P.; Condurier,G.; Primet,M. and Imelik,B. in ACS Symp. Ser. 40; Gould R.F. Ed.; 1977, 144.

84. Kuznetsov,V.L.; Bell,A.T. and Yermakov,Y.I. J. Catal. 1980, 65, 374.

85. Doi,Y. and Yano,K. Inorg. Chim. Acta 1976, 76, L71.

86. Theolier,A.; Choplin,A.; D'Ornelas,L.; Basset,J.M.; Zanderighi,G. and Sourisseau,C. Polyhedron 1983, 2, 119.

87. Simpson,A.F. and Whyman,R. J. Organomet. Chem. 1981, 213, 157.

88. Eckerdt,J.G. and Bell,A.T. J. Catal. 1979, 58, 170.

89. Vannice,M.A. In "CATALYSIS - Science and Technology"; Anderson,J.R.; Boudart,M., Ed.; Springer: Berlin, 1981; Vol.III, Chapter 3.

90. Brown,M.F. and Gonzalez,R.D. J. Phys. Chem. 1976, 80, 1731.

91. Bradshaw,A. J. Chem. Soc. Chem. Commun. 1980, 365.

92. Brenner,A. and Hucul,D.A. J. Am. Chem. Soc. 1980, 102, 2484.

93. Liu,D.K. and Wrighton,M.S. J. Am. Chem. Soc. 1982, 104, 898.

94. Simon,R.; Morse,D.L. and Gafney,H.D. Inorg. Chem. 1983, 22, 573.

95. Wrighton,M.S. et al. Pure Appl. Chem. 1975, 41, 671.

96. Gafney,H.D. E.C. Britton Memorial Symposium, Midland, Michigan, April 1982.

97. Jackson,R.L. and Trusheim,M.R. J. Am. Chem. Soc. 1982, 104, 6590.

98. Gerischer,H Discuss. Faraday Soc. 1974, 219.

99. Bach,W. and Breuer,H.D. ibid. 1974, 237.

100. Moesta,H. ibid. 1974, 244.

101. Elmer,T.H. J. Amer. Ceram. Soc. 1970, 53, 171.

102. Iler,R.K. "The Chemistry of Silica"; Wiley-Interscience: New York, 1979; p 551.

103. Kiselev,A.V. "The Structure and Properties of Porous Materials", Everett,D.H. and Stone,F.S., Eds.; Butterworth: London, 1958; p 195.

104. Strazhesko,D.N.; et al. J. Chromatog. 1974, 102, 191.

105. Vydra,F. and Markova,M. J. Inorg. Nucl. Chem. 1964, 26, 1319.

106. Arhland,S.; Grenthe,I.; Noren,B. Acta Chem. Scand. 1960, 14, 1059.

107. DeBoer,J.H. and Vleeskens,J.M. Proc. Koninkl. Ned. Akad. Wetenshap. Ser. B 1958, 61, 2.

108. Hockey,J.A. Chem. Ind. (London) 1965, 57.

109. Low,M.J.D. and Ramasubramanian,N. J. Chem. Soc. Chem. Comm. 1965, 499A.

110. Pfeifer,P. and Avnir,D. J. Chem. Phys. 1983, 79, 3558.

111. Avnir,D.; Farin,D.; Pfeifer,P. J. Chem. Phys. 1983, 79, 3566.

112. Avnir,D.; Farin,D.; Pfeifer,P. Nature 1984, 308, 261.

113. Jortner,J. Phys. Rev. Lett. 1984, 52, 2164.

114. Janowski,V.F. and Heyer,W. Z. Chemie 1979, 19, 1.

115. Allum,K.G.; Hancock,R.D.; Howell,I.V.; McKinzie,S.; Pitkethly,R.C. and Robinson, J. Organomet. Chem. 1975, 87, 203.

116. Pelz,J.; Unverferth,K. and Schwetlick,K. Z. Chem. 1974, 14, 370.

117. Imanaka,T; et al. Nippon Chem. Soc. Japan, Pure Chem. Sect. Kagaku Zasshi 1973, 421, 889.

118. Blomfield,G.A. and Little,L.R. J. Catal. 1969, 14, 213.

119. Kubota,S. and Higuchi,I. J. Chem. Soc. Japan, Pure Chem. Sect. (Nippon Kagaku Zasshi) 1967, 87, 417.

120. ibid. 1970, 91, 314.

121. Otsuka,K.; et al. Bull. Chem. Soc. Japan 1970, 50, 631.

122. Chapman,L.D. and Hair,M.L. J. Catal. 1963, 2, 145.

123. Lycourghiotis,A. React. Kinet. Catal. Lett. 1976, 5, 453

124. Koelling,J.G.; Kolb,K.E. J. Phys. Chem. 1971, 75, 3897.

125. Janowski,F.; et al. Chem. Techn. 1977, 29, 313.

126. Chapman,L.D. and Hair,M.L. J. Catal. 1963, 2, 145.

127. Wolf,F.; et al. Chem. Techn. 1976, 28, 610.

128. Janowski,F. and Wolf,F. Z. Chem. 1976, 16, 318.

129. Janowski,F.; et al. React. Kinet. Catal. Lett. 1978, 8, 437.

130. Janowski,F. and Wolf,F. ibid. 1977, 6, 253.

131. U.S. Patents 2403744; 2215089; 2286275; 2315329.

132. Wolf,F.; Renger,P.; Janowski,F.; Heyer,J. Z. Allg. Chem. 1977, 432, 249.

133. Adams,D.M.; Gardner,I.R.; Parkyns,N.D. J. Catal. 1976, 45, 145.

134. Vanderspurt,T.H. U.S. Patents 4020116, 4048110 1977.

135. Ziolo,R.F. and Lewis,R.B. German Patent 2740311 1978.

136. Ahmad,J.J. et al. Inorg. Synth. 1974, 15, 45.

137. Candlin,J.P. and Shortland,A.C J. Organomet. Chem. 1969, 16, 289.

138. Bruce,M.I.; Shaw,G.; Stone,F.G.A. J. Chem. Soc. Dalton 1972, 2094.

139. Ciapetta,F.G.; Plank,C.J. In "Catalysis"; Emmett,P.H. Ed.; Reinhold: New York, 1954; Vol. 1, p.315.

140. Higginson,G.W. Chem. Eng. (N.Y.) 1974, 81, 98.

141. Innes,W.B. In "Catalysis"; Emmett,P.H. Ed.; Reinhold: New York, 1954; Vol. 1, p. 245.

142. T. Kennelly, PH.D. Thesis, City University of New York, 1980.

143. Robert Simon, Ph.D. Thesis, City University of New York, 1983, p 47.

144. Hatchard,C.G. and Parker,C.A. ibid., 1956, 235, 518.

145. Calvert,J.G. and Pitts,J.N. "Photochemistry"; New York: Wiley, 1971.

146. Rodgers,V.E. and Angell,C.A. J. Chem. Educ. 1983, 60, 802.

147. Mirbach,M.F.; Mirbach,M.J. and Saus,A. Chem. Rev. 1982, 82, 59.

148. Williamson,D.E.; Nichols,I.A. and Schurin,B. Rev. Sci. Instrum. 1960, 31, 528.

149. Alt,H.C. and Kalus,J. Rev. Sci. Instrum. 1982, 53, 1235.

150. Buchter,H.H. "Apparate und Armaturen der Chemischen Hochdrucktechnik"; Springer: Berlin, 1967.

151. Spain,I.L. and Paauwe,J. "High Pressure Technology", Vol. I; Dekker: New York, 1977.

152. McDonald,R.S. J. Phys. Chem. 1958, 62, 1168.

153. Cant,N.W. and Little,L.H. Can. J. Chem. 1964, 42, 802.

154. Low,M.J.D. and Ramasubramanian,N. J. Phys. Chem. 1966, 9, 2740.

155. Eady,C.R.; Johnson,B.F.G.; Lewis,J. J. Chem. Soc. Dalton Trans. 1977, 838.

156. Lewis,J.; McPartlin,M.; Johnson,B.F.G. et al. J. Chem. Soc. Dalton Trans. 1980, 383.

157. Johnson,B.F.G.; Lewis,J.; Raithby,P.R.; Suess,G. J. Chem. Soc. Dalton Trans. 1979, 1356.

158. Poe,A. and Twigg,M.V. J. Chem. Soc. Dalton 1974, 1860.

159. Brevard,C. and Granger,P. J. Phys. Chem. 1981, 75, 4175.

160. Brevard,C. and Granger,P. Inorg. Chem. 1983, 22, 532.

161. Forster,A.; Johnson,B.F.G.; Lewis,J.; Matheson,T.W.; Robinson,B.H. and Jackson,W. J. Chem. Soc. Chem. Comm. 1974, 1042.

162. Johnson,B.F.G.; Lewis,J.; Reichert,B.E. and Schorpp,K. J. Chem. Soc. Dalton 1976, 1403.

163. Robertson,J. and Webb,G. Proc. Roy. Soc. A 1974, 341, 383.

164. Kettle,S.F.A. and Stanghellini,P.L. Inorg. Chem. 1979, 18, 2749.

165. Johnson,B.F.G.; Raithby,P.R. and Zuccaro,C. J. Chem. Soc. Dalton 1980, 99.

166. Besson,B.; Moraweck,B.; Smith,A.K. and Basset,J.M. J. Chem. Soc. Chem. Comm. 1980, 569.

167. Crooks,G.R.; Johnson,B.F.G.; Lewis,J. and Williams,I.G. J. Chem. Soc. (A) 1969, 797.

168. Nakamoto,K. "Infrared and Raman Spectra of Inorganic and Coordination Compounds", 3rd Ed.; Wiley-Interscience: New York, 1980; p 290.

169. Azam,K.A.; Deeming,A.J.; Kimber,R.E. and Shukla,P.R. J. Chem. Soc. Dalton 1976, 1853.

170. Johnson,B.F.G.; Raithby,P.R. and Zuccaro,C. J. Chem. Soc. Dalton 1980, 99.

171. Iwasaki,F.; Mays,M.J.; Raithby,P.R.; Taylor,P.L. and Wheatley,P.J. J. Organomet. Chem. 1981, 213, 185.

172. Churchill,M.R.; DeBoer,B.G. and Rotella,F.J. Inorg. Chem. 1976, 15, 1843.

173. Johnson,B.F.G. In "Transition Metal Clusters"; Johnson,B.F.G., Ed.; Wiley: New York, 1980; p 29.

174. Basset,J.M. and Choplin,A. J. Mol. Catal. 1983, 21, 95.

175. Tyler,D.R.; Levenson,R.A. and Gray,H.B. J. Am. Chem. Soc. 1978, 100, 7888.

176. Johnson,B.F.G.; Johnston,R.D.; Josty,P.L.; Lewis,J. and Williams,I.G. Nature 1967, 213, 901.

177. Bruce,M.I.; Shaw,G. and Stone,F.G.A. J. Chem. Soc. Dalton 1972, 2094.

178. Johnson,B.F.G.; Lewis,J. and Twigg,M.V. J. Chem. Soc. Dalton 1975, 1876.